Reply to all three reviews

The manuscript has been substantially revised. There are four main points:

1. The number of figures in the main body of the article is reduced from 23 to 15.
2. AON Linear Sampling produces better results with the recommended limiter condition.
3. The code has been polished (no csh, no sed).
4. A supplement with additional material is now included.

Authors of this paper test the behaviour of a numerical algorithm representing collisions between cloud and rain drops in Lagrangian microphysics schemes. They describe 3 versions of the algorithm (one of the versions is new) and test the convergence of the 3 versions in 3 different settings. The presented work is based on a similar suite of tests carried out by the same group of authors and published in GMD in 2017 (https://www.geosci-modeldev.net/10/1521/2017/gmd-10-1521-2017.html). In 2017 the tests were done in a 0-dimensional box setup. Now the tests are extended to a 1-dimensional column. I think that the presented tests are useful and the topic is interesting to the GMD community. However, the overall presentation of the convergence of the algorithm should be improved before publication. I couldn't find what is the criterion for reaching convergence in the tests. Despite being very thorough in testing different parameters and cases, the authors then use vague terms like "equally bad", "tend to approach the reference" or "seem to converge". The only way in which the authors show convergence is by plotting many lines on top of each other. This is not satisfying and results in a paper that is overflowing with figures that look the same. I suggest introducing a definition and quantitative measure of convergence. This would allow to change some of the repetitive concentration plots into plots showing convergence as a function of a tested parameter. I think that the paper should be more concise. The authors carried out a lot of tests but summarising some of them would improve the paper. For example Fig 10 shows results for slightly different initial condition and Fig 12 for a different kernel. Neither of these figures show anything new about the collision algorithm behaviour.

We agree that there are many similarly looking plots. With that we wanted to keep it simple and help the reader to interpret the results more easily when the same plot format is used. Moreover, this eliminated the need of introducing metrics which are sometimes more difficult to interpret.

On the other hand, we see that the manuscript is quite long. Hence, we follow your recommendation and identified sensitivity series where it is sufficient to show, e.g., only the moments after 60 minutes. The full time series plots are then moved to the newly introduced supplement. Moreover, the time evolution is shown for the range [30min,60min], where appropriate.

Similarly, the authors study the bin collision algorithm with upstream advection scheme and observe that the results are "slightly smeared out". The upstream advection scheme is known to be very diffusive and there were many papers published on that. This detracts from the main theme of the paper and the interesting parts of the study.

In previous publications, I faced sometimes concerns about EULAG/MPDATA as it based on the "infamous" upstream scheme. Hence, including both US1 and MPDATA should demonstrate that MPDATA does a better job. Nevertheless, we decided to remove all content that is related to the usage of the first order upstream scheme. The comparison with LCM should suffice to show the adequacy of MPDATA. By the way, we moved the PureSedi-test case in the previous section 3.1 to the Appendix.

Additional comments:

Table 1: German language in the caption

Sorry. Removed.

Page 3, line 13-14: "Moreover, we will use the term cloud droplets interchangeably with ice crystals to increase clarity in writing." - I don't think that this increases the clarity. The paper nowhere actually discusses issues related to ice crystals. I think that keeping the language focused on cloud and rain droplets is sufficient.

We removed the sentence and use the term droplet throughout the study. On the other hand, the text makes now more references to ice aggregation.

Figure 1: in SIP (Simulation particle) p should also be capitalised

Done.

Page 7 line 15: Smoluchowski equation

Thanks.

Page 8: Maybe it would make more sense to first describe the collision algorithms and then talk about the column model setup?

We would like to keep it our way. We think that first the basic properties of the column model should be introduced before going into the details of how collisional growth is implemented.

Figure 2,3 and later in the text: The abbreviations like AON, WM3D, etc were already defined and should not be defined again.

A table with all model versions and abbreviations is now included.

Page 9 line 5: I don't think it's legally allowed and generally acceptable to copy verbatim paragraphs from different papers (?). I would suggest to just refer to the relevant paragraph or to paraphrase.

We found it awkward to paraphrase our "own" text and thus we decided to copy paragraphs from our previous paper (it is also a GMD study). We were unsure if this plagiarism and we mentioned this when we submitted the manuscript. During the revision, we asked again the Editorial office and they confirmed that it is okay.

Algorithm 1 and 2 caption: The style convention of the code block should be repeated in its caption.

We moved the paragraph with the style convention to both captions.

Algorithm 2, line 16: iff

"iff" is a common term in mathematics meaning "if and only if". "iff" is replaced to avoid confusion.

Page 14 line 15: "For more sophisticated kernels, including, e.g., turbulence enhancement, the present approach may not be adopted easily as the driving mechanism for collisions to occur in the current model is differential sedimentation (...)." - This is very important for real applications of WM2D algorithm. Could you expand on this? How would you implement the WM2D ideas in a full 3D LES simulation focusing on turbulence effects on precipitation formation?

The extent of aggregation in pure ice clouds is not as much affected by turbulence as coalescence in warm clouds. So for aggregation studies with a classical hydrodynamic kernel, WM2D will be a suitable choice. The present WM2D version considers only vertical overtakes and can only be used with kernels that have a |wi-wj|-term. "Turbulence enhancement" kernels also account for collisions in the horizontal plane and such kernels usually do not have an

explicit |wi-wj|-term. So there is no straightforward way to use WM2D with such kernels and it is also not meaningful if a substantial fraction of collision appears due to turbulent motion. Moreover, this would also require making assumptions about the subgrid turbulent velocity of each SIP. That's another thread of research, namely, how subgrid information/processes are or should be incorporated in LCMs.

Paragraph 2.5: Please provide a table which summarises the combinations of different algorithm options and the labels used to distinguish them.

Included.

Paragraph 2.5: What is the added benefit of comparing the BIN Bott and Wang collection algorithms in a paper about Lagrangian collection algorithms?

The benefit is to put the comparison into a broader context. Bott and Wang are established solvers and it is important to see how differences between those two BIN models relate to differences among LCM versions or differences between LCM and BIN.

It also shows that Wang needs much smaller time steps than LCM for example. See also our reply on Figure 7 below.

Page 19 line 8: "We found that convergence is usually more easily reached for higher moments than for lambda_0" – Why is that? Would different method of initialising the SIPs make a difference?

These are good questions. And there is no simple answer. A few thoughts:

- In the base case, the decrease in lambda_0 is 4 orders of magnitudes, whereas lambda_2 increases by 8 orders of magnitude. This makes it difficult to define an objective metric that compares convergence in the zeroth and second moment. Hence, the above statement of an easier convergence is a bit subjective. So a possible answer to your question "Why is that" shouldn't be overrated.
- Our 'subjective' statement is mainly based on our experience gained from the 2017-paper. In particular, the supplement of the 2017-paper displays time evolutions of lambda_0, lambda_2 and lambda_3. There are several cases, where lambda_2-evolutions match better than lambda_0-evolutions. One example is Fig. 14 in SUPP of the present paper. There one can also find out about the effect of the various SIP initialization techniques.

Figure 7 and others: Could you show results for t> 30min only? The first half of all those plots shows nothing

The legends in the left column need some space, but the panels in the right column are shortened now. Thanks.

Figure 7 and others: Why are the Lagrangian schemes always predicting higher concentrations than the BIN scheme?

Good question. In U2017, we saw that the converged AON results predicted slightly smaller concentrations after 60 minutes. Dziekan & Pawlowska, 2017 (later in the year 2017) pointed out that AON results, at least in the limit of all SIP weighting factors approaching unity, solve the so-called master equation, and not the mean-state equation of Smoluchowski. This gave a posteriori one possible physical explanation of why AON and BIN results can differ and why there are more collisions in AON. In the end, the story is a different one, as we had a small bug in the 2017-program code. The present study uses a bug-free algorithm and AON produces fewer collisions. By the way, this gave the motivation for Figs. 9-11 (in the original manuscript),

where we wanted to see if this is a universal feature of AON and if this occurs also for other LWC- and DNC-values. Moreover, we compare LCM results to one specific BIN model. It could be that the underlying Bott model is diffusive in radius space and overestimates the amount of collisions. This is why we alternatively used the algorithm by Wang and find it important to include the fourth row of Fig.6 with bin sensitivities.

Figure 14: This figure is very interesting! It's staggering to see how very few of the tested combinations of SIPs lead to any collisions. A strong argument in favour of WM2D approach.

Indeed, very few of the tested combinations of SIPs lead to any collisions.

Figure 16: The figure is not clear, especially the yellow dash-dotted lines are hard to see.

We changed the selection of colours.

Page 34 lines 15-19: If the results are "identical" and "basically identical" then they don't have to be shown again.

We moved it to SUPP.

Page 35 line 4: This is not a new finding and is out of scope of the paper.

As written above, we removed all first-order upstream results in the collisional growth sections except for Figs. 4 & 5 (now Figs. A1 & A2).

Figure 21: It's very hard to distinguish between the two blue lines.

We now use a different colour table.

Page 40 line 14: necessary is repeated

Thanks.

Code availability: It would help to provide a Docker or a Singularity image in which the column model scripts could be run. It would eliminate the need to change any file paths or to install compilers and packages with specific versions. This would be helpful, especially because the provided code is not just pure Python code. I know that it is not a policy of GMD, so it's just a suggestion. In my case I tried compiling the code with gcc 8.3.0 and gcc/9.2.0 on a CentOS system with Python 3.7.0 and got an error:

AON_Alg.fpp:90:0: error: operator '*' has no right operand #if (KERNEL_INTPOL <= 1) /* logarithmic mass bin*/

I suspect it is some preprocessor issue but I didn't debug further. I then tried compiling with gcc/9.2.0 on an OSX system with Python 3.7.6 and got an error: sed: illegal option –

I guess it's an issue with OSX default sed, but I didn't debug further

The present study is my first open-source endeavour, and in the meantime I have come to the conclusion that not all aspects of the code design helped the interoperability. To give more tribute to the FAIR principles, I replaced the csh-script by a python script. Calls of sed are replaced by python internal commands (module re). So no more csh, no more sed. Unfortunately, gcc could not be replaced by python constructs. There are some modules promising to do the job of gcc, but they do not seem to be maintained or got stuck during their development.

Hereby I provide my comments to the manuscript entitled \Collection/Aggregation in a Lagrangian cloud microphysical model: Insights from column model applications using LCM12 (v0.9)"

Overall, I consider the submitted text a valuable contribution to the literature on particle-based cloud modelling as it provides detailed formulation of test cases that are essential in the development of new implementations of relevant algorithms. It thus clearly matches the journal scope.

Below, I list my major, minor and technical comments to the manuscript. I include also a comment to the enclosed software.

Major points

Unacknowledged performance trade-offs

Some performance trade-offs pertaining to the choice among linear and quadratic sampling are detailed. It is however not pointed out that QUADRATIC sampling precludes parallelisation of the collision computations (within a gridbox/column) due to introduced data dependency (page 11, line 22-23). This is particularly worth underlining, as the availability of shared-memory parallelisation with multi-core CPUs or GPUs allows for significant speed up (i.e., almost by the factor equal to the number of threads). In fact, all but the pair-shuffling and random number generation steps in the AON coalescence algorithm with linear sampling are embarrassingly parallel. Given the above, I find it at least misleading to say, without mentioning the precluded parallelisability, that:

• \simulations with linear sampling ... converges slower ... compared to quadratic" (p1/l14-15)

• \benefit of the reduced computational cost may be outweighed by the stronger requirements on Δt" (p24/l2)

• \restrictions on the timestep might cancel out the computational benefit gained by the reduced number of SIP combinations" (p39/l25-26)

Similarly, I doubt the statement on page 12, lines 2-3 (on performance superiority over integer preserving implementation) holds true in parallel context, where random numbers can be generated concurrently in large batches.
Finally, it is worth commenting on the parallelisability consequences of the requirement to perform collisions column-wise in the WM2D scheme.

The new LinSamp implementation with a new limiter version performs much better and statements that you found too critical are removed. Furthermore, comments on parallelisation are included in the LinSamp and WM2D sections.

Subrid-dynamics and WM2D

While it is acknowledged on page 14 (lines 15-17) that the WM2D scheme is somewhat incompatible with \sophisticated kernels", I highly recommend to extend the discussion also to the aspects of subgrid-scale dynamics representation in particle-based models { e.g., referring to the already cited work of Hoffmann et al. (2019). In short, in my understanding, the \information content" of SIP positions in particle-in-cell-type models is somewhat overestimated here. In particular, the prevalent Large-Eddy-Simulation context should be addressed. Candidate location: page 14 (lines 11-14)?

It is clear, that the complexity of AON when employed in 2D/3D cloud LES is in between of highly parametrised bulk approaches and DNS computing trajectories of single droplets. AON with WM2D is an effort to use slightly more information of the SIPs (i.e. their vertical position) than in the regular AON.

A possible route to consider the effects of subgrid-motions on collision in LCMs has recently been presented by Krueger and Kerstein (2018, https://doi.org/10.1029/2017MS001240). Their one-dimensional approach is able to represent droplet clustering and turbulence-induced relative droplet velocities in a realistic manner, and its implementation in already applied LCM subgrid-scale models (e.g., Hoffmann et al. 2019) is deemed straightforward. However, further research is required on how the limited number of SIPs in current LCM applications may corrupt the correct representation of such processes. We include a paragraph in the manuscript.

Rebutting your argument "positions in particle-in-cell-type models is somewhat overestimated here": If (subgrid) position of SIPs should not be overinterpreted, then it would not make sense to interpolate background Eulerian fields to SIP positions as is done in Grabowski et al 2018, GMD or GMDD paper of Shima et al., 2020.

Paper length

The article length is, in my opinion, impeding appreciation of its content. I include some detailed suggestions on what could be omitted from the text in Technical/editorial remarks below. Besides that, I consider it a malpractice to introduce an almost-page-long quote from an earlier study of the authors. I see also little benefit in repeating Figure. 3 here { please just refer to the relevant parts of the 2017 GMD paper which is readily available for all readers. I also suggest adding a table of contents (as done recently in GMD in Shima et al. [3]).

If I had cited the text of someone else in this way, I would consider it malpractice. In the present situation, it is fairer to simply copy the text. There's no benefit of rewriting it. As replied to Rev #1, the Editorial Office confirmed that it is legally okay.

The left side of Fig.3 was not part of the previous 2017-paper. Moreover, the two other algorithms (which performed mediocrely in the 2017-paper) are not actively used any longer (to our knowledge). So it makes sense to use this updated sketch in the future.

GMD Editorial Office is reluctant when it comes to including a printed table of contents. They say the PDF document contains a table of content. We drastically shortened the number of figures and hope that readers do not get lost that easily anymore.

Minor points

The title

First, why not to avoid a \slash" in the title, and use \Collisional growth" instead of \Collection/Aggregation". Second, I oppose to calling presented simulations \applications", suggest \simulations"?

Finally, I generally suggest to label the discussed microphysics modelling methods as \probabilistic particle-based" rather than \Lagrangian". First, \Lagrangian" is a much more broader term (consider e.g. the Lagrangian cloud models described in [2, 1]), and thus potentially misleading for readers from outside our niche. Second, the discussed model is not fully Lagrangian as it relies on Eulerian dynamical core. I am aware that the present title is a reference to the U2017 paper, but perhaps the above arguments outweigh it? On a related note, there is not a single mention of the \Monte-Carlo" keyword in the paper, please do cater to a wider community and use such keywords to give a good context for the readers.

Indeed, we wanted to stress the analogy with the 2017-paper. But we agree with your perspective. We will switch to the terms "collisional growth" and "particle based" in the title.

AON can be interpreted as a Monte-Carlo method as we average over 20 independent simulation realisations. Once AON is employed in higher-dimensional models, it is not foreseen to run multiple realisations in each grid box. Then, averaging is supposed to occur across grid boxes. In this context I would not call it a Monte-Carlo method. Then probabilistic method is a more appropriate term.

The limiter

The ad-hoc definition of the \limiter" (p15/l6) calls at least for a reference to the min() in the SDM paper's ~ $\gamma\alpha$:= min($\gamma\alpha$; [$\xi j\alpha$; $\xi k\alpha$]) expression (Shima et al. 2009, step (5) in the left column), if not for reformulating the \limiter" in a more robust manner.

Rev# 3 (S. Shima) had a similar comment and proposed to try his limiter variant. We carried out thorough tests with different limiter implementations. It was interesting to see how a seemingly small detail of an algorithm can have a large impact on the performance. We go into more detail in the reply to Rev #3.

Integer vs. real-valued weighting factors

I do not find enough grounds in the text for the statements on the superiority of real-valued vs. integer-valued weighting factors. Besides the above commented issue of parallel random number generation/multiple collisions, the statements on page 11, lines 30-31 seem to overlook the concept of spectrum estimation, see e.g. the third paragraph in section 5.1.4 in (Shima et al., 2009) (also, worth mentioning when discussing eq. 14).

Dealing with integers and preserving integer values for the weights needs some additional steps in the algorithm formulation. The number of FLOPS for computing a random number is high relative to the amount of computations in the remaining parts of the AON algorithm. In my opinion, dealing with integers makes sense in small discrete examples (as in the cited reference Dziekan & Pawlowska, 2017). In a setting, where SIP weights exceed, say 1e6, it is more appropriate to use floats. For me, nu_i= 3523496 pretends exactness which is not given.

Independent of these considerations, the question remains how one wants to reconstruct or derive physical quantities from a discrete SIP ensemble. Shima et al propose a statistical method called spectrum estimation where a continuous DSD is constructed from a discrete SIP ensemble. But I do not see how this is related to the aspect of integer/float weights.

CFL condition for sedimentation

I would argue that we should assume the CFL condition for particle sedimentation as well -- while it does not cause the numerics to fail as in Eulerian component, it is intuitively not fulfilling the assumptions (as acknowledged on p4/l12). Relevant statements: p8/l11, p12/l26, p21/l15, p34/l10.

In our current LCM model system only sedimentation and collisional growth are considered and it is perfectly fine to choose time steps that are larger than CFL. But we agree that in higher-dimensional models that include diffusional growth choosing a CFL-limited time step seems more appropriate. This holds in particular for warm clouds. From my experience, time step choice in a typical cirrus simulation is not that crucial. This depends on the time scale of deposition and also on the smoothness of the background fields.

At least, it is good to see that in the present model system fairly large time steps produce reasonable results. So time step requirements of collisional growth alone do not seem to be a bottleneck in LCMs. Including diffusional growth and its interaction with collisional growth process may, however, demand collisional growth time steps as small as those for diffusional

growth.
A discussion on this is included in the revised version.

Courant number values in section 3.1

Upwind and MPDATA convergence is dependent on the Courant number -- please indicate which was used in section 3.1. Perhaps worth checking the behaviour for a set of Courant numbers.

As stated in section 2.2 the maximum CFL number is 0.5. This was also used in section 3.1 (it is now part of the Appendix). Each bin has its own "local" CFL number that depends on w_{sed}, Δz, Δt and r_{CFL}. The figure included in this reply shows the bin-dependent local CFL number (top) and the number of subcycles (bottom) to maintain CFL numbers below r_{CFL}. It becomes obvious that for most bins the local CFL number is not close to r_{CFL}. Hence prescribing a theoretically advantageous value of $r_{CFL} = 0.5$ has no real practical consequences.

The supplement now discusses a variation of r_{CFL} and Δt (both parameters take values as in the plot in this reply) for BIN solutions for HalfDomLinDec setup. We find that the BIN solutions do not depend on the tested parameters.

Correlations

Please be more specific as to the mathematical meaning of \correlations" mentioned 12 times in the context of collisions but never defined.
We use the term correlation always in the same context, so there is no ambiguity in this respect. At several occasions we refer to the relevant literature (papers by first authors Bayewitz, Gillespie, Alfonso and Wang for example). Readers not familiar with the master equation, statistical fluctuations and correlations in the context of collisional growth are strongly advised to read the aforementioned publications to gain a deeper understanding of the matter. We believe this cannot be achieved in the present paper.

Classical/regular nomenclature

References to \classical/regular" \implementations/approaches/cases/versions/AON" (p8/l15, p8/l16, p8/l22, p8/l24, p9/l4, p11/l12, p12/l8, p12/l19, p12/l29, p12/l31, p14/l7, p14/l8, p14/l30, p15/l4, p17/l2, p19/l1, p25/l5, p25/l21, p29/l1, p30/l2, p37/l12) are not understandable, especially given that the authors introduce their own nomenclature for numerous notions named differently in literature. I am aware that there are some definitions of \regular" in the text, but it is an over 40-page long paper. Please come up with more precise and less subjective statements.

A table listing all model versions is introduced in order to have a clear location where everything is defined. The terms "implementations/approaches/cases/versions/variants" were used more or less interchangeably but with slightly different flavours. Apparently this caused more confusion than it helped. The revised manuscript contains a cleaner terminology.

Anyhow, regular AON always referred to the AON version described in section 2.3.1. The title of the section is "Regular AON collection algorithm (WM3D)". So I do not see that this is subjective in any way.

Technical/editorial remarks

Figures

I urge the authors to replace raster images in figures 1 and 4-23 by its vector-format equivalents (i.e., plt.savefig(format='png', ...) *;* plt.savefig(format='pdf', ...)). I suggest using *cm*-3 as the unit for $\lambda 0$ on the plots.

We switch to pdf versions of the mentioned figures. I favour units m^{-3}.

Text

p1/l2 the \high number" is equally (or even more) applicable to bin models, please rephrase and indicate with respect to which benchmark the value is high.

Clarified.

p1/l4 is the word \explicit" needed (suggest avoiding if the opposite \implicit" is not clear)
Removed

p1/l8 ditto
Removed

p1/l12 \accuracy" *;* \resolution"
Changed it to resolution.

p2/l28 please underline that it is you who introduce the AON term
Done.

p2/l22 why not in chronological order? (see also background works listed in Shima et al. [3] and dating back to 2004)
No real reason, why it is not chronological. Corrected.
If you refer to Paoli et al, 2004, it is true that they used a particle-based approach for modelling contrails. I did not add the paper to the list, as their model does not include processes of natural cirrus formation and hence its applicability is limited to the one specific purpose of the paper.

p2/l26 \abbreviated as ... in the following" *;* \hereinafter abbreviated ..."?
Done.

p3/Table 1 please remove non-English caption, and consider removing the table { given the multitude of symbols used in the text, it seems anecdotal to list 8 abbreviations in a table (moreover, the following are not listed: DNC, MPDATA, CFL, WM2D, WM3D, MC, BIN, US1, noSedi, LCM0D, LCM1D, LS, ...)
Table 1 is updated and lists frequently used abbreviations. Abbreviations with a local scope are not added.

p3/l3 suggest removing/rephrasing \relatively young modelling approach" { particle-in-cell method is 50-year old; same for Monte-Carlo for collision
added "in cloud physics" to make the statement more precise.

p3/l4 \aws" *;* \was"
Done.

p3/l12 \coalescence, aggregation, or accretion" { mention \riming", \self-collection", \wash-out" keywords as well?
These terms cover the general interactions of liquid-liquid, ice-ice, and ice-liquid hydrometeors, which include the interactions listed by the reviewer. To be slightly more inclusive, we changed our text to: „We will use the term collision, including various processes such as coalescence, aggregation, or accretion, as we focus on […]"

p3/l13-14 actually, ice crystals are mentioned only one after this statement { suggest removing
The text makes now more references to ice aggregation.

p3/l22 \(sometimes pedantically)" sounds negative ... suggest not being pedantic (see below) and removing the statement
Done.

p4/l3 suggest using subscripts for *Lz* and *nz*
Done.

p4/l6 no need to make it a separate numbered equation?
The reason for prominent placement is that ΔA is important for WM2D and a change in Δz implicitly changes ΔA if ΔV is kept constant.

p4/l8 no need to define volume of the sphere - just mention in the text

That's why I have written pedantic in the beginning☺. Even though it seems clear, the point is that in ice microphysics, this expression is usually replaced by mass-size relationships of the type $m = a L^b$. So in follow-up papers considering more specifically aggregation, it helps to say that Eq. (3) of the original formulation is replaced.

p4/l12 *K*(*mi; mj*) and *K*(*ri; rj*) would likely be better named differently
True.

p4/l15 \radius-dependent" *;* \sie-dependent"
Done.

p4/l17 \latter" *;* \last" (there are three assumptions listed before)
Corrected.

p4/l18 there is a bogus character before 500 *μ*m - garbage displayed in the pdf viewer I'm using
I cannot reproduce your error. The symbol is "\gtrsim" (in latex slang)

p5/l1 \collection" *;* \collisional growth"?
Changed.

p5/l9 \latter" *;* \last" (there are three assumptions listed before)
Corrected

p5/l12 no need to define factorial
Okay.

p5/l13 skip reference to Berry 1967, surely \mass density function with respect to the logarithm of radius" is enough
Those who are not familiar with the definition will be happy about the reference as it is nicely explained in Berry, 1967.

p5/l22 first sentence is a repetition from the Introduction
From this sentence on, section 2.1 treats LCM-specific definitions and settings. So one sentence that introduces LCM (for those who are not familiar with particle-based approaches) should be okay.

p5/l24-25 suggest rephrasing around \terms low and high"
Hopefully clearer now.

p6/l14 random interval should be [...) and not [...] (as per numpy.random docs)
Changed it.

p6/l14 \some threshold" { please be specific (also, worth mentioning the alternative formulation with integers)
"singleSIP-init" in U2017 describes it in more detail and also specifies the threshold.

p7/l3 \around" { please be specific
I do not really see your point. Eq. 16 gives a good rule of thumb. By the way, panel c) of Fig.5 lists both N_SIP and kappa. You can convince yourself that the factor 5 is a good approximation. I do not think it helps to be more specific as this factor depends on DSD properties. Or should I list the precise scaling factor for each kappa-value? But please be aware, that the initial N_SIP

can change by 1 or 2 across the different realisations. The listed kappa-values in the figure are actually rounded.

p7/l6 random number interval: [...)
Changed it.

p7/l6-7 unneeded sentence (Furthermore...)?
Why not needed? It is never stated explicitly elsewhere.

p7/l15 rephrase \to solve the Smoluchowski."
Done.

p7/l18 use partial derivatives
Thanks. Corrected.

p7/l21 constant-in-altitude air density implied: please mention (same concerns the assumption that *w*sed is constant
The only place, where rho_{air} matters, is in the computation of the fall speed using Beard's formula. We now state that rho_air = 1.225 kg/m³ is used, consistent with Bott's and Wang's specification.

The column model computations, in particular solving the sedimentation/advection part, do not need the information on air density. In the current setup, the subtlety between advecting mixing ratios and concentrations is not relevant here for hydrometeors (unlike to gases, which we do not treat here). But we now state clearly in the text, that we assume constant-in-altitude air density.

p7/l24 the two Smolarkiewicz papers list several flavours of MPDATA, which is used?
We use the basic MPDATA. For the given advection problem (non-divergent, constant in time advection speed), no extensions like infinite-gauge, variable-sign, non-oscillatory options had to be used. We added this piece of information to the manuscript.

p7/l26 \some value" ; \the value"?
Done.

p7/l30 why 0.5?
MPDATA has optimal performance for CFL number of 0.5. However, from the plot included here it should become obvious that the practical consequences of choosing 0.5 as upper threshold r_{CFL} are not too large. Having in mind that the bin-dependent CFL numbers can be far from the prescribed rCFL-value, we refrain from stating in the manuscript that r_{CFL}=0.5 is the optimal choice. This would give a wrong impression.

Description of the Figure:

The upper panel shows the bin-dependent CFL number for six different simulations. The y-axis uses a mixed linear/log-scale. The solid/dotted lines show simulations with Δt = 2s and 10s, respectively. The three colours denote r_{CFL} (in the inserted legend the quantity is called CFLmax). In the left part of the bin grid the local CFL number are much smaller than

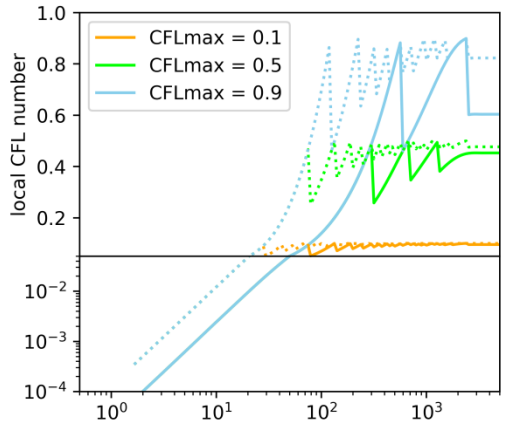

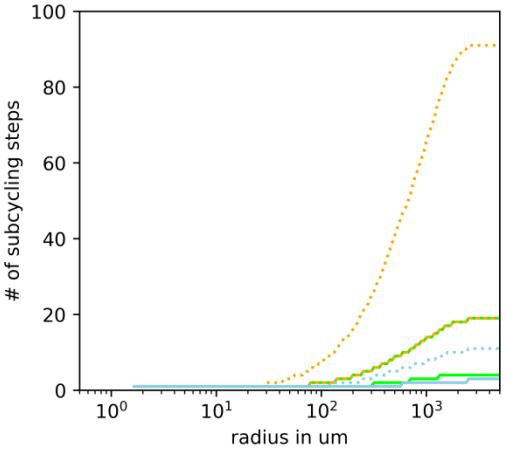

r_{CFL}. In the large-radius region the curves exhibit a saw-tooth pattern. Each time the number of subcycles is incremented (see bottom panel), the local CFL number drops.

SUPP now includes a sensitivity study where BIN simulations of the HalfDomLinDec setup were repeated with the Δt- and r_{CFL} -values used. It had no effect on the model outcome.

p8/l10 \Unlike to" ; \Unlike in"
Done.

p9/Fig 2 caption: \Wellmixed" ; \well-mixed" (twice)
Done.

p10/l4 is there any added-value in including the time loop in the pseudocode (same concerns listing on p13)
Is there any added value of removing it? I prefer to make clear that AON uses a prescribed time step. One cloudl also think of designing algorithm where the time advancement is computed based on the collision probability.

p10/l5 indicate that only for quadratic sampling
Nowhere is claimed that the presented pseudo-code treats the linear sampling version. So I do think adding 'quadratic sampling' confuses more than it helps.

p10/Alg. 1 caption random number interval: [...)
Done.

p11/l11 random number interval: [...)
Done.

p12/l29-31 use a proper big-oh (e.g., $O(n)$ with $\mathcal{O}(n)$)
Thanks.

p13/Alg. 2 caption random number interval: [...)
Done.

p14/l2 use a proper big-oh; nz inside the oh?
Done.

p14/l18-21 needed?
I prefer to keep it in order to see nicely the differences between both approaches.

p15/l19 comment that constant air density implied
See comment above (p7/l21)

p16/l12 remove \in the column model source code"
I wanted to make clear, that the new box model results (noSedi) also rely on the same source code.

p16/l16 omit \Validation exercises" from the section title (entirety of the paper is a validation exercise)
Done.

p17/Fig. 4 \at the indicated points in time" { cannot see any indicated points in time
I am confused. Figs. 4 & 5 both use a legend telling you which points in time are displayed.

p18/Fig. 5 ditto

I am confused. Figs. 4 & 5 both use a legend telling you which points in time are displayed.

p18/Fig. 5 \use different y-axis" { cannot see different y-axis
I am confused. The plots in Fig. 5 use different y-ranges!?

p18/l2 first mention of \lucky droplets" calls for a reference
Done.

p19/Fig 6 BoxModelEmul not mentioned before, used only in figure captions
Solved.

p19/l6 \surprisingly well" { please be more specific
Changed to "Hence, AON works well even for large time steps, […]"

p19/l7-8 \usually more easily reached" { please be more specific
Changes to "Generally, we find faster convergence for higher moments than for \lambda_0 (not shown)."

p19/9-10 \Even though..." { suggests this material can be skipped
Why? I think this is important for clarification.

p19/l12-14 sounds like a sentence for Introduction or Conclusions
Moved to the beginning of 3.1.

p19/Fig. 7 no units for dV (BTW, shouldn't it be ΔV ?)
Corrected. Yes ΔV.

p20/l3 \according" ; \relevant"?
I guess it is p21. Changed.

p20/l8 avoid \We believe"
Okay.

p16/l31 \agreement ... is good" { please be specific, provide quantitative measure
As mentioned in the reply to reviewer 1 introducing quantitative measures is difficult. And the interpretation based on a seemingly objective measure is again subjective.

p21/l24 \In a technical experiment" { suggest rephrasing
Changed.

p21/l30-32 \Nevertheless..." { suggest skipping the sentence
I do not see why this sentence should be removed.

p22/l24 first mention of Long kernel without reference or comment
We now mention the Long kernel in the beginning of section 3.1.

p22/l30 rephrase around \now f or"
Corrected.

p23/Fig. 8 no units for \dt" (BTW, shouldn't be Δt?)
It should be Δt. For consistency with other plots, units are added to the legend in Fig.4 (I believe you meant Fig.4, not Fig.8.).

p23/l3 \occur too often" - please be more specific
Rephrased paragraph.

p24/l3-4 \has to be solved" { subcycling seems to me as a preferable option than changing timestep of the whole simulation ... suggest skipping/rephrasing the sentence
Obsolete as paragraph has been removed.

p24/l4-5 please elaborate how/why inclusion of more SIP attributes would change the influence of LinSamp vs. QuadSamp choice?
Obsolete as paragraph has been removed.

p25/Fig. 10 add \, respectively" at the end of caption
Fig. 10 is not part of the manuscript any longer.

p25/l13 \Wang" ; \Wang et al."?
p25/l8 good place to mention performance trade-offs of the WM2D
Done here and also in section 2.3.1.

p25/l21 Bott/Bott's algorithm/model - please be consistent
Corrected.

p27/l5 \Bott's results are reliable" - rephrase
Changed to "While Bott yields stable results for $\Delta t \leq 100$ s, the results only converge for $\Delta t \leq 20$ s."

p28/l7&8 suggest renaming the section to \Algorithm profiling"
Changed. This sounds definitely better.

p29/Tab. 1 use the same exponential notation as elsewhere (i.e., $A \cdot 10^B$ instead of AeB)
The notation with "e" saves space. Otherwise the table width is too large.

p30/l6 \find their" { rephrase
Done.

p30/l23 \For small SIPs j" { what is a small SIP?
Small SIP is defined in section 2.1.

p31/l24 unit of \influx" should include 1/time
No value is given for the influx. So your comment is not applicable.

p32/Fig. 15 avoid using two acronyms for the same thing: LS, LinSamp
We reduced the occurrence of LS.

p33/Fig. 16 harmonise case for acronyms: Bin, BIN
Done.

p33/l2 \collector SIP" { please elaborate
Rephrased.

p34/l4 \sounds like a banal ..." sounds too colloquial
Rephrased.

p34/l14 what is the former effect?
Rephrased.

p35/l4 \superiority ... in BIN" - rephrase
The whole paragraph was re-written.

p35/l12 \improvement of this" -rephrase
Rephrased.

p37/l14 same remark regarding riming, etc as for p3/l12 p3/l12
Please check our previous comment on this aspect.

p37/l11-12 please clarify if this statement concerns just this section
Clarified.

p39/l11 \To bridge the gap" { puzzling, the gap was not mentioned earlier
Rephrased

References
Please harmonise the reference format:
I polished my paper reference database and all your suggested actions were implemented.

Enclosed software

I consider it awkward and confusing to use the GCC preprocessor with Python source code. Same concerns using csh and sed to generate preprocessor-directive-filled .py files with hardcoded system dependent paths. Altogether, the multi-platform and work-out-of-the-box advantages of Python were lost.

The new version v1.0 does not require sed and csh. However, gcc was not replaced as mentioned in the reply to Rev #1.

Note that in the CompSim.gcc.py file you are using two independent random-number-generation infrastructures available in Python, and I doubt setting the seed via random.seed() affects values returned via np.random.random(). Please avoid non-English comments in the code and marking changes with comments { it is the role of version control to track changes.

non-English comments were removed.

The seeding for np.random.random() was introduced.

Please indicate in the code availability section:

• the code availability (or lack thereof), version and license for \Bott" and \Wang" models

I obtained both BIN codes from the respective researchers. They are not published under a licence.

• the license the LCM1D is released on

Now included.

• the supported environments and dependencies of the implementation (python, numpy, gcc, csh, sed, ...)

The GitHub repository contains a document that lists the program/module versions with which I ran the simulations. The document has been updated as csh and sed are not mandatory any longer.

Thank you for a useful contribution to the field!

Hope the above comments help,

Sylwester

Many thanks for the thorough review, which triggered many improvements.

In this study, performance of several collection/aggregation algorithms for Lagrangian cloud models (LCMs) and bin models are compared in detail. The assessment was conducted in a one-dimensional columnar domain. Compared to their previous study in a single grid box, the tests are more relevant to three-dimensional cloud simulations, and hence the results are insightful. My major concern is the limiter introduced in p.15, l.5. I think this may considerably diminish the performance of WM3D LinSamp. Instead, I suggest that the authors consider splitting the SIP, as detailed below.

Major Comments

Now the limiter is implemented as follows: If $\nu_{coll} > \nu_j > \nu_i$,

$$\nu_i' = \nu_i, \quad \mu_i' = (\nu_i\mu_i + 0.99\nu_j\mu_j)/\nu_i,$$

$$\nu_j' = 0.01\nu_j, \quad \mu_j' = \mu_j.$$

I think this is not a good idea because this could oversample small droplets. Instead, I recommend you to split the SIP i as follows.

$$\nu_i' = \nu_j' = \nu_i/2, \quad \mu_i' = \mu_j' = (\nu_i\mu_i + \nu_j\mu_j)/\nu_i.$$

1) p.15, l.5, limiter

I think this is not a good idea because this could oversample small droplets. Instead, I recommend you to split the SIP as follows.

With this procedure, we can use more SIPs for large droplets. Then, we can expect that the number of limiter events decreases because tends to become smaller though the weighting factors of small SIPs ( ) are not changed. Note that similar procedure is already incorporated in Shima et al. (2009) (see (5b) on p.1313), but this is not the same because weighting factor (multiplicity) is considered as integer in Shima et al. (2009) and therefore (5b) rarely happens.

This rather small detail drastically improved the performance of the LinSamp version. So large parts of the sections concerned with LinSamp have been re-written.

Moreover, LinSamp simulations were added to many further test cases compared to the original script. A thorough discussion of the critical limiter choice is added to the Supplement. I am glad, that no results of the "flawed" LinSamp algorithm appear in the final paper. This avoids confusion in the community.

Minor Comments

2) p.4, l.17; p.26, Fig.12; collision efficiency

It is not clear which collision efficiency you are using for the default case.

Yes. We missed to write that the BoxModelEmul simulations used the Long kernel by default. This information is now included in the beginning of section 3.1.

3) p.14, ll.31-23

The feature that each SIP does not appear in two pairs enables parallel computation. Somewhere in the paper, this favorable property of WM3D LS should be mentioned.

Good point. It is mentioned now in section 2.3.3.

4) p.29, Table 2

From this result, I would conclude that WM3D LS is the most efficient.

Yes. Linear Sampling is the most efficient, but the table alone does not make a statement about effectiveness. Moreover, N_{comb} alone is not a perfect metric for computational cost, as in WM2D the cost per tested combination is smaller. In the revised version (with much better performance of LinSamp due to the modified limiter), it will be made clearer that LinSamp is the most efficient approach. See especially the new paragraph at the end of section 3.2.

5) p.31, Eq.(28c)

From this equation, we can derive the expected number of SIP pairs that actually collide:

$$N_{SIP}^{coll} = N_{combs}\overline{p_{crit}} \propto N_{SIP}^{\alpha+\beta-1}\delta t = N_{SIP}\delta t,$$

i.e., N_{SIP}^{coll} is proportional to N_{SIP}. This would imply that linear sampling is reasonable.

Many thanks for the derivation of the formula, but I doubt it is correct. Once $p_{crit} > 1$ occurs and multiple collections are implemented, the above formula is not valid as values $p_{crit} > 1$ should be rounded down to 1.

Imagine a hypothetical case with 200 combinations, where 100 combinations have $p_{crit} = 0.5$ and the other 100 combinations have $p_{crit} = 1.5$. Then your formula implies $N^{coll}_{SIP} = N_{comb}$. But the correct value is 100 * 0.5 + 100 * 1 = 150.

Kind regards,

Simon Unterstraßer, on behalf of all authors

~~Collection/Aggregation~~ Collisional growth in a ~~Lagrangian~~ particle-based cloud microphysical model: Insights from column model ~~applications~~ simulations using LCM1D (~~v0.9~~v1.0)

Simon Unterstrasser[1], Fabian Hoffmann[2,3], and Marion Lerch[1]

[1]Deutsches Zentrum für Luft- und Raumfahrt (DLR) – Institut für Physik der Atmosphäre, Oberpfaffenhofen, 82234 Wessling, Germany.
[2]Cooperative Institute for Research in Environmental Sciences (CIRES), University of Colorado Boulder, Boulder, Colorado, USA
[3]NOAA Earth System Research Laboratory (ESRL), Chemical Sciences Division, Boulder, Colorado, USA

Correspondence: Simon Unterstrasser: simon.unterstrasser@dlr.de

Abstract. Lagrangian cloud models (LCMs) are considered the future of cloud microphysical modeling. ~~However,~~ Compared to bulk models, however, LCMs are computationally expensive due to the typically high number of simulation particles (SIPs) necessary to represent microphysical processes such as ~~collection/aggregation~~ collisional growth of hydrometeors successfully. In this study, the representation of ~~collection/aggregation~~ collisional growth is explored in one-dimensional column simulations, allowing for the explicit consideration of sedimentation, complementing the authors' previous study on zero-dimensional collection in a single grid box. Two variants of the Lagrangian probabilistic all-or-nothing (AON) collection algorithm are tested that mainly differ in the assumed ~~spaatial~~ spatial distribution of the droplet ensemble: The first variant assumes the droplet ensemble to be well-mixed in a predefined three-dimensional grid box (WM3D), while the second variant considers ~~explicitly the vertical coordinate~~ the (sub-grid) vertical position of the SIPs, reducing the well-mixed assumption to a two-dimensional, horizontal plane (WM2D). Since the number of calculations in AON depends quadratically on the number of SIPs, an approach is tested that reduces the number of calculations to a linear dependence (so-called linear sampling). All variants are compared to established Eulerian bin model solutions. Generally, all methods approach the same solutions, and agree well if the methods are applied with sufficiently high ~~accuracy~~ resolution (foremost the number of SIPs, ~~timestep,~~ and to a lesser extent time step and vertical grid spacing). ~~However, it is found that the rate of convergence depends on the applied model variant~~Converging results were found for fairly large time steps, larger than those typically used in the numerical solution of diffusional growth. The dependence on the vertical grid spacing can be reduced if ~~AON WM2D~~ AON-WM2D is applied. The study also shows that ~~the AON~~ AON-WM3D simulations with linear sampling, a common speed-up measure, ~~converges slower , as smaller timesteps are required to reach convergence~~ converge only slightly slower compared to simulations with a quadratic ~~dependence on the number of SIPs.~~ SIP sampling. Hence, AON with linear sampling is the preferred choice when computation time is a limiting factor.

Most importantly, the study highlights that results generally require a smaller number of SIPs per grid box for convergence than previous one-dimensional box simulations indicated. The reason is the ability of sedimenting SIPs to interact with ~~an effectively~~ a larger ensemble of particles when they are not restricted to a single grid box. Since sedimentation is considered

in most commonly applied three-dimensional models, the results indicate smaller computational requirements for successful simulations~~than previously assumed~~, encouraging a wider use of LCMs in the future.

1 Introduction

Clouds are a fundamental part of the global hydrological cycle, responsible for the transport and formation of precipitation. While we expect a global increase in precipitation due to climate change, our knowledge on its spatial ~~redistribution, including~~ distribution, including even decreasing rainfall in some regions of the globe, is still uncertain (Boucher et al., 2013). The formation processes of precipitation are, however, reasonably understood and contain mechanisms that increase the size of hydrometeors. For liquid clouds, the coalescence of smaller cloud droplets is essential to form precipitating raindrops. In ice clouds, diffusional growth can produce precipitation-sized particles. The aggregation of ice crystals into larger clusters, snowflakes, also occurs frequently. And in mixed-phase clouds, ice crystals accrete supercooled liquid droplets forming graupel or hailstones.

The representation of these microphysical processes in climate models is impelled by the available computational resources, requiring necessary ~~idealizations~~idealisations. Primarily, this is the case for computationally efficient Eulerian bulk models that predict only a small number of statistical moments for each hydrometeor class (e.g., Kessler, 1969; Khairoutdinov and Kogan, 2000; Seifert and Beheng, 2001), with commensurate ~~effects on~~ limitations for the representation of clouds and precipitation. Of course, more detailed cloud microphysics models have ~~been also~~ also been developed: Eulerian bin models represent cloud droplets on a mass grid that consists of hundreds of bins sampling the droplet size distribution (DSD) (e.g., Berry and Reinhardt, 1974; Tzivion et al., 1987; Bott, 1998; Simmel et al., 2002; Wang et al., 2007). But even these models exhibit limitations and ~~idealizations~~idealisations. For instance, the coalescence of droplets is ~~modeled~~ modelled as a Smoluchowski (1916) process, describing the mean evolution of an infinitely large, well-mixed droplet ensemble. ~~The~~ But the underlying Smoluchowski equation (also called the kinetic collection equation or even the stochastic collection equation, although the equation is deterministic) ~~, however,~~ inherently neglects correlations and stochastic fluctuations known to be an integral part of the process chain that leads to precipitation (Gillespie, 1972; Bayewitz et al., 1974; Kostinski and Shaw, 2005; Wang et al., 2006; Alfonso et al., 2008).

In the last decade, Lagrangian cloud models (LCMs) emerged as a ~~valued~~ valid alternative to bin models ~~for the detailed modeling of clouds (e.g., Andrejczuk et al., 2008; Sölch and Kärcher, 2010; Shima et al., 2009; Riechelmann et al., 2012; Arabas et al., 20~~ These models use Lagrangian particles, so-called simulation particles (SIPs) (Sölch and Kärcher, 2010) or superdroplets (Shima et al., 2009), each representing an ensemble of identical real droplets. ~~Collection and aggregation~~ Collisional growth in LCMs has recently been rigorously evaluated in box model simulations by Unterstrasser et al. (2017) (hereinafter abbreviated as U2017~~in the following~~), who compared three ~~approaches~~ algorithms documented in the literature: the remapping algorithm (RMA) by Andrejczuk et al. (2010), the average-impact algorithm (AIM) by Riechelmann et al. (2012), and the all-or-nothing algorithm (AON) concurrently developed by Shima et al. (2009) and Sölch and Kärcher (2010). RMA and AIM are deterministic algorithms and, in theory, approach the Smoluchowski solution of a reference bin model. The actual convergence

of the ~~algorithm~~algorithms, however, was found to depend significantly on properties of the SIP ensemble and the chosen kernel. The probabilistic AON indicated much better convergence properties ~~, when it was~~ given the simulation outcome is averaged over sufficiently many instances. Furthermore, Dziekan and Pawlowska (2017) showed that AON approximates the stochastically complete Master equation including aforementioned correlations and stochastic fluctuations (Gillespie, 1972; Bayewitz et al., 1974). In fact, AON solutions are identical to the Master equation solutions (Alfonso and Raga, 2017) when the weighting factors (the number of real droplets represented by a SIP) ~~are set to unity.~~ approach unity. The name AON was introduced in U2017. Note that in the literature, the term super-droplet method (SDM) is not used such that it refers to the class of particle-based microphysics models in general, but to the particular model introduced in Shima et al. (2009) . Hence, AON with linear sampling (this will be explained later) is typically referred to as SDM method (Shima et al., 2019) .

However, many aspects of this relatively young ~~modeling approach~~ modelling approach in cloud physics have not been tested thoroughly. One important message of our previous box simulations in U2017 ~~aws~~ was that the representation of ~~collection~~ collisional growth exhibits considerably more freedom in setting up a simulation than in bin models. Accordingly, in this study, we are going to extend the box simulations of U2017 by ~~analyzing collection~~ analysing collisional growth in a vertical column, including sedimentation, as it has been done in previous studies for Eulerian bulk and bin models (e.g., List et al., 1987; Tzivion (Tzitzvashvili) et al., 1989; Hu and Srivastava, 1995; Prat and Barros, 2007; Stevens and Seifert, 2008; Seifert, 2008). All simulations will use the AON ~~collection~~ algorithm since it outperformed RMA and AIM in the box simulations, and we do not expect that this general ~~behavior~~ behaviour is reversed here. The simulations will be compared to established Eulerian bin references. ~~Note that although the following analysis~~ U2017 demonstrated that numerical convergence is harder to achieve for typical liquid cloud kernels (Long, 1974; Hall, 1980) than for a typical aggregation kernel with constant aggregation efficiency. Hence, the present study focuses on cloud ~~droplets,~~ droplet coalescence as benchmarking exercise. But we expect that the results can be ~~generalized~~ generalised for the LCM representation of ice crystal aggregation and the accretion of supercooled droplets. ~~Therefore, we~~ We will use the term collection~~to address~~ , comprising coalescence, aggregation, ~~or accretionas we will~~ and accretion, as we focus on the numerical treatment, which is similar for all ~~three~~ these process, and not on ~~the physics. Moreover, we will use the term cloud droplets interchangeably with ice crystals to increase clarity in writing.~~ their particular physics.

The paper is structured as follows. First, Sec. 2 will give an overview on the applied models, their foundations, and basic setup. The results are presented in Sec. 3, divided into ~~validation studies (Sec.A), highly idealized~~ highly idealised applications in which the column model emulates a box model (Sec. 3.1), process-level analysis of the applied algorithms (Sec. ~~??~~3.2), and finally realistic applications (Sec. 3.3). The paper is concluded in Sec. 4. The Appendix presents pure-sedimentation test cases. The supplement (SUPP from now on) contains additional material and figures (enumerated as S1, S2, and so on)

2 Numerical model and setup

Two column models, which consider collection and sedimentation, have been implemented, the first one represents a traditional Eulerian bin scheme and the second model uses a particle-based approach. Before we describe both models in some detail,

Table 1. List of frequently used abbreviations. ~~(Am Ende Text nochmal durchgehen um auch durchgehend die Abkuerzungen zu benutzen)~~

AON	~~All-or-nothing~~ All-Or-Nothing algorithm
BC	boundary condition
DNC	droplet number concentration
DSD	~~Droplet~~ droplet size distribution
GB	~~Grid~~ grid box
LCM	Lagrangian cloud model
LWC	~~Liquid wter~~ liquid water content
MC	multiple collection
SIP	Simulation particle
SUPP	supplement
U2017	Unterstrasser et al. (2017)

we will ~~(sometimes pedantically) write out~~ write down basic relations, which will help disentangling the effects of particular parameter variations later.

2.1 Basic relations and definitions

We use a column with ~~nz~~ n_z grid boxes (GBs). Each GB has the volume ΔV and a height of Δz. The total column height is thus

$$Lz L_z = nz n_z \times \Delta z. \tag{1}$$

We define that the GB k with ~~$1 \leq k \leq nz$~~ $1 \leq k \leq n_z$ extends from z_{k-1} to $z_k := k \times \Delta z$, hence the GB with $k = 1$ is the lowest GB.

The horizontal area of the column is given by

$$\Delta A = \Delta V / \Delta z. \tag{2}$$

Throughout this study, we implicitly assume that air density ρ_{air} is constant in time and space.

The droplets are assumed to be spherical with a density of ~~$\rho_w = 1000\,\mathrm{kg/m^3}$~~ $\rho_{\mathrm{w}} = 1000\,\mathrm{kg/m^3}$ and the mass-size relation is simply given by

$$m = \frac{4}{3}\pi r^3 \rho_{w\mathrm{w}}. \tag{3}$$

Following Gillespie (1972) and Shima et al. (2009), the probability ~~P_{ij}^{WM3D}~~ P_{ij}^{WM3D} that one droplet with mass m_i coalesces with one droplet with mass m_j inside a small volume δV within a short time interval δt is given by

$$p^{WM3D\mathrm{WM3D}}_{ij} = K_{ij}\,\delta t\,\delta V^{-1}, \tag{4}$$

where ~~$K_{ij} = K(m_i, m_j)$ or equivalently~~ the collection kernel K_{ij} can be expressed as a function of droplet radii, $K(r_i, r_j)$, or equivalently droplet masses, $\tilde{K}(m_i, m_j)$. We suppose that δt is sufficiently small in order to assure ~~$p_{ij}^{WM3D} \leq 1$~~ $p_{ij}^{\mathrm{WM3D}} \leq 1$.

The hydrodynamic collection kernel, driven by differences in the droplet vertical velocity, is given by

$$K^{WM3D\,\mathrm{WM3D}}(r_i, r_j) = E_{\mathrm{cc}}(r_i, r_j)\,\pi (r_i + r_j)^2\,|w_{sed\,\mathrm{sed},i} - w_{sed\,\mathrm{sed},j}|, \tag{5}$$

where ~~w_{sed} is the radius-dependent~~ w_{sed} is the size-dependent droplet fall speed and ~~$E_c = E \times E_{\mathrm{coal}}$~~ $E_{\mathrm{c}} = E \times E_{\mathrm{coal}}$ is the collection efficiency, which is the product of the collision efficiency E and the coalescence efficiency E_{coal}. In this study, we use the ~~w_{sed}~~ w_{sed}-parametrisation of Beard (1976), the tabulated E-values of Hall (1980), and the coalescence efficiency E_{coal} is assumed to be 1. The ~~latter~~ last assumption is an oversimplification for large droplets with radii $\gtrsim 500\,\mu\mathrm{m}$ for which E_{coal} is significantly smaller than 1 (Beard and Ochs III, 1984; Ochs III and Beard, 1984), but does not limit the generality of our findings. For the computation of w_{sed}, $\rho_{\mathrm{air}} = 1.225\mathrm{kg/m^3}$ is assumed analogously to Bott (1998) as this enables conclusive comparisons with bin and box model results.

The average number of collisions from ν_i droplets of mass m_i and ν_j droplets of mass m_j (which are assumed to be well-mixed in the volume δV) within time δt is

$$\nu_{coll\,\mathrm{coll}} = K^{WM3D\,\mathrm{WM3D}}{}_{ij}\,\nu_i\,\nu_j\,\delta t\,\delta V^{-1}, \tag{6}$$

or equivalently

$$\nu_{coll\,\mathrm{coll}} = E_{\mathrm{cc}}(r_i, r_j)\pi (r_i + r_j)^2\,|w_{sed\,\mathrm{sed},i} - w_{sed\,\mathrm{sed},j}|\nu_i\,\nu_j\,\delta V^{-1}\delta t. \tag{7}$$

By dividing the above equation by δV, we obtain the common relationship in terms of concentrations, given by $n = \nu/\delta V$,

$$n_{coll\,\mathrm{coll}} = E_{\mathrm{cc}}(r_i, r_j)\pi (r_i + r_j)^2\,|w_{sed\,\mathrm{sed},i} - w_{sed\,\mathrm{sed},j}|n_i\,n_j\,\delta t. \tag{8}$$

Sedimentation and ~~collection~~ collisional growth are the only processes considered in this study, and any effects of diffusional growth are neglected.

An exponential DSD is used to prescribe the cloud droplets in the beginning

$$f_{\mathrm{m}}(m) = \frac{DNC}{\bar{m}} \exp\left(-\frac{m}{\bar{m}}\right). \tag{9}$$

As in U2017, Berry (1967), or Wang et al. (2007), we choose by default a mean mass $\bar{m} = LWC/DNC$ that corresponds to a mean droplet radius of ~~$r_0 = 9.3\,\mu\mathrm{m}$~~ $r_{\mathrm{init}} = 9.3\,\mu\mathrm{m}$ and a droplet number concentration ~~$DNC = 2.97 \times 10^8$~~ $DNC_{\mathrm{init}} = 2.97 \times 10^8\,\mathrm{m^{-3}}$ (resulting in a droplet mass concentration of ~~$LWC = 10^{-3}$~~ $LWC_{\mathrm{init}} = 10^{-3}\,\mathrm{kg\,m^{-3}}$). The function $f_{\mathrm{m}}(m)$ is the number density function with respect to mass. The moments are defined as

$$\lambda_l(t) = \int m^l f_{\mathrm{m}}(m,t)\mathrm{d}m, \tag{10}$$

with order l, which gives $DNC = \lambda_0, LWC = \lambda_1$ and $Z = \lambda_2$. We will refer to ~~the latter quantity~~ Z as radar reflectivity since the radar reflectivity is proportional to λ_2.

For an exponential DSD, the moments can be expressed analytically as

$$\lambda_{l,\mathrm{anal}} = (l-1)!\; DNC\; \bar{m}^l, \tag{11}$$

~~where $l!$ is the factorial of l.~~

Using the terminology of Berry (1967), we introduce the mass density function with respect to the logarithm of droplet radius $\ln r$

$$g_{\ln \mathrm{r}}(r) = 3m^2 f_{\mathrm{m}}(m), \tag{12}$$

taking into account the transformation property of distributions ($f_{\mathrm{y}}(y)\mathrm{d}y = f_{\mathrm{x}}(x(y))\mathrm{d}x$).

The DSD is usually discretised using exponentially increasing bin sizes. In analogy to U2017, the bin boundaries are defined by the masses

$$m_{bbbb,p+1} = m_{bbbb,p}\; 10^{1/\kappa}. \tag{13}$$

Note that many other studies use a factor of $2^{1/s}$ for discretisation. The parameters s and κ are related via $s = \kappa\, \log_{10}(2) \approx 0.3\,\kappa$.

In an LCM, real droplets are represented by simulation particles (SIPs, also called super droplets). Each SIP has a discrete position (vertical coordinate z_p in our column model applications) and represents ν_p identical real droplets with an individual droplet mass μ_p. The total droplet mass in a SIP is then $\nu_p \mu_p$. In conjunction with SIPs, we define that the terms ~~low and high~~ "low" and "high" relate to the SIP vertical position~~and the terms small and large~~, whereas "small" and "large" relate to the droplet mass μ_p. The number of SIPs in a GB is defined as ~~$N_{SIP,GB}$~~ $N_{\mathrm{SIP,GB}}$ and the total SIP number is given by ~~$N_{SIP,tot} = \sum_{k=1}^{nz} N_{SIP,GB}(k)$~~ $N_{\mathrm{SIP,tot}} = \sum_{k=1}^{nz} N_{\mathrm{SIP,GB}}(k)$.

The moments λ_l of order l in a GB are computed via a simple summation

$$\lambda_{l,\mathrm{SIP}} = \left(\sum_{p=1}^{N_{\mathrm{SIP,GB}}} \nu_p\, \mu_p^l \right) \Big/ \Delta V\,, \tag{14}$$

Here and in the following, index p refers to any single bin or SIP. If we want to stress that the combination of two SIPs or bins matters, we use indices i and j. Index k is used for altitude and l for the order of the moments by convention.

How to represent an ensemble of droplets in an Eulerian or Lagrangian cloud model? Their size distribution can be uniquely described in a bin model by simply accounting for each real droplet in its respective bin, where its boundaries are given by the bin model (see illustration in Fig. 1 top). In the Lagrangian approach, however, the weighting factor ν_i and the droplet mass μ_i can be chosen independently. Accordingly, there is no unique SIP representation of an ensemble of real droplets; two possible SIP ensemble realisations are illustrated in Fig. 1 bottom.

Various techniques to generate a SIP ensemble in an LCM for a given (analytically prescribed) DSD exist (see section 2.1 in U2017). In this study, we use a SIP initialisation technique (termed "singleSIP-init" in U2017), for which Lagrangian collection algorithms, and in particular AON, achieved the best results in box model tests. In the singleSIP-init, the DSD, more

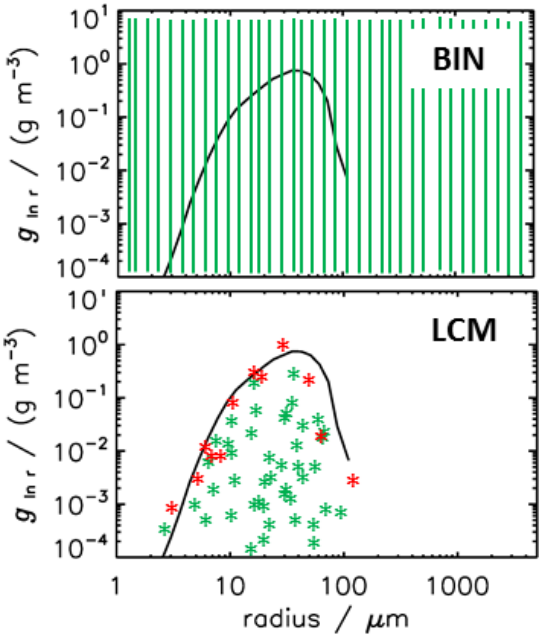

Figure 1. ~~schematic~~ Schematic plot of how a droplet ~~dize~~ size distribution is ~~discretized~~ discretised in a bin model and represented by a SIP (SImulation ~~particle~~Particle) ensemble in a Lagrangian cloud model (LCM). The red and green stars shows two different realisations of a SIP ensemble.

specifically f_m, is ~~discretized~~ discretised in exponentially increasing mass intervals and a single SIP is generated for each bin (see section 2.1.1 in U2017 for details). The SIP weight is given by

$$\nu_{\mathrm{p}p} = f_{\mathrm{m}}(\mu_{\mathrm{p}p})\,\Delta m_{\mathrm{bb},p}\Delta V, \tag{15}$$

where ~~μ_{p}~~ μ_p is chosen randomly from the interval ~~$[m_{\mathrm{bb},p}, m_{\mathrm{bb},p+1}]$~~$[m_{\mathrm{bb},p}, m_{\mathrm{bb},p+1})$. The generation of SIPs with ~~ν_{p}~~ ν_p below some threshold is discarded. Due to the probabilistic component, different realisations of SIP ensembles can be created for the same prescribed DSD, yet the ~~init~~ initialisation technique guarantees that the moments $\lambda_{l,\mathrm{SIP}}$ are close to $\lambda_{l,\mathrm{anal}}$. The number of generated SIPs depends on the width of the mass bins and hence on κ, as well as the other parameters of the prescribed DSD. A change of the "system size" ΔV does not change the number of SIPs, but simply leads to a rescaling of the SIP weights ν_i. For the exponential DSD given above, around

$$N_{SIP,GB\,\mathrm{SIP,GB}} = 5 \times \kappa \tag{16}$$

SIPs are initialised (the scaling factor depends on the width of DSD and the choice of the lower cut-off threshold). Finally note that if the DSD is prescribed in a specific GB, the position z_p of each SIP in this GB is randomly chosen from ~~$[z_k, z_{k+1}]$~~$[z_k, z_{k+1})$. Furthermore, δt and δV of the conceptual model take the values Δt and ΔV in the numerical models.

2.2 Eulerian column model

Eulerian column models have been widely employed in cloud physics and the present bin implementation is conceptually similar to previous ones (e.g. Prat and Barros, 2007; Stevens and Seifert, 2008; Hu and Srivastava, 1995). We use exponentially increasing bin sizes as defined in Eq. 13. The smallest mass ~~$m_{bb,0}$~~ $m_{\mathrm{bb},0}$ is chosen suitably small (corresponding roughly to a droplet radius of $1\,\mu\mathrm{m}$), and the grid resolution parameter s sufficiently large (4 by default), i.e. the mass doubles every four bins.

The variable $g_{\ln \mathrm{m}} = \frac{1}{3} g_{\ln \mathrm{r}}$ will be ~~discretized~~ discretised in mass space and used as a prognostic variable. The droplet mass concentration in each bin p and height k is given by $g_{p,k} \times \mathrm{d} \ln m$ and approximates $\int_{m_{\mathrm{bb},p}}^{m_{\mathrm{bb},p+1}} g_{\ln \mathrm{m}}(m, z_k) \mathrm{d} \ln m$. For each GB k, Bott's exponential flux method (Bott, 1998, 2000) is used to solve the Smoluchowski equation. Bott's method is a one-moment scheme and $g_{\ln \mathrm{m}}$ is the only prognostic variable. Alternatively, the collection algorithm by Wang et al. (2007) is employed, which additionally employs a prognostic equation for the droplet number concentrations in each bin.

In a second step, the mass concentrations are advected vertically according to the classical advection equation

$$\frac{d\, g_{\ln \mathrm{m}}}{dt} \frac{\partial\, g_{\ln \mathrm{m}}}{\partial t} = w_{sed\mathrm{sed}} \frac{d\, g_{\ln \mathrm{m}}}{dz} \frac{\partial\, g_{\ln \mathrm{m}}}{\partial z}. \tag{17}$$

For its numerical solution, two different positive definite advection algorithms have been used. The first option is the classical first-order upwind scheme (known for its inherent numerical diffusivity). For ~~$w_{sed} \geq 0$~~ $w_{\mathrm{sed}} \geq 0$, it is simply given by

$$g_{p,k}(t + \Delta t) = g_{p,k}(t) + \frac{\Delta t}{\Delta z} w_{sed\mathrm{sed}}(\bar{m}_{\mathrm{bb},p})(g_{p,k+1}(t) - g_{p,k}(t)). \tag{18}$$

The above equation is solved independently for each bin p, where ~~w_{sed}~~ w_{sed} is evaluated at the arithmetic bin ~~center~~ centre $\bar{m}_{\mathrm{bb},p} = 0.5(m_{\mathrm{bb},p+1} + m_{\mathrm{bb},p})$[1] ~~. A second (better)~~ . [1] A second option is the popular MPDATA algorithm, which is an iterative solver based on the upwind scheme, yet drastically reduces its diffusivity (Smolarkiewicz, 1984, 2006). By default, ~~MPDATA is employed~~the basic MPDATA with two passes is employed as described in section of 2.1 of Smolarkiewicz and Margolin (1998) .

Irrespective of the chosen advection solver, the prediction of the "new" $g_{p,k}$ depends on $g_{p,k}$ and $g_{p,k+1}$ (i.e. the GB above the one of interest). For the prediction of ~~$g_{p,nz}$~~ $g_{p,nz}$ at the model top, it is necessary to prescribe ~~some value $g_{p,nz+1}$~~ the value $g_{p,nz+1}$, which defines the upper boundary condition (this is detailed in section 2.4).

If the prescribed Δt is too large and the Courant-Friedrichs-Levy (CFL) criterion ~~$\frac{\Delta t}{\Delta z} w_{sed}(\bar{m}_{\mathrm{bb},p}) \leq r_{CFL} < 1$~~ $\frac{\Delta t}{\Delta z} w_{\mathrm{sed}}(\bar{m}_{\mathrm{bb},p}) \leq r_{\mathrm{CFL}} <$ is violated, subcyling is introduced. As ~~$w_{sed}(\bar{m}_{\mathrm{bb},p})$~~ $w_{\mathrm{sed}}(\bar{m}_{\mathrm{bb},p})$ does not change over the course of a simulation, the (bin-dependent) number of subcycles ~~$n_{subc,p}$~~ $n_{\mathrm{subc},p}$ is determined in the beginning, such that ~~$r_{CFL} = 0.5$~~ $r_{\mathrm{CFL}} = 0.5$ holds for the reduced ~~timestep~~ ~~$\frac{\Delta t}{n_{subc,p}}$~~ time step $\frac{\Delta t}{n_{\mathrm{subc},p}}$.

After one call of ~~the Bottalgorithm, $n_{subc,p}$~~ Bott's algorithm, $n_{\mathrm{subc},p}$ calls of the selected advection algorithm with reduced time step ~~$\frac{\Delta t}{n_{subc,p}}$~~ $\frac{\Delta t}{n_{\mathrm{subc},p}}$ follow for each bin p.

[1] ~~Evaluating w_{sed} at the geometric bin centers did not change the results.~~

[1] Evaluating w_{sed} at the geometric bin centres did not change the results.

The moments are computed by

$$\lambda_{l,\mathrm{BIN}} = \sum_{p=1}^{N_{\mathrm{BIN}}} g_{p,k}\ (\tilde{m}_{\mathrm{bb},p})^{l-1} \frac{\ln 2}{3\,s} \tag{19}$$

as given in Eq. 48 of Wang et al. (2007), where $\tilde{m}_{\mathrm{bb},p} = m_{\mathrm{bb},p} \times 2^{1/(2\,s)}$ is the geometric bin ~~center~~centre.

2.3 Lagrangian column model

In a Lagrangian model, the inclusion of sedimentation (obeying the transport equation ~~$dz/dt = -w_{sed}$~~$dz/dt = -w_{\mathrm{sed}}$) is straightforward. For each SIP the particle position is updated via

$$z_p(t + \Delta t) = z_p(t) - w_{\mathrm{~~sed~~sed}}(\mu_p(t))\ \Delta t. \tag{20}$$

Unlike ~~to~~ in Eulerian methods, sedimentation in a Lagrangian approach is independent of the chosen mesh and the time step is not restricted by numerical reasons. If z_p becomes negative at some point in time, the SIP crossed the lower boundary and is removed.

For the collection process, it assumed that each SIP belongs to a certain GB k obeying $z_{k-1} \leq z_p < z_k$ and that the real droplets of each SIP are well-mixed in the GB volume (WM3D). The collection process is treated with the probabilistic AON algorithm. In the regular version (see section 2.3.1), AON is called for each GB and accounts for all possible collisions among any two SIPs of the same GB. By construction, the information on the vertical position is irrelevant inside the regular AON, and is only used in the SIP-to-GB assignment.

In the version with explicit overtakes (WM2D, see section 2.3.2), for any two SIPs (of the whole column) it is checked if the higher SIP (i.e. with larger z_p) overtakes the lower SIP within the current time step. This may have several advantages: First, only 2D well-mixedness in a horizontal plane is assumed and possible size sorting effects within a GB are accounted for. Moreover, in Lagrangian methods the time step is not restricted by the CFL criterion and the largest SIPs may travel through more than one GB. In the classical approach, such a SIP can only collect SIPs from the GB where it was present in the beginning of the time step. In the second approach, collections can also occur across GB boundaries (see section 2.3.2).

In the remainder of this paper, the classical approach is referred to as ~~"3D Well-Mixed" (WM3D) AON~~ AON-regular and the new approach as AON-WM2D. Figure 2 sketches how the SIP properties (location, weighting factor, sedimentation speed) are interpreted in either approach. For simplicity, a single GB with one SIP pair is displayed.

AON is probabilistic and an individual realisation does usually not reproduce the mean state as predicted by deterministic methods like Eulerian approaches. The extent of deviations from the mean state is exemplified in Fig. 15 of U2017 for a box model application of AON. Hence, the discussed AON results in the present study are usually ensemble averages over ~~$nr_{inst} = 20$~~ $nr_{\mathrm{inst}} = 20$ realisations.

Pseudo-code of both algorithm implementations is given. For the sake of readability, the pseudo-code examples show easy-to-understand implementations. The actual codes of the algorithms are, however, optimised in terms of computational efficiency. The style conventions for the pseudo-code examples are as follows: commands of the algorithms are written in upright

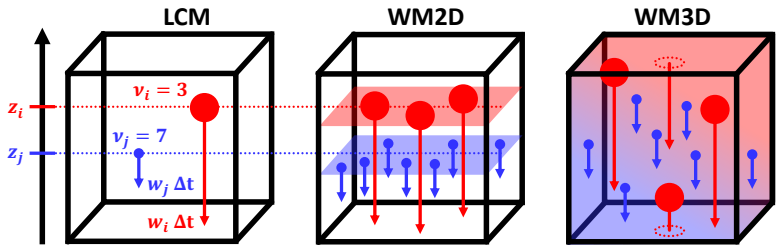

Figure 2. Grid box with a SIP pair in the LCM world (left) and its respective interpretation in the 2D ~~Wellmixed~~ well-mixed (WM2D, ~~center~~centre) and 3D ~~Wellmixed~~ well-mixed (WM3D, right) approach of the AON ~~collection~~ collisional growth algorithm.

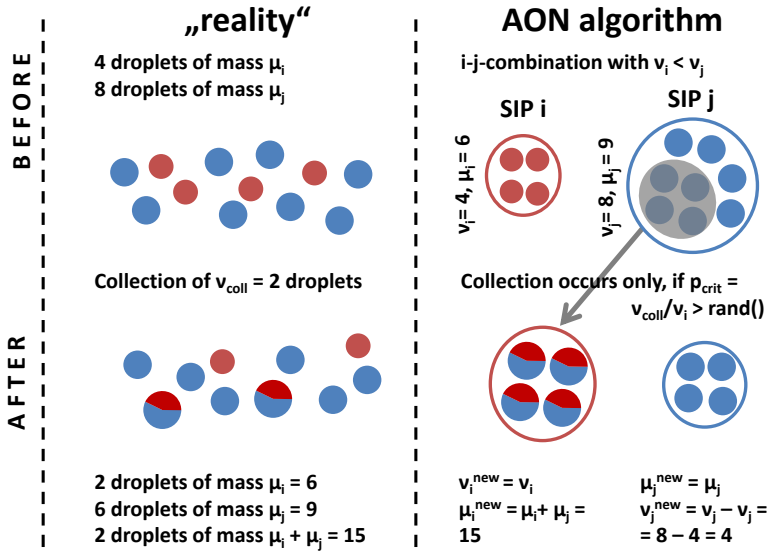

Figure 3. Treatment of a collection between two SIPs in the All-Or-Nothing Algorithm (AON) algorithm, partially adopted from Fig. 2 of Unterstrasser et al. (2017).

font with keywords in boldface. Comments appear in italic font (explanations are enclosed by {} and headings of code blocks are in boldface).

2.3.1 Regular AON ~~collection~~ algorithm (~~WM3D~~AON-regular)

Here we basically repeat the AON description of U2017 (their section 2.5).

"Figure 3 illustrates how a collection between two SIPs is treated. SIP i is assumed to represent fewer droplets than SIP j, i.e. $\nu_i < \nu_j$. Each real droplet in SIP i collects one real droplet from SIP j . Hence, SIP i contains $\nu_i = 4$ droplets, now with

Algorithm 1 Pseudo-code of the ~~WM3D~~ regular all-or-nothing ~~algorithm~~ (AON) algorithm; style conventions are explained right before Section 2.3.1 starts; rand() generates uniformly distributed random numbers ~~$\in [0,1]$~~ $\in [0,1)$. This AON version is called independently for each grid box.

INIT BLOCK
Given: Ensemble of SIPs of a specific grid box; Specify: Δt
TIME ITERATION
while t<Tsim **do**
  {Check each $i-j$-combination for a possible collection event}
  for all $i < j \leq N_{\mathrm{SIP}}$ **do**
    Compute ~~ν_{coll}~~ ν_{coll} according to Eq. 7
    ~~$\nu_{\mathrm{new}} = \min(\nu_i, \nu_j)$~~ $\nu_{\mathrm{new}} := \min(\nu_i, \nu_j)$
    ~~$p_{\mathrm{crit}} = \nu_{coll} / \nu_{\mathrm{new}}$~~ $p_{\mathrm{crit}} := \nu_{\mathrm{coll}} / \nu_{\mathrm{new}}$
    {Update SIP properties on the fly}
    ~~***MULTIPLE COLLECTION*** *{can occur when ν_i and ν_j differ strongly and be regarded as special case; see text for further explanation}*~~ assume $\nu_i < \nu_j$, otherwise swap i and j in ~~the following lines~~ all following lines
    if $p_{\mathrm{crit}} > 1$ **then**
      {~~$p_{\mathrm{crit}} > 1$ is equivalent to $\nu_{coll} > \nu_i$~~ can occur when ν_i and ν_j differ strongly and be regarded as special case; see text for further explanation}
      if $\nu_{\mathrm{coll}} > \nu_j$ **then**
        ~~*{transfer ν_{coll} droplets with μ_j from SIP j to SIP i, allow multiple collections in SIP i, i.e. one droplet of SIP i collects more than one droplet of SIP j.}*~~***LIMITER***
        {Special treatment necessary, otherwise the new ν_j would be negative}
        {Limit ν_{coll} to ν_j, then ν_i droplets with mass $(\nu_i \mu_i + \nu_j \mu_j)/\nu_i$ remain}
        {Distribute those droplets among SIPs i and j; use a 60%,40%-partitioning}
        $\mu_j := (\nu_i \mu_i + \nu_j \mu_j)/\nu_i$ and $\mu_i := \mu_i$
        $\nu_j := 0.6\,\nu_i$ and $\nu_i := 0.4\,\nu_i$
      else
        MULTIPLE COLLECTION
        {$p_{\mathrm{crit}} > 1$ is equivalent to $\nu_{\mathrm{coll}} > \nu_i$}
        {transfer ν_{coll} droplets with μ_j from SIP j to SIP i, allow multiple collections in SIP i, i.e. one droplet of SIP i collects more than one droplet of SIP j}
        SIP i collects ~~ν_{coll}~~ ν_{coll} droplets from SIP j and distributes them on ν_i droplets: ~~$\mu_i = (\nu_i \mu_i + \nu_{coll} \mu_j)/\nu_i$~~ $\mu_i := (\nu_i \mu_i + \nu_{\mathrm{coll}} \mu_j)/\nu_i$
        SIP j loses ~~ν_{coll}~~ ν_{coll} droplets to SIP i: ~~$\nu_j = \nu_j - \nu_{coll}$~~ $\nu_j := \nu_j - \nu_{\mathrm{coll}}$
      end if
    else if p_{crit} >rand() **then**
      RANDOM SINGLE COLLECTION
      ~~assume $\nu_i < \nu_j$, otherwise swap i and j in the following lines~~ *{transfer ν_i droplets with μ_j from SIP j to SIP i}*
      SIP i collects ν_i droplets from SIP j: ~~$\mu_i = \mu_i + \mu_j$~~ $\mu_i := \mu_i + \mu_j$
      SIP j loses ν_i droplets to SIP i: ~~$\nu_j = \nu_j - \nu_i$~~ $\nu_j := \nu_j - \nu_i$
    end if
  end for

mass $\mu_i+\mu_j = 15$. *SIP* j *now contains* $\nu_j-\nu_i = 8-4 = 4$ *droplets with mass* $\mu_j = 9$. *Following Eq. (7), only* ~~$\nu_{coll} = 2$~~ $\nu_{\mathrm{coll}} = 2$ *pairs of droplets would, however, merge in reality. The idea behind this probabilistic AON is that such a collection event is realised only under certain circumstances in the model, namely such that the expectation values of collection events in the model and in the real world are the same. This is achieved if a collection event occurs with probability*

$$p_{\mathrm{crit}} = \nu_{coll\,\mathrm{coll}}/\nu_i \tag{21}$$

in the model. Then, the average number of collections in the model,

$$\bar{\nu}_{coll\,\mathrm{coll}} = p_{\mathrm{crit}}\nu_i = (\nu_{coll\,\mathrm{coll}}/\nu_i)\nu_i, \tag{22}$$

is equal to ~~ν_{coll}~~ ν_{coll} *as in the real world. A collection event between two SIPs occurs if* $p_{\mathrm{crit}} >$*rand(). The function rand() provides uniformly distributed random numbers* $\in [0,1]$. *Noticeably, no operation on a specific SIP pair is performed if* $p_{\mathrm{crit}} <$*rand().*

The treatment of the special case ~~$\nu_{coll}/\nu_i > 1$~~ $\nu_{\mathrm{coll}}/\nu_i \geq 1$ *needs some clarification. This case is regularly encountered when SIPs with large droplets and small* ν_i *collect small droplets from a SIP with large* ν_j. *The large difference in droplet masses* μ *led to large kernel values and high* ~~ν_{coll} *with* $\nu_i < \nu_{coll} < \nu_j$~~ ν_{coll} *with* $\nu_i \leq \nu_{\mathrm{coll}} \leq \nu_j$. *[. . .] If* $p_{\mathrm{crit}} > 1$, *we allow multiple collections, as each droplet in SIP* i *is allowed to collect more than one droplet from SIP* j. *In total, SIP* i *collects* ~~ν_{coll}~~ ν_{coll} *droplets from SIP* j *and distributes them on* ν_i *droplets. A total mass of* ~~$\nu_{coll}\mu_j$~~ $\nu_{\mathrm{coll}}\mu_j$ *is transferred from SIP* j *to SIP* i *and the droplet mass in SIPs* i *becomes* ~~$\mu_i^{\mathrm{new}} = (\nu_i\,\mu_i + \nu_{coll}\,\mu_j)/\nu_i$~~ $\mu_i^{\mathrm{new}} = (\nu_i\,\mu_i + \nu_{\mathrm{coll}}\,\mu_j)/\nu_i$. *The number of droplets in SIP* j *is reduced by* ~~ν_{coll} *and* $\nu_j^{\mathrm{new}} = \nu_j - \nu_{coll}$~~ ν_{coll} *and* $\nu_j^{\mathrm{new}} = \nu_j - \nu_{\mathrm{coll}}$. *Keeping with the example in Fig. 3 and assuming* ~~$\nu_{coll} = 5$~~ $\nu_{\mathrm{coll}} = 5$, *each of the* $\nu_i = 4$ *droplets would collect* ~~$\nu_{coll}/\nu_i = 1.25$~~ $\nu_{\mathrm{coll}}/\nu_i = 1.25$ *droplets. The properties of SIP* i *and SIP* j *are then* $\nu_i = 4$, $\mu_i = 17.25$, $\nu_j = 3$ *and* $\mu_j = 9$. *[. . .] So far, we explained how a single* $i-j$ *combination is treated in AON. In every time step, the full algorithm simply checks each* $i-j$ *combination for a possible collection event. To avoid double counting, only combinations with* $i < j$. *Pseudo-code of the algorithm is given in Algorithm (1). The SIP properties are updated on the fly. If a certain SIP is involved in a collection event in the model and changes its properties, all subsequent combinations with this SIP take into account the updated SIP properties. [. . .] For the generation of the random numbers, the well-proven (L'Ecuyer and Simard, 2007) Mersenne Twister algorithm by Matsumoto and Nishimura (1998) is used."*

The AON treatment of ~~self-collections and of~~ collection of droplets within one SIP, as well as the collection of two SIPs with equal weighting factors are described in U2017. In the simulations presented here these aspects are not relevant and thus omitted.

The current implementation differs in several aspects from the version in Shima et al. (2009). First, they use a linear sampling approach (which will be described in subsection 2.3.3). Second, the weighting factors are considered to be integer numbers, whereas we use real numbers ν. Integer values are appropriate in discrete test cases of small sample volumes such as the validation test case in section 3 of Dziekan and Pawlowska (2017). For comparing AON with bin model references, usually continuous DSDs are prescribed. Then a SIP ensemble with real-values weighting factors is more appropriate in our opinion. Third, multiple collections (MC) are differently treated. For ~~$p_{crit} = (\nu_{coll}/\nu_i) > 1$, either $\lfloor p_{crit} \rfloor \nu_i$ or $\lceil p_{crit} \rceil \nu_i$~~

$p_{crit} = (\nu_{coll}/\nu_i) > 1$, either $\lfloor p_{crit} \rfloor \nu_i$ or $\lceil p_{crit} \rceil \nu_i$ droplets of SIP j merge with ν_i droplets of SIP i depending on the probability ~~$p_{crit} - \lfloor p_{crit} \rfloor$~~ $p_{crit} - \lfloor p_{crit} \rfloor$. This maintains the integer property of the SIP weights. As the latter feature is not required in our approach, we deterministically merge ~~$p_{crit}\nu_i = \nu_{coll}$~~ $p_{crit}\nu_i = \nu_{coll}$ droplets from SIP j with ν_i droplets of SIP i. This is computationally more efficient than the integer-preserving implementation. Test simulations showed that both MC treatments produce similar results.

2.3.2 AON algorithm with explicit use of vertical coordinate (~~WM2D~~AON-WM2D)

We now introduce the AON version based on an idea by Sölch and Kärcher (2010) where the vertical position z_p of the SIPs is explicitly considered. The approach and its implications will be detailed next. Pseudo-code of this AON ~~variant~~ version ("WM2D") is given in Algorithm 2.

Unlike to the classical case where 3D well-mixedness has to be assumed, droplets of a SIP are now assumed to be well mixed on the ~~x-y-plane~~ $x-y$-plane at $z = z_p$ within the GB (horizontally well-mixed instead of the traditional ~~isotropic assumption~~ well-mixed assumption for the entire three-dimensional GB) and represent a "concentration" of $n_{2D} = \nu/\delta A$ (units L^{-2}, where L is a length scale). We introduce an adapted kernel definition where the relative velocity term ~~$|w_{sed,i} - w_{sed,j}|$~~ $|w_{sed,i} - w_{sed,j}|$ is dropped from Eq. 5:

$$K^{WM2D\,\mathrm{WM2D}}_{ij} := E_{cc}(r_i, r_j)\pi(r_i + r_j)^2. \tag{23}$$

The AON algorithm is split into two steps:

1. Based on the evaluation of the vertical positions z_i and z_j at times t and $t + \Delta t$, it is checked if SIP i overtakes SIP j within a time step Δt. Given $z_i(t) \geq z_j(t)$ (otherwise swap i and j) an overtake takes place in the time interval Δt if $z_i(t + \Delta t) < z_j(t + \Delta t)$.

2. In case of such an overtake: Compute the average number of droplet collections by

$$\nu_{coll\,\mathrm{coll}} = K^{WM2D\,\mathrm{WM2D}}_{ij} \nu_i \, \nu_j \, \Delta A^{-1}. \tag{24}$$

   Analogous to the classical implementation, a collection in the model is performed with a probability ~~ν_{coll}/ν_i~~ ν_{coll}/ν_i and SIP i may collect ν_i from SIP j (in this step i and j are chosen, such that $\nu_i < \nu_j$).

Similarly to the WM3D version, it happens that ~~ν_{coll}~~ ν_{coll} is larger than ν_i and multiple collections ~~should be considered in the algorithm~~are also considered in AON-WM2D.

Specifically to WM2D, it is also possible that a SIP interacts with other SIPs located not only in one but several GBs. Accordingly, it is not only necessary to check overtakes of other SIPs in the original GB (more specifically, SIPs that lie in the same GB at time t), but also the SIPs that are located underneath, depending on the prescribed time step.

In a Lagrangian model, the time step choice is not numerically restricted by the CFL criterion and in particular the largest collecting drops may fall through several GBs during the time period Δt. Hence, their collections are underrated unless potential overtakes are checked among all ~~$N_{SIP,tot}$~~ $N_{\mathrm{SIP,tot}}$ SIPs of the entire column. Even if the CFL criterion is obeyed, SIPs

Algorithm 2 Pseudo-code of the ~~WM2D all-or-nothing algorithm (AON)~~AON-WM2D; style conventions are explained right before Section 2.3.1 starts; rand() generates uniformly distributed random numbers ~~$\in [0,1]$~~$\in [0,1)$. This AON version is called once for the total column.

INIT BLOCK
Given: Ensemble of SIPs of the total column, in particular also their positions Specify: Δt
TIME ITERATION
while t<Tsim **do**
    {Sort SIPs by position, the highest SIP will be the first SIP.}
    Sort SIPs by position, such that $z_i(t) \geq z_j(t)$ for $i < j$
    {Check for overtakes}
    for ~~$i = 1, N_{SIP,tot} - 1$~~$i = 1, N_{\mathrm{SIP,tot}} - 1$ **do**
        for ~~$j = i + 1, N_{SIP,tot}$~~$j = i + 1, N_{\mathrm{SIP,tot}}$ **do**
            if $z_i(t + \Delta t) \geq z_j(t)$ **then**
                exit ~~j-loop~~ j-loop and proceed with next SIP i *{if end position of SIP i is above departure point of ~~SIPs~~SIP j, then no overtakes are possible for any remaining SIP j.}*
            end if
            if $z_i(t + \Delta t) \geq z_j(t + \Delta t)$ **then**
                proceed with next SIP j *{no overtake ~~occured~~ occurred as SIP i is still above SIP j at $t + \Delta t$}*
            end if
            {the above conditions guarantee that the following code is executed ~~iff~~ if and only if SIP i overtakes SIP j}
            Compute ~~ν_{coll}~~ ν_{coll} according to Eq. 24 *{instead of Eq. 7 as in the WM3D version}*
            {all the following operations are identical to the WM3D version and accompanying explanations are removed}
            ~~$\nu_{\mathrm{new}} = \min(\nu_i, \nu_j)$~~ $\nu_{\mathrm{new}} := \min(\nu_i, \nu_j)$
            ~~$p_{\mathrm{crit}} = \nu_{coll} / \nu_{\mathrm{new}}$~~ $p_{\mathrm{crit}} := \nu_{\mathrm{coll}} / \nu_{\mathrm{new}}$
            assume $\nu_i < \nu_j$, otherwise swap i and j in ~~the following lines~~ all following lines
            if $p_{\mathrm{crit}} > 1$ **then**
                ~~$\mu_i = (\nu_i \mu_i + \nu_{coll} \mu_j) / \nu_i$~~ *{for brevity, the **LIMITER**-block is left out in this code listing}*
                ~~$\nu_j = \nu_j - \nu_{coll}$~~ $\mu_i := (\nu_i \mu_i + \nu_{\mathrm{coll}} \mu_j) / \nu_i$
                $\nu_j := \nu_j - \nu_{\mathrm{coll}}$
            else if $p_{\mathrm{crit}} >$rand() **then**
                ~~assume $\nu_i < \nu_j$, otherwise swap i and j in the following lines~~ $\mu_i := \mu_i + \mu_j$
                ~~$\mu_i = \mu_i + \mu_j$ $\nu_j = \nu_j - \nu_i$~~ $\nu_j := \nu_j - \nu_i$
            end if
        end for
    end for
    ~~$t = t + \Delta t$~~ $t := t + \Delta t$
end while

close to the lower GB boundary will mostly collect SIPs from the GB underneath. Hence, seeking collision candidates only in the present GB is never a good choice.

In a naive implementation, this would dramatically increase the computational costs. In the regular (WM3D~~implementation, nz~~) version, n_z calls of AON with ~~$O(N_{SIP,GB}{}^2)$~~ $\mathcal{O}(N_{\mathrm{SIP,GB}}{}^2)$ (for simplicity lets assume ~~$N_{SIP,GB}$~~ $N_{\mathrm{SIP,GB}}$ is the same in all GBs) give a total cost of ~~$nz \times O(N_{SIP,GB}{}^2)$~~ $n_z \times \mathcal{O}(N_{\mathrm{SIP,GB}}{}^2)$. Contrarily, AON-WM2D is called once for all SIPs of the column. Hence the cost is ~~$1 \times O(N_{SIP,tot}{}^2) = nz^2 \times O(N_{SIP,GB}{}^2)$~~ $1 \times \mathcal{O}(N_{\mathrm{SIP,tot}}{}^2) = {n_z}^2 \times \mathcal{O}(N_{\mathrm{SIP,GB}}{}^2)$ and a factor ~~nz~~ n_z higher than the regular ~~implementation.~~ AON version. However, the WM2D ~~implementation~~ version can be sped up by first sorting all SIPs by their position (if sorting is done independently in each GB, the complexity is ~~$nz \times O(N_{SIP,GB} \log(N_{SIP,GB}))$~~ $n_z \times \mathcal{O}(N$ and second by taking into account that the final position $z_i(t+\Delta t)$ of the potentially overtaking SIP i must be below the initial position $z_j(t)$ of SIP j. Finding possible candidates for SIP i within the sorted SIP list can be stopped once a SIP j with $z_j(t) < z_i(t+\Delta t)$ is encountered (see condition in line 10 of Algorithm 2).

For the smallest SIPs, which often travel only a small distance inside a GB, the list of SIPs that may be overtaken is commensurately small and overtakes have to be checked for a fraction of SIPs of the GB only (that means the actual computational work is smaller than in the regular version). On the other hand, imagine the largest SIPs travel through three GBs, then overtakes have to be tested for roughly three times more SIPs than in the regular version. Moreover, testing for overtakes (step 1) is computationally less demanding than calculating the potential collections (step 2). In WM3D we have always the workload of step 2 for all tested combinations, whereas in WM2D only the cheaper step 1 is executed in case of no overtake.

Besides the weaker assumption of 2D well-mixedness, the present approach is actually more intuitive (even though it may first be regarded counter-intuitive by those who are familiar with traditional Eulerian grid-based approaches). Moreover, this approach complies better with the Lagrangian paradigm of a grid-free description (the present approach is independent of ~~nz~~ n_z and Δz, yet some horizontal "mixing area" ΔA has to defined, over which the droplets of a SIP are assumed to be dispersed). In the regular AON, the aspect ratios of the grid box do not matter, only the grid box volume ΔV enters the computations. In WM2D, on the other hand, the value of ΔV is insignificant and ΔA enters the computations. In a column model with sedimentation, results also depend on Δz as it determines the travel time through a grid box. Note that a variation of Δz can implicitly change also ΔV or ΔA.

For more sophisticated kernels, including, e.g., turbulence enhancement, the present approach may not be adopted easily as the driving mechanism for collisions to occur in the current model is differential sedimentation~~(see also discussions~~. Related to this are studies on cylindrical vs. spherical formulations of kernels in ~~(Saffman and Turner, 1956) and Wang et al. (1998, 2005)).~~ Saffman and Turner (1956) and Wang et al. (1998, 2005) . A possible route to consider the effects of subgrid-motions on collision in LCMs has recently been presented by Krueger and Kerstein (2018) . Their one-dimensional approach is able to represent droplet clustering and turbulence-induced relative droplet velocities in a realistic manner, and its implementation in already applied LCM subgrid-scale models (e.g. Hoffmann et al., 2019; Hoffmann and Feingold, 2019) is deemed straightforward. However, further research is required on how the limited number of SIPs in current LCM applications may corrupt the correct representation of such processes.

Finally, we shortly ~~summarize~~ summarise the differences between the WM2D and WM3D approach. The standard kernel ~~K^{WM3D}~~ K^{WM3D} as given by Eq. 5 has units L^3/T (where L and T are a length and time scale, resp.). Multiplying it by concentrations n_i and n_j (units L^{-3}), one obtains the rate of a concentration increase of merged droplets (L^{-3}/T) which is finally multiplied by δt (unit T) to obtain ~~n_{coll}~~ n_{coll} (see Eq. 8). Since SIPs represent droplet concentrations of $n_i = \nu_i/\delta V$ and $n_j = \nu_j/\delta V$, Eq. 7 follows. In the WM2D approach, the kernel ~~K^{WM2D}~~ K^{WM2D} as given by Eq. 23 has units L^2. Multiplying it by "2D" concentrations ~~$n_{2D,i}$ and $n_{2D,j}$~~ $n_{\mathrm{2D},i}$ and $n_{\mathrm{2D},j}$ (units L^{-2}) one obtains the collected 2D concentration ~~$n_{2D,coll}$~~ $n_{\mathrm{2D,coll}}$ (units L^{-2}). Since SIPs represent "2D" droplet concentrations of ~~$n_{2D,i} = \nu_i/\delta A$ and $n_j = \nu_{2D,j}/\delta A$~~ $n_{\mathrm{2D},i} = \nu_i/\delta A$ and $n_j = \nu_{\mathrm{2D},j}/\delta A$, Eq. 24 follows. A collection can only occur, if a larger droplet (or SIP) i overtakes a smaller droplet (or SIP) j. First, $z_i > z_j$ and ~~$w_{sed,i} > w_{sed,j}$~~ $w_{\mathrm{sed},i} > w_{\mathrm{sed},j}$ must hold and second the overtake time ~~$\Delta t_{OT} := (z_i - z_j) \times (w_{sed,i} - w_{sed,j})^{-1}$ must fulfill $\Delta t_{OT} \leq \delta t$~~ $\Delta t_{\mathrm{OT}} := (z_i - z_j) \times (w_{\mathrm{sed},i} - w_{\mathrm{sed},j})^{-1}$ must fulfil $\Delta t_{\mathrm{OT}} \leq \delta t$. One can define the overtake probability ~~p^{OT}~~ p^{OT} being 0 for ~~$\Delta t_{OT} > \delta t$~~ $\Delta t_{\mathrm{OT}} > \delta t$ and 1 for ~~$\Delta t_{OT} \leq \delta t$~~ $\Delta t_{\mathrm{OT}} \leq \delta t$, and the "2D" collection probability ~~$p_{ij}^{WM2D} = K_{ij}^{WM2D} \delta A^{-1}$. Simulations will~~ $p_{ij}^{\mathrm{WM2D}} = K_{ij}^{\mathrm{WM2D}} \delta A^{-1}$. Simulations in SUPP demonstrate that the WM2D and WM3D formulations are statistically equivalent~~under certain conditions~~, i.e. ~~$p^{OT} \times p_{WM2D}$ equals p_{WM3D}.~~ $p^{\mathrm{OT}} \times p^{\mathrm{WM2D}}$ equals p^{WM3D}, under certain conditions (see Fig. S9).

From a technical point of view, it might be challenging to implement the WM2D-version in full 2D/3D cloud models, as one has to keep track of all SIPs in a grid box column. If domain decomposition is used in vertical direction, collision candidates had to be searched across multiple processors.

2.3.3 Linear sampling ~~variant~~version (AON-LinSamp)

The regular AON ~~variant~~ version can be sped up by introducing a linear sampling technique (LinSamp) as done in Shima et al. (2009) or Dziekan and Pawlowska (2017). $\lfloor N_{\mathrm{SIP}}/2 \rfloor$ combinations of pairs $i-j$ are randomly picked, where each SIP appears exactly in one pair (if N_{SIP} is odd, one SIP is ignored). As only a subset of all possible combinations is numerically evaluated, the extent of collisions is underestimated. To compensate for this, the probability p_{crit} (or equivalently ~~ν_{coll}~~ ν_{coll}) is upscaled by a scaling factor

$$\gamma_{\mathrm{corr}} = N_{\mathrm{SIP}}(N_{\mathrm{SIP}} - 1)/(2\,\lfloor N_{\mathrm{SIP}}/2 \rfloor) \tag{25}$$

to guarantee an expectation value as desired. Clearly, this reduces the computational complexity of the algorithm from ~~$O(N_{\mathrm{SIP}}{}^2)$ to $O(N_{\mathrm{SIP}})$~~ $\mathcal{O}(N_{\mathrm{SIP}}{}^2)$ to $\mathcal{O}(N_{\mathrm{SIP}})$. Multiple collections are more likely than in the regular ~~quadratic implementation~~AON version. The LinSamp ~~variant~~ version becomes the preferred choice if N_{SIP} is large. ~~If ν_{coll}~~

If ν_{coll} is larger than both, ν_i and ν_j, all AON versions as introduced so far would produce negative weights. In order to prevent this, ~~ν_{coll}~~ ν_{coll} is artificially reduced to ~~$0.99 \max(\nu_i, \nu_j)$~~ ν_j in such a case ~~. This limiter is applied in all AON implementations, but~~ (let us assume that $\nu_i < \nu_j$). The standard procedure would then produce a SIP j with zero weight, which allows splitting the updated SIP i with weight ν_i (the weight ν_i remains unchanged during the update) into two SIPs. We

choose a $60\%, 40\%$-partitioning and the operations are as follows:

$$\mu_j := (\nu_i\,\mu_i + \nu_j\,\mu_j)/\nu_i \tag{26a}$$

$$\mu_i := \mu_j \tag{26b}$$

$$\nu_j := 0.6\,\nu_i \tag{26c}$$

$$\nu_i := 0.4\,\nu_i \tag{26d}$$

SUPP demonstrates that it is critical how the limiter is implemented. We thank reviewer S. Shima for pointing us to a better limiter implementation which has been already described in Shima et al. (2009) . There, a $50\%, 50\%$-partitioning was implemented. We avoid this equal splitting as it produces two identical SIPs. In our implementation with floating point weights, SIPs with identical weights are extremely rare and no special care is taken of this. Hence, including an operation that produces identical weights is unfavourable. The dependence of the AON-LinSamp performance on the limiter definition is showcased in SUPP (Figs. S3 to S7, S15, S16 and Table S1).

Employing a limiter is recommended for all AON versions (even though we never encountered a limiter event in QuadSamp-simulations), but it is particularly significant in the LinSamp version due to the upscaling of p_{crit}. Moreover, note that LinSamp can be reasonably used only in conjunction with AON-WM3D, not AON-WM2D.

In addition to the favourable linear computational complexity, LinSamp can be easily parallelised, in particular on shared-memory multi-processor architectures as used by Arabas et al. (2015) or Dziekan et al. (2019) . Once the SIP pairs are determined in the beginning of each time step, each processor treats a subset of SIP pairs. After an collection event, SIP properties are updated on the fly. By the way, the need to do updates on the fly precludes simple parallelisation strategies in the quadratic sampling version, where all SIPs are interconnected.

2.4 Boundary condition

At the lower boundary, droplets leave the domain according to their fall speed. Using the LCM, the moment outflow $F_{l,\mathrm{out}}$ is determined by accumulating the contributions $\nu_p(\mu_p)^l$ of all SIPs p that cross the lower boundary $z = 0\,\mathrm{m}$. Due to the discreteness of the crossings, instantaneous fluxes are actually averages of the past $200\,\mathrm{s}$. Using the bin model, $F_{l,\mathrm{out}}$ is diagnosed by

$$F_{l,\mathrm{out}} = \sum_{p=1}^{N_{\mathrm{BIN}}} g_{p,k=1}\,(\tilde{m}_{\mathrm{bb},p})^{l-1} w_{sedsed}(\tilde{m}_{\mathrm{bb},p}) \frac{\ln 10}{3\,\kappa}. \tag{27}$$

At the model top, the simplest condition is to have a zero influx. In this case, the column integrated droplet mass will decrease once a non-zero flux across the lower boundary occurs. To ~~realize~~ implement a zero-influx condition in the Eulerian model, the mass concentrations at the ghost cell level ~~$nz+1$~~ n_z+1 are simply set to zero. In the Lagrangian model, a zero influx condition is naturally implemented when no new ~~SIP~~ SIPs are created at the top of the column.

Table 2. Summary of AON versions.

AON feature	QuadSamp	LinSamp
WM3D	AON-reg	AON-LinSamp
WM2D	AON-WM2D	*n.a.*
WM3D, noSedi	AON-noSedi	AON-LinSamp-noSedi

In both models, also a non-zero influx at the model top can be prescribed. One ~~variant~~ option is to use periodic boundary conditions. In the Lagrangian approach this is done by increasing the ~~height~~ altitude z_p of ~~affected SIPs by Lz, once their height~~ an affected SIP by L_z, once z_p drops below 0. In the Eulerian model, ~~$g_{p,nz+1}$~~ $g_{p,nz+1}$ is identified with $g_{p,1}$. A second non-zero influx ~~variant~~ option is a prescribed size distribution that is advected into the domain with its respective fall speed. In the bin model, the prescribed DSD simply defines the ~~$g_{i,nz+1}$~~ $g_{i,nz+1}$-values. In the Lagrangian model, new SIPs have to be introduced close to the model top. For this, a new SIP ensemble is drawn from the prescribed DSD at each time step using the SingleSIP-init method. In order to place the SIPs in the column, it is considered how far it would fall at most from the model top during one ~~timestep: $z_\Delta(p) = w_{sed,p} \times \Delta t$~~time step: $z_\Delta(p) = w_{sed,p} \times \Delta t$. In a straightforward implementation, one would create one SIP from each bin with a position $z_{new,p}$ uniformly drawn from ~~$[Lz, Lz - z_\Delta(p)]$~~ $[L_z, L_z - z_\Delta(p))$ and weighting factor $\nu_{new,p} = \nu_p \times (z_\Delta(p)/\Delta z)$. This implementation has, however, several undesirable side-effects. For small, slowly falling SIPs $z_\Delta(p)$ is much smaller than Δz. Applying this procedure in every time step leads to $\Delta z / z_\Delta(p)$ SIPs per GB in the end. Hence, we refine this procedure by creating a SIP with probability ~~$z_\Delta(p)/\Delta z$~~ $p_{init,p} := z_\Delta(p)/\Delta z$, a weighting factor $\nu_{new,p} = \nu_p$ and ~~$z_{new,p} \in [Lz, Lz - z_\Delta(p)]$~~ $z_{new,p} \in [L_z, L_z - z_\Delta(p))$. Note that if ~~$z_\Delta(p)/\Delta z > 1$~~ $p_{init,p} \geq 1$, then either ~~$\lfloor z_\Delta(p)/\Delta z \rfloor$ or $\lceil z_\Delta(p)/\Delta z \rceil$~~ $\lfloor p_{init,p} \rfloor$ or $\lceil p_{init,p} \rceil$ SIPs are created depending on the probability ~~$(z_\Delta(p)/\Delta z) - \lfloor z_\Delta(p)/\Delta z \rfloor$~~ $p_{init,p} - \lfloor p_{init,p} \rfloor$. This establishes a similar spatial SIP occurrence across the size spectrum with one SIP per GB and bin on average. Moreover, SIP numbers do not scale any longer with Δt.

2.5 Terminology

Before we start discussing the results, we outline the terminology of the various model versions. On a first level, we differentiate between Eulerian (~~BIN~~"BIN") and Lagrangian approaches (~~LCM~~"LCM"), which can be both applied in a box ("0D") or column model ("1D") framework. By default, BIN uses the MPDATA advection algorithm (clearly only in 1D) and Bott's collection algorithm. Alternatively, MPDATA can be replaced by the 1st order upstream scheme ("US1") and Bott's collection algorithm by Wang's ~~(Wang~~algorithm ("Wang"). The Lagrangian model versions differ only in the way AON is employed. The various model versions are summarised in Table 2. By default, 3D well-mixedness ("WM3D") is assumed and a quadratic sampling (~~QuadSamp~~"QuadSamp") of the SIP combinations is used. Those simulations are ~~also~~ referred to as "regular". A second type of QuadSamp simulation assumes 2D well-mixedness ("WM2D"). Linear sampling of SIP combinations ("LinSamp") can be alternatively used for the WM3D-version. Accordingly, ~~only~~ the terms "regular", "WM2D" and "LinSamp" each refer to a ~~specific type of simulation, while~~ one specific AON version. On the other hand, "QuadSamp" and "WM3D" ~~may denote~~

options in several simulations (each denote two AON versions: "QuadSamp" can be used with WM3D and comprises "regular" and "WM2D, and ", whereas "WM3D" can be used with QuadSamp and LinSamp). comprises "regular" and "LinSamp".

By switching off sedimentation in the column model source code (as done in section 3.1), box model results are produced in each GB. In order to distinguish the latter simulations from AON box model results in U2017 they are refered referred to as "noSedi"(implicitly assuming WM3D). . In LCM1D-noSedi simulations, the vertical position is not updated from time step to time step. Hence, this implicitly calls for the usage of AON-WM3D, as AON-WM2D relies on checking overtakes based on the vertical SIP positions. Simulations with switched on sedimentation are the default; for better discrimination from the noSedi-case we refer to all such simulations optionally as "full" simulations.

If the space in figure legends is limited, abbreviations "LS" and "nS" are used for "LinSamp" and "noSedi", respectively.

3 Results

3.1 Validation exercises: pure sedimentation

Pure Sedimentation test case: Comparison of BIN and LCM (solid) advection. BIN uses either MPDATA (dashed) or 1st order Upstream scheme (dotted). EmptyDom (upper row) and HalfDom (lower row) setup are used with an exponential distribution with $r_0 = 50\,\mu$m as influx condition. Displayed are vertical profiles of normalised zeroth and second moment at the indicated points in time.

Pure Sedimentation test case: Comparison of BIN and LCM advection. EmptyDom setup with an exponential distribution with $r_0 = 50\,\mu$m as influx condition. Displayed are vertical profiles of normalised mass within specified size ranges (see on top of each panel) at the indicated points in time. Note that most panels use different y-axis ranges and do not show all six points in time. Before we start comparing collection collisional growth in column model applications, we highlight should first demonstrate that the differences introduced by the different numerical treatment of the sedimentation process are small to negligible. This exercises is deferred to the Appendix.

We find the discrepancies introduced by the different sedimentation treatment small enough as long as the MPDATA advection algorithm is employed in BIN. Hence, all following BIN simulations rely on MPDATA and we can attribute the differences that we may see in the following validation exercises to the different numerical treatment of collisional growth.

Two simple setups with an influx of an exponential DSD with $r_0 = 50\,\mu$m is prescribed. In the first case the domain is initially empty and fills over time (EmptyDom). In the second case, the upper half of the domain is filled and LWC and DNC decrease linearly to zero from the domain top to the domain middle (HalfDom). Fig. A1 shows the vertical profiles of normalised zeroth (left) and second (right) moments for EmptyDom (top) and HalfDom (bottom). Because of the lack of numerical diffusion, the solid LCM curves show the exact results, except for the error introduced by discretizing the influx DSD with a probabilistic approach. Each panel showcases a convincing agreement between the Eulerian and Lagrangian approach. Only the BIN-US1 solutions are slightly smeared out. The small wiggles in the LCM curves originate from the probabilistic influx condition. Even though the above agreement is favourable, it might be that the advection errors of differently sized droplets compensate each other in the Eulerian approaches. Hencein a second validation step, the computation of mass profiles is confined to certain

~~droplet size ranges. Figure A2 shows such vertical profiles for EmptyDom. We see that for all four size ranges, the BIN results are smeared out relative to LCM. For the smallest size ranges both BIN versions are equally "bad" (top left panel). For the three remaining panels, the MPDATA curves (dashed) are closer to the LCM reference than the US1 curves (dotted). On the other hand, the MPDATA curves in the bottom right panel show some wiggles. Overall, the agreement between LCM and BIN-MPDATA is good. The discrepancies introduced by the different sedimentation treatment seem to be small enough to focus on the collection process in the following comparisons.~~

3.1 Box model emulation simulations

3.1.1 ~~Regular AON version~~

~~BoxModelEmul setup:Temporal evolution of column-averaged DNC and Z over one hour for various time steps Δt (see inserted legend for Δt-values in seconds). All other parametes take the default values as given in the caption of Fig. 5.~~

~~BoxModelEmul setup:Temporal evolution of column-averaged moment λ_0 (i.e. droplet concentration) over one hour. The default setting is $nz = 50, nr_{inst} = 20, \Delta V = 1\,\mathrm{m}^3, \Delta t = 10\,\mathrm{s}, \Delta z = 10\,\mathrm{m}, \kappa = 40$ and $L_z = nz \times \Delta z$. The microphysical parameters of the initial exponential droplet size distribution are $LWC = 1\mathrm{g/m}^3, r_0 = 9.3\,\mu\mathrm{m}$ and $DNC = 297\,\mathrm{cm}^{-3}$ as in many previous studies (Berry, 1967; Wang et al., 2007) . The parameter or parameter pair that is varied is written on top of each panel and the legend lists the parameter values for the different colours. If further parameters (besides the varied parameter) take non-default values, it is indicated in a black box. In any case, the total number of GBs is $nr_{inst} \times nz = 1000$. By default, sedimentation is switched on. Simulations without sedimentation and independent rain formation in each GB (identical to a box model treatment) are labelled as "noSedi" (appear only in the left column).~~

In this section, we choose a column model setup that is supposed to produce results that are similar to box model results. For this, we initialise the default DSD in all GBs of the column and use periodic boundary conditions. In LCM1D, different SIP ensemble realisations of this DSD are initialised in each GB.

The deterministic ~~bin column~~ BIN1D model predicts identical DSDs in all GBs, as in each GB the divergence of the sedimentation flux is zero. Hence, for this specific setup, the attained BIN1D results are identical to those of a corresponding BIN0D model or the data of Wang et al. (2007, see their Tables 3 and 4).

In LCM1D, the combination of homogeneous initial conditions and periodic BCs results in statistically identical results across all GBs. However, the averaged results may not be the same as in LCM0D, as lucky droplets/SIPs (Telford, 1955; Kostinski and Shaw collect other droplets/SIPs not only from a single GB as in LCM0D, but from any GB (depending on how fast they fall), creating potentially larger and/or faster growing lucky droplets/SIPs than in LCM0D. In other words, the number of SIPs interacting with each other is increased in LCM1D. This, as we will show below, accelerates the convergence of the simulations.

~~Within the LCM1D-implementation~~Within the LCM1D-model, pure box model results can be obtained by switching off sedimentation ("noSedi"). Without sedimentation, the GBs of the column are not interconnected and the ~~collection~~ collisional growth process proceeds independently. ~~In the following, we refer to those simulations as "noSedi".~~

All figures related to the box model emulation setup start their caption with the label **BoxModelEmul setup**.

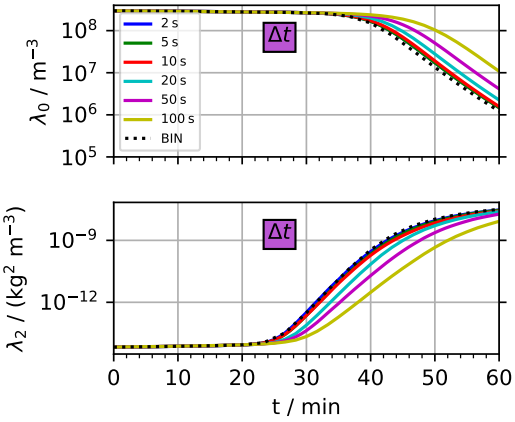

Figure 4. BoxModelEmul setup: Temporal evolution of column-averaged moments λ_0 and λ_2 over one hour for various time steps Δt (see inserted legend for Δt-values for the regular AON version. All other parameters take the default values as given in the caption of Fig. 5.

By default, we use ~~$nz = 50$~~ $n_z = 50$ GBs with $\Delta z = 10\,\mathrm{m}$ (giving a column height of ~~$Lz = 500\,\mathrm{m}$, $\Delta V = 1\,\mathrm{m}^3$, $\Delta z = 10\,\mathrm{m}$, $\Delta t = 10\,\mathrm{s}$~~ $L_z = 500\,\mathrm{m}$), $\Delta V = 1\,\mathrm{m}^3$, $\Delta t = 10\,\mathrm{s}$ and $\kappa = 40$ throughout section 3.1. The results are averaged over ~~$nr_{inst} = 20$ realisations. AON-WM3D is employed in LCM1D and sedimentation~~ $nr_{\mathrm{inst}} = 20$ independent realisations. Hence, the present AON application can be viewed as a Monte-Carlo method.

Moreover, we use the Long kernel (Long, 1974) as default in BoxModelEmul simulations, as U2017 revealed that numerical convergence is harder to reach for the Long kernel than for the Hall kernel or a hydrodynamic kernel with constant aggregation efficiency typical used for cirrus simulations (Sölch and Kärcher, 2010) .

3.1.1 Regular AON version

This subsection presents results obtained with the regular AON, i.e. with quadratic sampling of SIP combinations ("QuadSamp") and 3D well-mixed assumption (WM3D). Sedimentation is switched on unless noted (for better discrimination from the ~~noSedi, those~~ "noSedi"-cases, these simulations will be referred to as "full"). ~~Moreover, the regular AON-WM3D version uses a quadratic sampling of SIP combinations (referred to as "QuadSamp").~~

Figure 4 shows the temporal evolution of column-averaged LCM1D moments λ_l ($l = 0$ and 2) over one hour for various time steps Δt. The box model data serve as orientation in this and following Figures 4~~-??~~–7. We find that in terms of λ_0 and λ_2 LCM1D results converge for $\Delta t \leq 10\,\mathrm{s}$. The noSedi simulations show a similar time step dependence (not shown). Hence, AON works ~~surprisingly well~~ well even for large time steps; a fact that was already shown with the AON box model (see Fig. 18 of U2017).

Next, we discuss the sensitivity to ~~more~~ further physical and numerical parameters. ~~We found that convergence is usually more easily reached~~ Generally, we find faster convergence for higher moments than for λ_0 (not shown). Hence in the following, we confine our analysis to the most "critical" quantity, and Fig. 5 displays the λ_0-evolution for various sensitivity experiments.

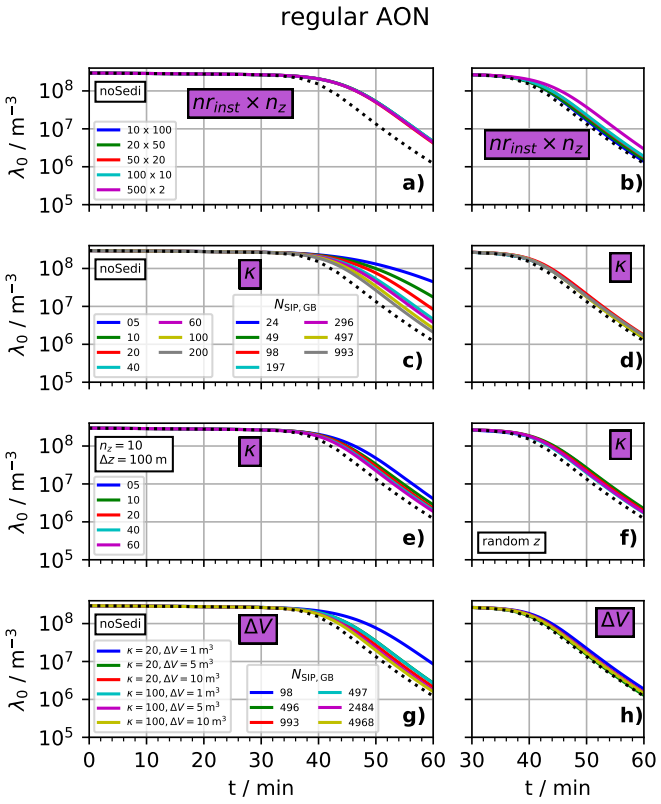

Figure 5. BoxModelEmul setup: Temporal evolution of column-averaged moment λ_0 (i.e. droplet concentration) over one hour for the regular AON version. The default setting is $n_z = 50, nr_{\text{inst}} = 20, \Delta V = 1\,\text{m}^3, \Delta t = 10\,\text{s}, \Delta z = 10\,\text{m}, \kappa = 40$ and $L_z = n_z \times \Delta z$. The microphysical parameters of the initial exponential droplet size distribution are $LWC_{\text{init}} = 1\,\text{g/m}^3, r_{\text{init}} = 9.3\,\mu\text{m}$ and $DNC_{\text{init}} = 297\,\text{cm}^{-3}$ as in many previous studies (Berry, 1967; Wang et al., 2007) . The parameter or parameter pair that is varied is added in a purple box to each panel and the legend lists the parameter values for the different colours. If further parameters (besides the varied parameter) take non-default values, it is indicated inside a black rectangle. In any case, the total number of GBs is $nr_{\text{inst}} \times n_z = 1000$. By default, sedimentation is switched on. Simulations without sedimentation and independent rain formation in each GB (identical to a box model treatment) are labelled as "noSedi" (appear only in the left column). The panels on the right use a shortened time range.

Even though we analyse the results in some detail, we want to mention that the observed differences are in principle not substantial. In fact, results differ ~~often~~ much more due to a different collection kernel or slightly varied initial DSDs (see section 3.1.4). Nevertheless, the analysis will help to understand more deeply how ~~collection~~ collisional growth works in an LCM with AON. This pronounced effort is justified, as precipitation initiation is still not fully understood and a well-validated Lagrangian approach may lead to new insights (Dziekan and Pawlowska, 2017; Grabowski et al., 2019).

In a first simple step, we vary ~~nz~~ n_z (see first row of Fig. 5), which changes two aspects of the numerical setup. The number of GBs over which interactions can occur and secondly the height of the column. This implicitly changes the time it takes for SIPs to fall through the total column and hence changes the "recycling" time scale ~~L_z/w_{sed}~~ L_z/w_{sed}. Together with ~~nz, nr_{inst}~~ n_z, nr_{inst} is varied such that ~~$nz \times nr_{inst}$~~ $n_z \times nr_{\mathrm{inst}}$ is always 1000. Accordingly, all simulation results are averaged over the same number of GBs and we avoid that simulations with smaller ~~nz~~ n_z produce noisier data.

In the noSedi-simulations (panel a), the moment evolution is not affected by varying (~~nz, nr_{inst}~~n_z, nr_{inst}). This is trivial, as in any case the average is taken over 1000 independent GBs. At least, these results demonstrate that averaging over that many GBs suffices by far to produce robust averages. In the full simulations (panel b), the λ_0-decrease is more pronounced and the various setups produce nearly identical results (except for the case with ~~$nz = 2$~~ $n_z = 2$, which is in between the other full simulations and the noSedi simulations). From this finding alone one may argue that the ~~collection~~ collisional growth process is more efficient in LCM1D than in LCM0D.

The second row shows a variation of κ which reveals qualitatively different convergence properties of the noSedi simulations (panel c) and the full simulations (panel d). In the noSedi simulations, an increase of κ (and ~~N_{SIP}~~ N_{SIP}; see extra legend for according ~~N_{SIP}~~ N_{SIP}-values) leads to a faster decrease of λ_0. Large differences between $\kappa = 5$ and 40 simulations are apparent; above $\kappa = 40$, an increase of κ leads only to marginal improvements. Also for the highest κ, the λ_0-values remain ~~slightly above the bin~~ above the BIN0D reference. For the smallest κ-value, only 24 SIPs are created according to Eq. 16 and interactions among that few computational particles ~~overemphasize~~ overemphasise the impact of correlations. It is well-known that for small ensembles of real droplets correlations become important (Bayewitz et al., 1974; Wang et al., 2006). ~~Analougusly~~Analogously, we introduced correlations in our numerical approach by using too few computational particles. We ~~believe~~ speculate that this hinders the formation of lucky droplets and fewer droplets get collected (hence λ_0 is larger for smaller κ). Another more technical explanation is that the ν_p-distribution of the SIP ensemble is such that the formation of lucky SIPs is not supported. Ideally, there is a reservoir of SIPs with small ν-values ~~which~~ that can become lucky SIPs. There might be too few SIPs with small ν for small κ.

Contrarily, the full simulations (panel d) give nearly identical results independent of κ. We obtain converged results with as few as 24 SIPs in each GB. Compared to $\kappa = 200$ with 1000 SIPs, the simulations are a factor 40^2 faster. The reason for the much faster convergence in terms of ~~$N_{SIP,GB}$~~ $N_{\mathrm{SIP,GB}}$ is that the GBs are interconnected which effectively raises the number of potential collision partners. Drops with ~~radius~~ radii of 100 and $500\,\mu\mathrm{m}$ have fall speeds of around $0.7\,\mathrm{m\,s^{-1}}$ and $4\,\mathrm{m\,s^{-1}}$, respectively. Thus it takes them around 14 s and 2.5 s to fall through a $\Delta z = 10\,\mathrm{m}$-GB and they enter a new GB every or every few time steps given $\Delta t = 10\,\mathrm{s}$.

How strongly SIPs are interconnected across GBs in LCM1D should depend also on geometrical properties of the column. In the next setup, we investigate the κ-sensitivity in a column with ~~$nz = 10$~~ $n_z = 10$ and $\Delta z = 100\,\mathrm{m}$ instead of ~~$nz = 50$~~ $n_z = 50$ and $\Delta z = 10\,\mathrm{m}$ (panel e). Then, SIP interactions can occur only across 10 GBs and overall five times fewer SIPs are present in the column than for the default case with ~~$nz = 50$~~$n_z = 50$. Moreover, the domain is stretched by increasing Δz to $100\,\mathrm{m}$, which increases the residence time of a SIP in a GB by a factor 10, slowing down additionally SIP interactions across GBs. Those two changes introduce a weak κ-dependence, yet it is much weaker than in the corresponding noSedi-simulations (panel c).

In ~~a technical~~ an even more academic experiment, sedimentation is turned off, but SIPs are randomly redistributed inside the column after each time step (panel f) similar to Schwenkel et al. (2018). Again, we find converged results for small κ-values down to 5 (panel f). This elucidates that convergence is improved once some process exchanges SIPs between GBs, may it be for physical reasons like sedimentation or by an artificial operation as the ~~randomized~~ randomised SIP re-location. We speculate that in full 2D/3D LCM-simulations turbulent motions and sedimentation increase the SIP exchange across GBs and hence may additionally increase the performance of AON. The two ~~latter~~ last simulation series are promising, as they suggest that in a column model (and probably also 2D/3D model) convergence is potentially reached with fewer SIPs per GB than in a box model. Nevertheless the tests also highlight that convergence with κ depends on many circumstances and convergence tests are prerequisite to any LCM simulation with AON.

In bin models, the Smoluchowski equation, which is strictly valid only for an infinite volume and hence an infinite number of well-mixed droplets, is solved. Accordingly, only concentrations are prescribed in bin model algorithms. Neither ΔV nor the absolute number of droplets is considered in this approach. At least in the limit of all SIPs having weighting factor $\nu = 1$, the AON algorithm solves the master equation (Dziekan and Pawlowska, 2017) which takes into account ΔV and results may depend on the actual number of involved droplets. Clearly, correlations (which are accounted for in the master equation) are larger in smaller volumes (Bayewitz et al., 1974; Wang et al., 2006; Alfonso and Raga, 2017).

For ~~the given~~ our SIP-initialisation procedure, ~~$N_{SIP,GB}$~~ $N_{\mathrm{SIP,GB}}$ depends solely on the chosen κ-values and is independent of ΔV. By construction, a ΔV-variation does not affect at all the simulation results, as all SIP weights are simply rescaled. Indeed, we obtain nearly bit-identical results for a ΔV-variation. To explore the ΔV-sensitivity in our LCM1D, the SIP-init procedure has to be adapted. In the adapted version the SIP number increases proportionally with ΔV as it would in reality. As computational requirements increase quadratically with ~~$N_{SIP,GB}$~~ $N_{\mathrm{SIP,GB}}$, the variation of ΔV and ~~$N_{SIP,GB}$~~ $N_{\mathrm{SIP,GB}}$ can be performed only for a small range of ΔV-values. ΔV is increased by a factor of five or ten. As a base case, we use the simulations with $\kappa = 20$ and $\kappa = 100$ and define $\Delta V := 1\,\mathrm{m}^3$. The fourth row shows results for the noSedi (panel g) and the full simulations (panel h). Apparently, the noSedi-simulations with larger ΔV converge to the solution we obtained before by using a sufficiently large κ. In full simulations, a ΔV-variation has basically no effect. The $\kappa = 100, \Delta V = 10\,\mathrm{m}^3$-simulation considered on average collisions between 5000 SIPs in each GB. Yet, the results are basically identical to the case $\kappa = 5, \Delta V = 1\,\mathrm{m}^3$ with 24 SIPs in each GB (which runs nearly 40000 times faster).

In the present simulations where SIPs with weights $\nu > 1$ are used, variations of the numerical parameter κ and the physical parameter ΔV are interconnected and their effects cannot be disentangled. Hence, the AON algorithm can only answer

whether correlations matter in systems with a certain number of SIPs. These correlations are not necessarily the correlations one would see in a real system with millions to billions of real droplets. Nevertheless, the last sensitivity series implies that at least in our model system the importance of correlations are likely the same in a system with ~~$N_{SIP,GB} = 24$ and with $N_{SIP,GB} \approx 5000$~~ $N_{\mathrm{SIP,GB}} = 24$ and with $N_{\mathrm{SIP,GB}} \approx 5000$. Assuming that the importance of correlations in a real system with billions of droplets is similar to that of a system with 5000 SIPs, the latter finding demonstrates that LCMs can capture the ~~collection~~ collisional growth process with astonishingly few SIPs.

The noSedi κ-sensitivity series as shown in panel c) was already presented in Fig. 18 of U2017. There ~~it was~~ we found that for high enough κ the LCM0D results lie below the BIN0D reference contradictory to the present noSedi simulations. The reason for this inconsistency is a programming bug in the LCM0D-AON version used in U2017. The Hall/Long kernel values are stored in look-up tables and were wrongly accessed (overestimating the actual mass of the involved droplets by 2%). Hence, the ~~collection~~ collisional growth process proceeded more rapidly in U2017. Despite this flaw, the main findings of U2017 remain valid. Yet, the more rapid ~~collection~~ collisional growth of LCM0D-AON in U2017 should clearly not be attributed to conceptual differences of AON and BIN algorithms.

3.1.2 ~~AON with linear sampling~~

~~BoxModelEmul setup:The plots are analogous to Fig. 5 (all setup parameters are listed in that caption), now simulations with linear sampling (as described in section 2.3.3) are depicted. The left column shows noSedi simulations, the right column shows LCM1D simulations..~~

~~Figure ?? displays again the~~ In the discussion of the subsequent sensitivity studies, we refrain from showing time series of λ_0 ~~-evolution in Δt~~as done in Fig. 5. Instead we only evaluate λ_0 at $t = 1\,\mathrm{h}$ as this is a suitable metric for the algorithm performance in the BoxModelEmul setup. Figure 6 comprises Δt- and κ-sensitivity ~~studies, now f or the WM3D~~ series of all subsequent BoxModelEmul simulations. The black dotted (horizontal) line depicts the reference BIN result obtained with Wang's algorithm with $s = 16$ and $\Delta t = 1\,\mathrm{s}$ and was already added in Fig. 5 for orientation.

3.1.2 AON with linear sampling

This subsection discusses the AON version with linear sampling~~(LinSamp). The left/right column of the figure shows results without/with sedimentation. For the default time step of $\Delta t = 10\,\mathrm{s}$, results do not converge and are far off the desired result (first row). Reducing the time step to $\Delta t = 1\,\mathrm{s}$ increases the number of tested collisions by a factor of 10. This seems to be a crucial point as the results now converge (second row); for the noSedi-case only for the highest~~ Both, full simulations and noSedi simulations have been carried out. The first row of Figure 6 shows sensitivity of $\lambda_0(t = 1\,\mathrm{h})$ to κ ~~-values, for the full simulation~~ (left) and Δt (right), respectively. The grey curves repeat the regular AON results (i.e. with quadratic sampling); they show the endpoints of curves shown in Fig. 4 top and Fig. 5 c) and d). We find that the qualitative behaviour does not differ between LinSamp and regular AON.

In the full simulations (solid lines), simulations converge for any κ.~~-~~

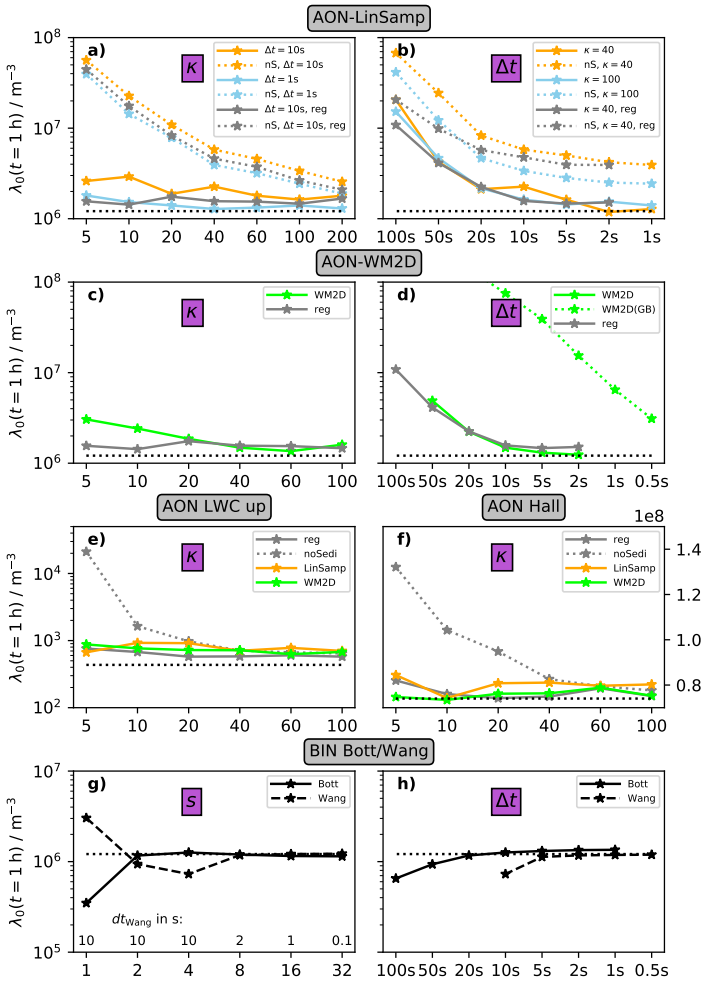

Figure 6. BoxModelEmul setup: This figure summarises results of many sensitivity studies for various AON versions and BIN simulations by displaying DNC after one hour as a function of resolution κ (or analogously s in BIN models) and time step Δt. The default parameter settings are listed in Fig. 5 and the horizontal black dotted curve shows the BIN benchmark reference. For example, the information of panels c) and d) in Fig. 5 is compressed into the two grey curves in panel a). Panels a) and b) additionally show AON simulations with linear sampling (as described in section 2.3.3), unless "reg" in the legend indicates regular AON with quadratic sampling. "nS" is short for "NoSedi". The second row shows simulations with explicit overtakes and a 2D well-mixed assumption ("WM2D", as described in section 2.3.2). Again, the regular AON with WM3D serves as reference. In the simulation labelled "WM2D(GB)", overtakes are considered only between SIPs inside the same GB, whereas "WM2D" checks overtakes in the full column. Panel e) shows a scenario with (increased) $LWC_{\mathrm{init}} = 1.5\,\mathrm{g/m^3}$ and panel f) uses the Hall kernel instead of the Long kernel. Note that the y-ranges are different in the third row. The fourth row shows BIN results with Bott's and Wang's algorithms. The default parameters are $s = 4$ and $\Delta t = 10s$.

Finally, Δt is varied between 1 and 20 s. This is roughly the Δt-range for which the QuadSamp simulations produced more or less converged results. Here, we find convergence only for time steps as small as 5 s. We attribute this , whereas for the noSedi-simulations (dotted, "delayednS" Δt-convergence to the fact that SIP combinations, where ν_{coll} is limited to $0.99 \max(\nu_i, \nu_j)$, occur too often and that this "limiter" effect becomes negligible only for small enough time steps.

In general, we find that switching off sedimentation in the LinSamp simulations deteriorates the convergence properties, as already seen in the QuadSamp simulations.

All in all, convergence in the in the legend) convergence is reached only for largest κ-values. Using the default time step $\Delta t = 10$ s, the LinSamp simulations is reached only for smaller Δt relative to the QuadSamp simulations. Hence, the potential benefit of results (orange curves) are slightly further away from the BIN reference (black dots) than the regular results. A second LinSamp series with $\Delta t = 1$ s (blue) produces better results than the regular AON version with $\Delta t = 10$ s.

The Δt-sensitivity series shown in the reduced computational cost may be outweighed by the stronger requirements on Δt. In particular, in full 2D/3D LCMs also condensation/deposition and sedimentation has then to be solved more often unless subcycling is introduced. Whether LinSamp or QuadSamp is in the end more efficient in a full 2D/3D LCM may depend also on the simulated cloud type and the complexity of right panel demonstrates that LinSamp results are slightly worse than the regular results for the LCM (inclusion of aerosol physics, chemistry or different hydrometeor types, e.g. as in Jaruga and Pawlowska, 2018; Brdar And indeed, Dziekan et al. (2019) presents 2D and 3D LCM simulations using the LinSamp approach and they see convergence only for a rather small time step of $dt = 0.1$ s, which is probably caused by the slow convergence of LinSamp default resolution $\kappa = 40$. Using LinSamp with a finer resolution of $\kappa = 100$ produces better results than the regular AON with $\kappa = 40$. In LinSamp simulations with large time steps, limiter cases occur quite often and one may expect that the artificial reduction of collection events strongly deteriorates the model outcome. However, we see that the performance in the high-Δt range drops similarly in the LinSamp and regular AON version.

3.1.3 AON version with explicit overtakes

3.1.4 AON version with explicit overtakes

BoxModelEmul setup:The plots are analogous to Fig. 5 (all setup parameters are listed in that caption), now simulations with explicit overtakes and a 2D well-mixed assumption (as described in section 2.3.2) are depicted. In the top panel overtakes are considered only between SIPs inside the same GB, whereas the other panels show the regular version where overtakes are tested for all SIPs of the column..

Next, we will discuss results of the AON-WM2D version with explicit overtakes. Figure ?? displays again the temporal evolution of λ_0.Results are presented in the second row of Fig. 6. For the chosen setup with homogeneous initial conditions and periodic boundary conditions, 3D well-mixedness of the SIPs is expected to be maintained over the course of the simulation. Hence, the AON-WM3D and AON-WM2D version are supposed to produce similar outcomes. Panel a

The dotted, green curve in panel d) shows results for the version where only intra-GB overtakes are considered. Results are far off the benchmark curve, only for the smallest time step of $\Delta t = 0.5$ s they tend to approach become close to the reference.

~~Panel b shows the same~~ The solid, green curve shows a Δt-variation (down to $\Delta t = 2\,\mathrm{s}$) for the version where overtakes are considered across the full column. In the present example, it was also necessary to check for overtakes across the periodic boundary. Then, convergence is reached for $\Delta t \leq 10\,\mathrm{s}$, very similar to the regular ~~AON-WM3D version . The bottom row (WM3D) version (see grey curve for comparison). Panel c)~~ shows a slight dependence on κ, yet ~~AON-WM2D results seem to converge to the WM3D-results~~the performance of AON-WM2D is almost comparable to that of the regular AON results.

Overall, we can conclude that the feasibility and correct implementation of the ~~WM2D-variant~~ WM2D-version was demonstrated, with the caveat that overtakes have to be considered in the full column. Checking for overtakes outside of the "own" GB can cause some computational overhead in implementing the WM2D-version in higher-dimensional cloud models, which are typically parallelised. If the chosen time step for collection obeys the CFL criterion (as argued in Shima et al., 2019) , SIPs can at most travel from one GB to the one right below. Then, potential collision partners can only appear in two different GBs.

As noted in section 2.3.2, the WM2D version can only be used in conjunction with kernels where the differential sedimentation term $|w_{\mathrm{sed},i} - w_{\mathrm{sed},j}|$ is explicitly included and can be dropped. Typically, this is not fulfilled for kernels accounting for turbulence enhancement, in which motions in all spatial directions need to be accounted for. Turbulence in cirrus clouds is often weak. Moreover, cirrus clouds often show a strong layering by ice crystal size possibly making the 3D well-mixed assumption overly simplistic. Hence, the WM2D version appears to be a reasonable alternative to the regular (WM3D) version. Furthermore, the mixed-phase LCM of Shima et al. (2019) used for the simulation of a cumulonimbus employs a hydrodynamic kernel. Hence, the WM2D version would be applicable in this context as well.

3.1.4 Microphysical and bin model sensitivities

So far, all simulations were initialised with the same initial DSD, the same collection kernel, and the results ~~are~~ have always been compared to the same ~~bin reference .~~ BIN reference simulation.

Accordingly, in this section, we perform simulations with modified ~~LWC, r_0 and DNC~~ $LWC_{\mathrm{init}}, r_{\mathrm{init}}$ and DNC_{init}. Moreover, we highlight the effect of the employed kernel on the AON performance. And finally, we also present ~~bin model~~ BIN sensitivities (namely, we switch from Bott's algorithm to Wang's algorithm and vary the bin resolution and the time step).

~~BoxModelEmul setup:Figure analogous to Fig. 5 (all setup parameters are listed in that caption), now displaying also the temporal evolution of the mean diameter (top row) and the second moment λ_2 (bottom row) additional to λ_0 (middle row). Variations of the initial size distribution parameters $LWC = \lambda_1(t=0), r_0$ and $DNC = \lambda_0(t=0)$ are performed. The first and second column show a variation of LWC (see inserted legend) for either fixed DNC or r_0. The third column shows a DNC-variation for fixed LWC. Four different models are used (AON-WM3D, AON-WM2D, noSedi and BIN1D; see legend in top right panel).~~

~~BoxModelEmul setup:The plots are analogous to Fig. 5 (all setup parameters are listed in that caption) and the sensitivity to κ is shown for simulations with the Hall kernel. The left and right panel juxtapose noSedi and full simulations. Unlike to previous plots, the y-axis uses a linear scale.~~

In a first experiment, we increase ~~LWC~~ LWC_{init} by a factor of 1.5 and ~~do again a~~ repeat the κ-sensitivity test~~(~~, see panel e) of Fig. ~~??~~)6. We keep ~~DNC~~ DNC_{init} fixed and hence the mean radius is ~~$r_0 = 9.3\,\mu\mathrm{m} \times 1.5^{(1/3)} = 10.7\,\mu\mathrm{m}$~~ $r_{\mathrm{init}} = 9.3\,\mu\mathrm{m} \times 1.5^{(1/3)} = 10.7\,\mu\mathrm{m}$

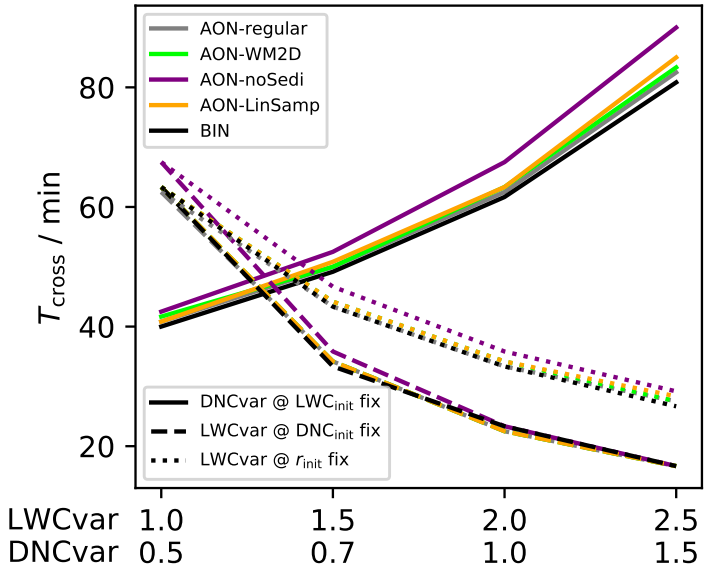

Figure 7. BoxModelEmul setup: ~~The plots are analogous~~ Sensitivities to ~~Fig. 5 (all setup~~ the initial size distribution parameters ~~are listed in that caption)~~ LWC_{init}, r_{init} and DNC_{init} are summarised by showing T_{cross}, which is defined as the ~~sensitivity to κ~~ time when λ_0 drops below $10^7\,\mathrm{m}^{-3}$. LWC_{init} is ~~depicted~~ varied (the x-axis shows the scaling factor LWCvar relative to the default LWC_{init}) for ~~simulations with initial $LWC = 1.5\,\mathrm{g/m}^3$~~ either fixed DNC_{init} (dashed lines) or r_{init} (dotted lines). The solid lines depicts a DNC_{init}-variation for fixed LWC_{init}. Again, the scaling factor DNCvar is depicted on the x-axis. Five different model versions, as indicated in the top left ~~and right panel juxtapose~~ legend, are used: regular AON (reg), AON-WM2D, regular AON with noSedi ("nS"), AON with LinSamp ("LS") and ~~full simulations~~BIN.

Compared to the base case with ~~$LWC = 1$~~$LWC_{init} = 1\mathrm{g/m}^3$, λ_0 starts to decrease after 20 minutes (instead of 40 min~~) and~~ , see Fig. S10). Eventually, λ_0 decreases below $10^4\,\mathrm{cm}^{-3}$ (instead of $10^6\,\mathrm{cm}^{-3}$). In the full simulations (~~right panel~~all solid curves), we again find results nearly independent of κ for all tested AON versions (regular, LinSamp and WM2D). In the ~~noSedi-sims (left panel~~noSedi simulations (grey, dotted curve), fewer SIPs are necessary to obtain reasonable results compared to the base case ~~(see Fig 5c~~in panel a).

In a next step, the characteristics of the initial DSD are more ~~flexibly~~ systematically varied for fixed $\kappa = 40$. For such a κ-value the noSedi-simulation of the base case was considerably off the reference. ~~Figure 7 shows the temporal evolution of~~ $LWC_{init} = \lambda_1(t_0)$ is varied, for either fixed droplet number or fixed mean radius. The default value is scaled by factor of 1.5, 2.0 or 2.5. Similarly, DNC_{init} is varied by factor of 0.5, 0.7 or 1.5 keeping LWC_{init} constant.

A more detailed presentation of simulation results with time series of the mean diameter, λ_0 and λ_2 ~~(from top to bottom)~~ over 100 min ~~.~~is deferred to SUPP (see Fig. S11). Here, we focus on a single metric again. We define T_{cross} as the time, when λ_0 drops below $10^7\,\mathrm{m}^{-3}$. The smaller T_{cross}, the faster precipitations sets in. Figure 7 shows T_{cross} for all three sensitivities series (see lower left legend for the various linestyles). Simulations with the ~~Bott model~~ BIN are contrasted with the regular ~~AON-WM3D~~AON, AON-WM2D and AON-noSedi ~~. The first two columns show simulations for a variation of the initial~~

~~$LWC_0 = \lambda_1(t_0)$, for either fixed droplet number or fixed mean radius. The right-most column shows a variation of the initial droplet number. The default value (denoted as "1" in~~ and AON-LinSamp (see upper left panel for the ~~legend) is scaled by factor of 1.5, 2.0 or 2.5 (for a LWC-variation) and 0.5, 0.7 or 1.5 (for a DNC-variation). We find for most cases, that the three model versions produce very similar λ_2-evolutions. The bin model~~ various colours). T_{cross} and with it precipitation onset changes strongly with LWC_{init} and DNC_{init}. Generally, we find a similar behaviour across all tested models. The AON-noSedi version features the largest T_{cross}-values. This is consistent with previous noSedi-results in Fig. 5 where the decrease in λ_0 lags behind. All other AON versions match well and are close to the BIN results. Only for the largest DNC_{init}-value some spread in T_{cross} exists. Fig. S11 shows that BIN predicts in all cases slightly ~~higher droplet numbers λ_0 than the AON version. The WM2D are in between the WM3D and the bin model. As a consequence, the mean droplet diameter increases the fastest with the WM3D version.~~

~~Figure ?? shows simulations where the~~ lower droplet numbers similar to what we already observed for the default microphysical initialisation in Fig. 5. Nevertheless, we can confirm the very good agreement of BIN and all full AON simulations.

As a last AON sensitivity study, the default Long kernel is replaced by the Hall kernel. Panel f) of Fig. 6 shows the according results. The decrease in ~~DNC~~ λ_0 occurs at a slower rate (the y-scale now uses a linear scale). For the full simulations (~~right~~solid curves), we obtain perfect agreement for any chosen κ-value and for all three model versions. Moreover, convergence with κ in the noSedi-simulations (~~left~~dotted curve) is less critical than in the base case (compare with panel a) again) and results converge for $\kappa \geq 40$. Timeseries of λ_0 of all Hall kernel simulations are shown in Fig. S12.

~~BoxModelEmul setup:The plots are analogous to Fig. 5. The left and right panel juxtapose BIN results with Bott's and Wang's algorithms. The default parameters are $s = 4$ and $dt = 10s$. Unlike to the AON case, the choice of nz is irrelevant.~~ So far, all reference BIN results were obtained with Wang's algorithm, using a time step $\Delta t = 1\,\mathrm{s}$ and resolution $s = 16$. We conclude the box model emulation section by showing sensitivities of ~~the bin model approach~~two BIN versions. For this, we vary the bin resolution s and the time step for the base case with ~~$LWC = 1$~~$LWC_{\mathrm{init}} = 1\,\mathrm{g/m^3}$ and Long kernel and apply either Bott's or Wang's algorithm. The default time step is ~~again $dt = 10\,\mathrm{s}$~~ $\Delta t = 10\,\mathrm{s}$ as in the AON simulations and the bin resolution is $s = 4$. The ~~left and right column~~ fourth row of Fig. ~~??~~ 6 show results obtained with Bott's and Wang's algorithm, respectively. ~~The black reference curve in Figs. 4 to ?? are data from Wang's algorithm with $s = 16$ and $dt = 1\,\mathrm{s}$ and is also added to the present plot for orientation.~~ Again, λ_0-timeseries of these BIN simulations are shown in Fig. S13.

We find that Bott's algorithm converges for $s \geq 2$ ~~. For higher resolutions,~~ (left panel). Wang's algorithm, on the other hand, does not produce stable results for ~~$dt \geq 10\,\mathrm{s}$ and~~ higher resolutions and $\Delta t = 10\,\mathrm{s}$. Thus, the time step had to be reduced (see inserted legend, for the combination of s and ~~dt~~Δt). For $s \geq 8$ results have converged to the reference. The ~~second row~~ right panel shows the time step dependency for a medium resolution of $s = 4$. ~~Bott's results are reliable for dt as high as $100\,\mathrm{s}$ and converge for $dt \leq 20\,\mathrm{s}$. On the other hand,~~ While Bott yields stable results for $\Delta t \leq 100\,\mathrm{s}$, the results only converge for $\Delta t \leq 20\,\mathrm{s}$. We can even see a slight dependence of $\lambda_0(t = 1\,\mathrm{h})$ on Δt. As as side note, this is is a clear indication that the BIN reference values used for orientation so far should not be interpreted as absolute reference and it would be premature to discredit AON results being slightly above the BIN reference.

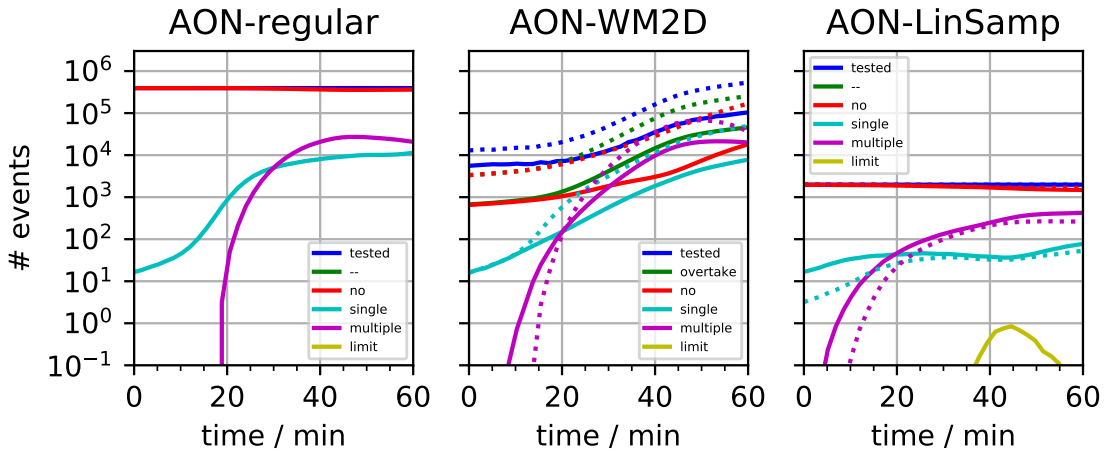

Figure 8. BoxModelEmul setup: Time series of number of events in the various AON ~~implementation~~versions. Shown are the number of tested SIP combinations, of overtakes, of no collection, of a single collection, of a multiple collection in every time step. Additionally, the number of limiter cases, where ~~n_{coll}~~ ν_{coll} had to be artificially reduced, is shown (occurs only in the LinSamp-panel). The parameter setup is given in the text. In the WM2D-panel, the dotted lines show the case with ~~$dz = 10\,\text{m}$~~$\Delta z = 10\,\text{m}$. In the LinSamp-panel, the dotted lines show the 1 s-simulation. The displayed numbers can be below unity, as averages over 20 instances are shown.

Wang's algorithm~~requires $dt \leq 10\,\text{s}$~~, on the other hand, requires $\Delta t \leq 10\,\text{s}$ for stable results, and convergence is reached for ~~$dt \leq 5\,\text{s}$~~$\Delta t \leq 5\,\text{s}$. Overall, we can conclude that both algorithms converge to basically the same values, given a sufficiently high s and ~~low dt~~ small Δt is chosen. As Bott's algorithm ~~seems~~ appears to be more robust than Wang's algorithm, all following ~~bin model~~ BIN simulations are carried out with this algorithm.

Comparing the various ~~collection~~ collisional growth algorithms, we find that Bott's algorithm has the least requirements in terms of bin resolution and time step as we have converged results for t up to 100 s and s as low as 2. AON simulations may converge for $\kappa = 5$ (corresponds roughly to $s = 2$) and ~~$dt = 10\,\text{s}$~~ $\Delta t = 10\,\text{s}$ if GBs of the column are sufficiently interconnected and averaging over several realisations is done. Wang's algorithm produces correct solutions for $s = 4$ and ~~$dt = 5\,\text{s}$~~$\Delta t = 5\,\text{s}$, yet increasing the bin resolution has to be done hand in hand with a reduction of the time step.

3.2 ~~Analysis of the "algorithmic interior"~~Algorithm profiling

Now, we turn the attention to ~~the processes in the "algorithmic interior"~~ an algorithm profiling of the various AON versions.

Figure 8 and ~~Tab.~~Table 3 give an example of how often collections occur in the model. For AON-WM2D, also the number of overtakes is given. The listed numbers give a rough indication of the importance of the various events (overtake, no collection, single collection, multiple collection, limiter), yet we want to note the caveat that the relative importance changes with a change of the parameter setup. Here, results are shown for the specific setup with ~~$nz = 20, nr_{inst} = 10, \Delta V = 1\,\text{m}^3, \Delta t = 5\,\text{s}, \Delta z = 50\,\text{m}$~~ $n_z = 20, nr_{\text{inst}} = 10, \Delta V = 1\,\text{m}^3, \Delta t = 5\,\text{s}, \Delta z = 50\,\text{m}$ and $\kappa = 40$. The figure shows qualitatively the number of ~~occurences~~

Table 3. BoxModelEmul setup: Number of events for various AON ~~model variants~~ versions for the parameter setup given in the text. ~~N_{comb}~~ N_{comb} is the number of tested SIP combinations and ~~N_{LI}~~ N_{LI} is the number of limiter cases, where ~~n_{coll}~~ n_{coll} had to be artificially reduced. Moreover, ~~$\eta_{OT}, \eta_{NO}, \eta_{SI}$~~ $\eta_{\mathrm{OT}}, \eta_{\mathrm{NO}}, \eta_{\mathrm{SI}}$ and ~~η_{MU}~~ η_{MU} specify the number of overtakes, no collections, single collections and multiple collections divided by ~~N_{comb}~~ N_{comb}. The two last columns shows summed up p_{crit} (summed over all times and SIP combinations/overtakes) and the average p_{crit}. For each ~~model variant~~AON simulation, the first three rows show aggregate values over three time periods ($0-20\,\mathrm{min}, 20-40\,\mathrm{min}$ and $40-60\,\mathrm{min}$) and the fourth row values for the full time period.

Model ~~variant~~version	tested SIP combinations ~~N_{comb}~~ N_{comb}	overtakes ~~η_{OT}~~ η_{OT}	no collision ~~η_{NO}~~ η_{NO}	single collision ~~η_{SI}~~ η_{SI}	multiple collision ~~η_{MU}~~ η_{MU}	limiter event ~~N_{LI}~~ N_{LI}	$\sum p$
	9.44e7	-	100.0%	0.0%	0.0%	0	2.91
block #1	9.44e7	-	97.0%	1.2%	1.8%	0	4.25
~~AON-WM3D~~ AON-WM3D	9.45e7	-	91.2%	2.5%	6.3%	0	1.95
	2.83e8	-	96.1%	1.3%	2.7%	0	2.38
	1.49e6	13.9%	12.7%	0.8%	0.3%	0	2.70
block #2	3.83e6	34.7%	11.9%	4.5%	17.8%	0	3.64
~~AON-WM2D~~ AON-WM2D	1.77e7	44.1%	12.1%	6.4%	25.3%	0	2.15
	2.30e7	40.6%	12.2%	5.8%	22.5%	0	2.52
	3.64e6	28.6%	27.7%	0.7%	0.0%	0	2.85
block #3	1.53e7	43.9%	22.0%	6.5%	14.9%	0	3.62
~~AON-WM2D, $dz = 10\,\mathrm{m}$~~ AON-WM2D, $\Delta z = 10\,\mathrm{m}$	8.89e7	47.5%	23.9%	8.4%	15.0%	0	1.79
	1.08e8	46.4%	23.8%	7.9%	14.5%	0	2.15
	4.76e5	-	~~98.0%~~97.9%	1.6%	0.5%	0	~~2.89~~
block #4	4.76e5	-	90.9%	2.2%	6.9%	~~122~~11	~~3.48~~
~~AON-WM3D~~AON-WM3D, LS	4.76e5	-	~~76.3%~~78.7%	~~3.2%~~2.6%	~~20.5%~~18.7%	~~1343~~87	~~3.21~~
	1.43e6	-	~~88.4%~~89.2%	~~2.3%~~2.1%	~~9.3%~~8.7%	~~1465~~99	~~3.56~~
	2.38e6	-	99.3%	0.6%	0.1%	0	~~3.31~~
block #5	2.38e6	-	~~93.0%~~92.9%	1.7%	~~5.3%~~5.4%	~~14~~0	~~4.45~~
~~AON-WM3D~~AON-WM3D, LS, ~~$dt = 1\,\mathrm{s}$~~ $\Delta t = 1\,\mathrm{s}$	2.38e6	-	~~84.6%~~85.0%	~~2.1%~~2.0%	~~13.3%~~12.9%	~~24~~0.40	~~2.14~~
	7.14e6	-	~~92.3%~~92.4%	~~1.5%~~1.4%	6.2%	~~38~~0.40	~~2.58~~

occurrences as a function of time, whereas the table gives aggregate values for three 20 min blocks and the total 60 min simulation period. In both WM3D versions (regular ~~QuadSamp~~ and LinSamp), the number of tested SIP combinations N_{comb} is constant over time. Clearly, the LinSamp value is smaller by a factor of 200 ($= N_{\mathrm{SIP}}$) and implies a faster execution. For the ~~WM2D-approach~~WM2D-version, on the other hand, N_{comb} increases over time as the DSD gets more mature and larger droplets fall faster. Relative to the regular (WM3D) version, N_{comb} of WM2D is at any time smaller. In the beginning of the simulation, possible overtakes occur among relatively few SIPs; much fewer on average than there are in a GB, hence the total N_{comb} is around a factor 60 smaller (in the first 20 minutes; $9.44 \cdot 10^7$ vs. $1.49 \cdot 10^6$). Even towards the end of the simulation, many SIPs are still small and travel through a small fraction of the GB. Only few SIPs grow to rain drop size and travel distances of order Δz. The table shows that the total (time-integrated) N_{comb} is more than a factor 12 smaller for WM2D than for WM3D ($2.30 \cdot 10^7$ vs. $2.83 \cdot 10^8$). This demonstrates the numerical efficiency of the current WM2D implementation despite a theoretically unfavorable computational complexity with a factor ~~nz~~ n_z higher N_{comb} compared to the regular WM3D version.

Moreover, the workload per time step is constant in ~~the~~ both WM3D-versions and determined solely by N_{SIP}. In the WM2D-version, the workload depends additionally on the properties of the DSD and also on Δz. If Δz is reduced by a factor of 5 (see block #3 in the table), N_{comb} roughly increases by the same factor. Similarly, we found a longer execution time of WM2D in the LWCup-series than in the base case (not shown).

In the table, the ratios ~~η_{NO}, η_{ST} and η_{MU} (find their definitions in the caption of the table)~~ η_{NO}, η_{SL} and η_{MU} specify the number of no collections, single collections and multiple collections divided by N_{comb}, and add up to 100% for both WM3D ~~(QuadSamp and LinSamp)~~versions. In the regular WM3D version, only 1.3% and 2.7% of all tested ~~combination~~ combinations lead to a single or multiple collection. So, for most combinations p_{crit} is close to zero and makes a collection unlikely. On the other hand, for favourable SIP combinations p_{crit} can be far above 1 (imagine a SIP combination with $\nu_i = 10^6, \nu_j = 10^2$ and ~~$\nu_{coll} = 10^4$~~ $\nu_{\mathrm{coll}} = 10^4$ yielding $p_{\mathrm{crit}} = 100$). This also explains the somewhat surprising fact that the average $\bar{p}_{\mathrm{crit}}$ is close to unity ($= 0.83$, see right-most column). The PDF (probability density function) of all p_{crit}-values is strongly right-skewed (not shown). In the LinSamp case, single and multiple collections occur in ~~2.3% and 9.3%~~ 2.1% and 8.7% of the tested combinations. Collections are more likely as $\bar{p}_{\mathrm{crit}}$ is larger due to the upscaling. Moreover, ~~ν_{coll}~~ ν_{coll} had to be artificially reduced in ~~$N_{LI} \approx 1400$~~ $N_{\mathrm{LI}} \approx 100$ cases. Note that such limiter cases do not appear in ~~the QuadSamp simulations~~any QuadSamp version (regular and WM2D). In the LinSamp version, ~~N_{LI}~~ N_{LI} can be cut down by choosing a smaller time step (see ~~fourth~~ fifth block in table). Using ~~$dt = 1\,\mathrm{s}$~~ $\Delta t = 1\,\mathrm{s}$ leads to 5 times smaller p_{crit}-values, increases ~~η_{NO}~~ η_{NO}, and decreases ~~η_{ST} and η_{MU}~~ η_{SL} and η_{MU}. Limiter cases ~~appear only in 38 of all combinations~~are now an extremely rare event. For clarification, p_{crit} of a single SIP combination scales with ~~dt^{-1}~~ Δt^{-1}; from this, however, does not follow that the listed $\bar{p}_{\mathrm{crit}}$-values of the two LinSamp simulation differ by a factor of ~~10~~5, as the DSDs and SIP ensembles/weights evolve differently in the two simulations.

Finally, we focus on the WM2D-version (block #2). Here, the sum of ~~η_{NO}, η_{ST} and η_{MU} yields η_{OT},~~ η_{NO}, η_{SL} and η_{MU} yields η_{OT}, the number of overtakes divided by N_{comb}, and not 100% as before. In the end, around 40% of all tested SIP combinations undergo an overtake. This quite large fraction comes from the fact that the DSD (or more precisely the size distribution of the SIPs) features a strong bimodal spectrum. So most tested combinations are combinations between a large collector SIP i and a small SIP j with $z_i > z_j$. ~~Tested SIP combinations fulfill~~ These tested SIP combinations fulfil by design

$z_i(t+\Delta t) < z_j(t)$. For small SIPs j, ~~$z_j(t+\Delta t) = z_j(t+\Delta t) - \epsilon$~~ $z_j(t+\Delta t) = z_j(t) - \epsilon$ holds. As ϵ is a small distance, it is likely that $z_i(t+\Delta t) < z_j(t+\Delta t)$ is fulfilled, i.e. SIP i overtakes SIP j. In more than every second overtake, a multiple collection occurs (i.e. ~~$\eta_{MU}/\eta_{OT} = 0.56$~~)$\eta_{\mathrm{MU}}/\eta_{\mathrm{OT}} = 0.56$). In one eights/one third of the overtakes a single/no collection happens. So the relative importance of the various events is quite different compared to the regular AON and also $\bar{p}_{\mathrm{crit}}$ is three times larger (2.69 vs. 0.83). Note that ~~Changing dz~~ changing Δz in the WM2D-simulation (block #3) also affects the relative ~~occurences~~ occurrences of no/single/multiple collections. In the WM3D-versions, the overall workload is proportional to Δt^{-1}. This is different in the WM2D-version. With increasing time step, droplets travel longer distances. Hence, the number of tested combinations and overtakes per time step increases.

Note that the relative occurrence frequency of p_{crit}-values may depend also on the spectrum of given ν_p values (i.e. on the SIP initialisation method).

~~In all five setups we find,~~ Figure S14 demonstrates that all five AON simulations converge and show a basically identical time evolution of λ_0. The analysis here shows that in the end more multiple collections than single collections appeared. ~~Except for the LinSamp version with $dt = 10\,\mathrm{s}$, the simulations converge.~~ Clearly, the ~~occurence~~ occurrence of multiple collections in a simulation does not necessarily deteriorate the simulation results. It is certainly not the case, that the time step choice or adaptation must be such that multiple collections barely appear in a simulation. ~~The present analysis only shows a correlation between the appearance of limiter cases and a non-converged simulation. Strictly speaking, we cannot even say that the limiter cases are the reason for the failure~~Beyond that, limiter events occurred in the LinSamp-simulation with $\Delta t = 10\,\mathrm{s}$ did not avert convergence. So even a certain amount of limiter events seems to be acceptable in terms of performance. Fig. 6b) showed that even for $\Delta t = 100\,\mathrm{s}$ LinSamp and regular AON produce similarly good results, albeit off from the reference.

Several of the above findings may hold only for the specific setup used here. To put the findings into a broader context, we next derive scaling relations for basic numerical quantities and, in particular, discuss their sensitivity to the time step and the number of SIPs. For a simplified presentation, we limit ourselves to the ~~WM3D versions with QuadSamp and LinSamp~~ regular and LinSamp-version and assumed converged simulation results and no limiter events. Moreover, we assume that an increase of ~~N_{SIP} leads to an~~ N_{SIP} leads to a uniform decrease of all SIP weights ν_p.

For the following basic quantities we have

$$\nu_p \propto \frac{1}{N_{SIP}} \frac{1}{N_{\mathrm{SIP}}};\quad nt \propto \frac{1}{\delta t};\quad N_{combs\mathrm{comb}} \propto {N_{SIP\mathrm{SIP}}}^{\alpha};\quad \gamma_{\mathrm{corr}} \propto {N_{SIP\mathrm{SIP}}}^{\beta}, \tag{28}$$

where γ_{corr} is the correction factor defined in Eq. 25. For QuadSamp $\alpha = 2, \beta = 0$ and for LinSamp $\alpha = 1, \beta = 1$.

Accordingly,

$$\nu_{coll\,\mathrm{coll}} \propto \frac{1}{{N_{SIP}}^2}\,\frac{1}{{N_{\mathrm{SIP}}}^2} \times \delta t, \tag{29a}$$

$$\nu_{sum} := \sum^{nt,\,N_{combs}\,nt,\,N_{\mathrm{comb}}} \left(\nu_{coll\,\mathrm{coll}}\,\gamma_{\mathrm{corr}}\right) \propto \frac{{N_{SIP}}^{\alpha+\beta}}{{N_{SIP}}^2}\,\frac{{N_{\mathrm{SIP}}}^{\alpha+\beta}}{{N_{\mathrm{SIP}}}^2} = 1, \text{ and} \tag{29b}$$

$$\bar{p}_{crit\,\mathrm{crit}} := \frac{1}{N_{combs}\,nt}\,\frac{1}{N_{\mathrm{comb}}\,nt} \sum^{nt,\,N_{combs}\,nt,\,N_{\mathrm{comb}}} (\nu_{coll\,\mathrm{coll}}/\nu_p\,\gamma_{\mathrm{corr}}) \propto {N_{SIP}}_{\mathrm{SIP}}{}^{\beta-1}\,\delta t. \tag{29c}$$

In ~~all versions~~both versions, ν_{sum} is independent of ~~N_{SIP}~~ N_{SIP} and δt. Clearly, ν_{sum} should have the same value (not only the same asymptotic ~~behavior~~behaviour) across all AON versions in order to obtain consistent results. The average probability ~~$\bar{p}_{crit}$~~ $\bar{p}_{\mathrm{crit}}$ scales, not surprisingly, linearly with δt. For QuadSamp, ~~$\bar{p}_{crit}$~~ $\bar{p}_{\mathrm{crit}}$ is inversely proportional to ~~N_{SIP}~~ N_{SIP} and an increase of ~~N_{SIP} decreases the occurence~~ N_{SIP} decreases the occurrence of multiple collections and limiter events. In the LinSamp case, ~~$\bar{p}_{crit}$~~ $\bar{p}_{\mathrm{crit}}$ is independent of ~~N_{SIP}~~ N_{SIP} (as already pointed out by Shima et al., 2009, end of their section 5.1.3) implying that an increase of ~~N_{SIP}~~ N_{SIP} does not decrease the number of multiple collections and limiter events. Nevertheless, an ~~N_{SIP}~~N_{SIP}-increase is also beneficial in LinSamp as it increases the number of trials and reduces the variance of the results.

3.3 ~~Full~~ Realistic column model simulations

The box model emulation simulations presented in Sec. 3.1 used an academic and irrealistic setup, not yet exploiting the capabilities of a column model framework. The following two subsections treat realistic setups.

3.3.1 Half domain setup

We initialise droplets in the upper half of a $4\,\mathrm{km}$ column. In each GB the mean radius of the DSD is fixed at the default value ~~$r_0 = 9.3\,\mu\mathrm{m}$. LWC~~ $r_{\mathrm{init}} = 9.3\,\mu\mathrm{m}$. LWC_{init} (and with it ~~DNC~~DNC_{init}) decreases linearly from $3\,\mathrm{g/m^3}$ at the model top to zero at $z = 2\,\mathrm{km}$. At the model top, a constant influx of a DSD with ~~$LWC = 3$~~ $LWC_{\mathrm{init}} = 3\,\mathrm{g/m^3}$ is prescribed which guarantees a smooth profile over time. Otherwise, a discontinuity would occur at the top-most GB which may raise problems in the ~~bin model.~~

BIN model. The further settings are ~~$nz = 400$, $\Delta z = 10\,\mathrm{m}$, $\Delta t = 10\,\mathrm{s}$, $nr_{inst} = 20$, $\kappa = 40$.~~ $n_z = 400$, $\Delta z = 10\,\mathrm{m}$, $\Delta t = 10\,\mathrm{s}$, $nr_{\mathrm{inst}} =$
All figures related to this setup start their caption with the label **HalfDomLinDec setup**.

Figure 9 shows the temporal evolution of the mean diameter and the moments λ_0, λ_1 and λ_2. Due to the influx condition, the total mass increases during the first 10 minutes, barely visible in the third panel. During this period, however, ~~collection~~ collisional growth is already efficiently reducing the droplet number. This is accompanied by an increase of the mean diameter and radar reflectivity. Soon after, the first droplets reach the surface, the mass declines rapidly, and the whole column is more or less washed out after 30 minutes. We find an excellent agreement among the ~~three model versions BIN1D, AON-WM3D and~~ four model versions BIN, AON-regular, AON-WM2D ~~. Using LinSamp in AON-WM3D, agreement with the other models is reached only if the time step is reduced (here from $\Delta t = 10\,\mathrm{s}$ to $1\,\mathrm{s}$).~~ and AON-LinSamp.

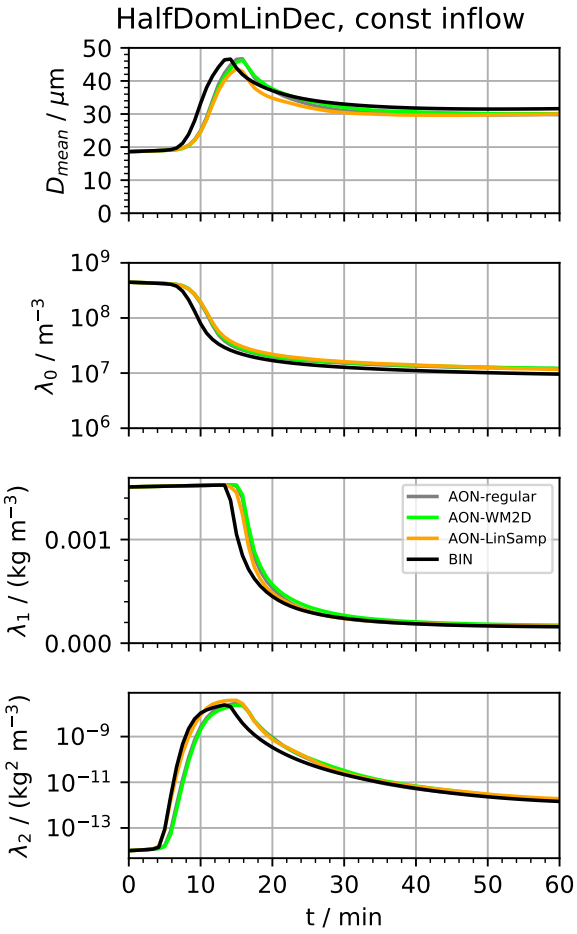

Figure 9. HalfDomLinDec setup: Temporal evolution of ~~D_{mean}~~ D_{mean} and column-averaged moments λ_0, λ_1 and λ_2 for various model versions (see inserted legend; "LS" is short for linear sampling). .

Figure 10 shows vertical profiles of DNC, LWC, Z and ~~$N_{SIP,GB}$~~ $N_{\text{SIP,GB}}$ for times $t = 0, 10\,\text{min}, 20\,\text{min}, 30\,\text{min}$ and $60\,\text{min}$. In the upper half, droplet number is roughly homogeneously distributed and decreases over time. In the lower half, droplet number concentrations are several orders of magnitude smaller than in the upper half and increase over time. The profile of the radar reflectivity shows the highest values after 10 minutes with a pronounced peak in the middle of the domain. Soon after, the Z-profiles become smooth and increase monotonically towards the surface. The sedimentation flux also increases towards the surface and hence λ_2-values decrease over time.

In the upper half, ~~$N_{SIP,GB}$~~ $N_{\text{SIP,GB}}$ is fairly constant over altitude and time with around 200 SIPs. As the LWC is initially highest at the model top, ~~collections are~~ collisional growth is most frequent there. Most likely, SIPs from that layer turn into collector SIPs~~and~~ , meaning they fall through the total column and collect many other SIPs. Consistently, ~~$N_{SIP,GB}$~~ $N_{\text{SIP,GB}}$ decreases over time close to the model top. Yet overall, only a small fraction of the SIPs becomes rain drops eventually (see

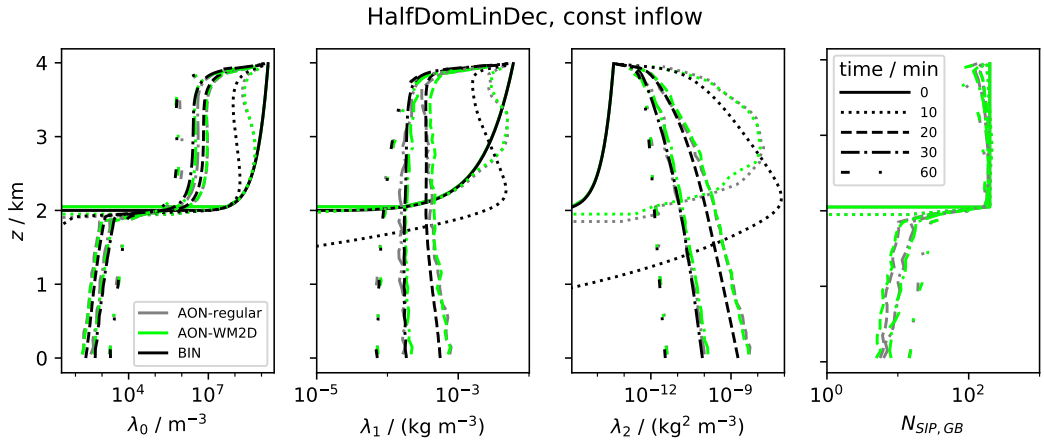

Figure 10. HalfDomLinDec setup: Vertical profiles of moments $\lambda_0, \lambda_1, \lambda_2$ and ~~$N_{SIP,GB}$~~ $N_{\mathrm{SIP,GB}}$ for various model versions (AON-WM3D, AON-WM2D, Bin; see ~~color~~ colour legend in left-most panel) and times $(0, 10, 20, 30, 60\,\mathrm{min}$; see linestyle legend in right-most panel).

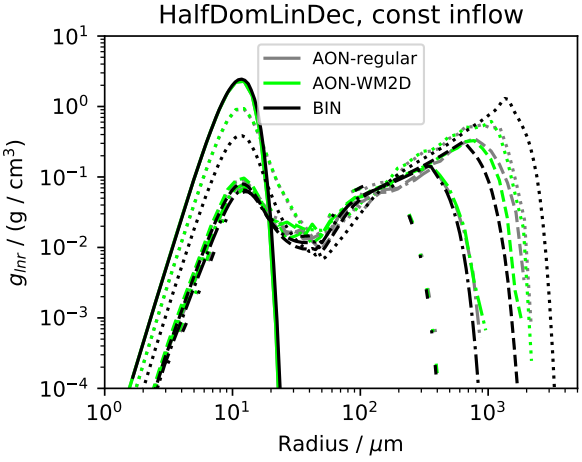

Figure 11. HalfDomLinDec setup: Size distribution g_{lnr} for various model versions and times as in Fig. 10 (see legends there).

e.g. Fig. 4 in U2017) and hence the SIP number is substantially smaller in the lower half. There, each GB is populated roughly by 10 SIPs. Despite this rather small value, convergence in DNC and Z seems to be ubiquitous.

Figure 11 depicts column-averaged DSDs for various points in time. The precipitation mode develops rapidly, and 2 to 3 mm-sized drops are produced within 10 minutes. Those drops soon reach the surface and remove a significant amount of liquid water from the column. Due to this wash-out effect, the rain drops cannot grow that large any longer and the precipitation mode peaks at smaller sizes at later times.

For a cleaner presentation, AON-LinSamp results were not shown in Figs. 10 and 11, but we confirm that these are very similar to those from AON-regular and AON-WM2D.

Overall, the agreement between the ~~three~~ four model versions is remarkable given the completely different numerics of the Eulerian and Lagrangian approach.

Next, the vertical resolution Δz is varied in ~~all three model versions .~~ the model versions AON-regular, AON-WM2D and BIN (see Fig. S17). Even though this ~~sounds like a banal~~ may look like a trivial sensitivity study, the effect of a Δz-variation has different implications in the various ~~model variants and the~~ models and AON versions. The differences are rather subtle. First, Δz affects the number of GBs ~~nz~~ n_z and with it the total SIP number ~~$N_{SIP,tot}$ (as $N_{SIP,GB}$~~ $N_{\mathrm{SIP,tot}}$ (as $N_{\mathrm{SIP,GB}}$ is unchanged with the standard SIP init technique). To eliminate this unwanted numerical side effect in LCM1D, we increase ~~$N_{SIP,GB}$~~ $N_{\mathrm{SIP,GB}}$ proportionally to Δz (analogous to the ΔV-sensitivity tests in section 3.1). Second, the advection by sedimentation changes in BIN as the CFL number changes and the subcycling has to be adapted. In LCM1D, the SIP transport by sedimentation is independent of the assumed grid and clearly unaffected by a Δz-variation. Third, there is a physical effect as Δz determines the layer depth of the well-mixed volume (effective only in ~~AON-WM3D~~ AON-regular and BIN).

It follows that the results of the ~~AON-WM2D~~ AON-WM2D version should be independent of Δz. Moreover, the ~~AON-WM3D variant~~ AON-regular version can be used to determine if the size (more specifically the depth) of the well-mixed volume is a crucial parameter. In bin models in general, ~~the latter effect~~ this sensitivity could not easily be singled out as sedimentation numerics also change with Δz.

~~Figure ?? depicts the evolution of λ_0 and λ_2 for~~ Given a constant column height $L_z = 4\,\mathrm{km}$, Δz ~~ranging from $2\,\mathrm{m}$ to $100\,\mathrm{m}$.~~takes the values $2\,\mathrm{m}, 10\,\mathrm{m}, 50\,\mathrm{m}$ or $100\,\mathrm{m}$ and we find $\lambda_0(t)$ to be independent of Δz (see Fig. S17). As expected, the ~~AON-WM2D~~ AON-WM2D simulations are not at all affected by Δz~~(left column). The middle column shows the AON-WM3D simulations . The $\Delta z = 10\,\mathrm{m}$ simulation uses $N_{SIP,GB} = 200$ and the $\Delta z = 100\,\mathrm{m}$-simulation $N_{SIP,GB} = 2000$. Hence, a factor 100 more SIP combinations are tested for possible collections in the latter case. Nevertheless, the results are basically identical, implying~~ . In particular, the AON-regular simulations are insensitive to a change in Δz and imply that the depth of the well-mixed volume has a negligible impact on the extent of collections in the present ~~example. The right column shows the BIN results which are again basically identical, using the MPDATA scheme (solid) and the 1st order upwind scheme (dotted). The slight deviations in λ_0 may be due to the fact, that in a bin model the vertical redistribution by sedimentation is also affected by Δz. Due to stability issues, the time step (for collection) had to be reduced from $\Delta t = 10\,\mathrm{s}$ to $1\,\mathrm{s}$ for US1. Then, reasonable results are achieved for $\Delta z \geq 10\,\mathrm{m}$. For the highest resolution $\Delta z = 2\,\mathrm{m}$, however, numerical instabilities are still present (see outlier curve). This is a clear indication for the superiority of MPDATA in BIN.~~

setup. Interestingly, the $\Delta z = 10\,\mathrm{m}$ simulation uses $N_{\mathrm{SIP,GB}} = 200$ and the $\Delta z = 100\,\mathrm{m}$-simulation $N_{\mathrm{SIP,GB}} = 2000$. Hence, a factor 100 more SIP combinations are tested for possible collections in the latter case, yet with no effect on the physical evolution.

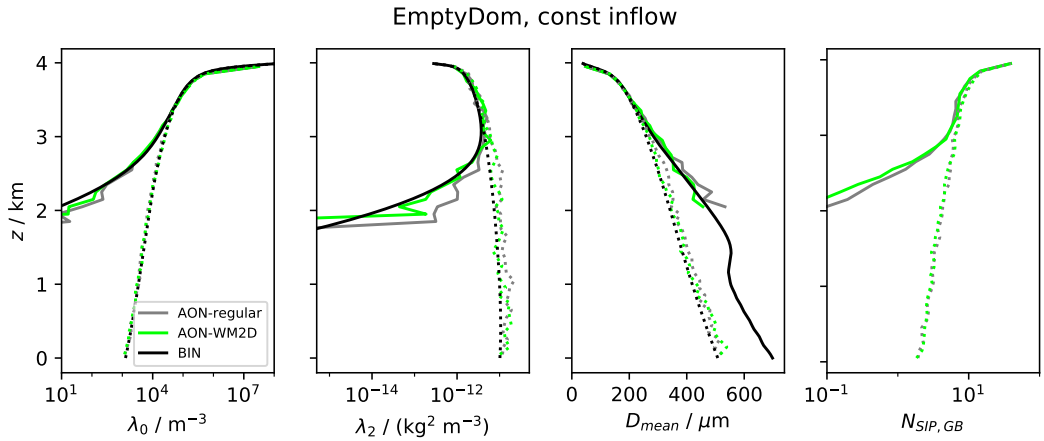

Figure 12. EmptyDom setup: Vertical profiles of moments ~~$\lambda_0, \lambda_2, D_{mean}$~~ $\lambda_0, \lambda_2, D_{\text{mean}}$ and ~~$N_{SIP,GB}$~~ $N_{\text{SIP,GB}}$ for various model versions (see legend). Depicted are the times $t = 30$ and 60 minutes (solid, dotted).

3.3.2 Empty domain setup

In this section, the $4\,\text{km}$ deep column is initially devoid of droplets and a time-constant influx of a DSD with ~~$r_0 = 16.9\,\mu\text{m}$ and $LWC = 6\,\text{g/m}^3$~~ $r_{\text{init}} = 16.9\,\mu\text{m}$ and $LWC_{\text{init}} = 6\,\text{g/m}^3$ is prescribed. As in the box model emulation setup, the according ~~DNC~~ DNC_{init} is $297\,\text{cm}^{-3}$. All figures related to this setup start their caption with the label **EmptyDom setup**.

Over time the column fills with droplets, a distinct size sorting is established and DSDs at a specific altitude are expected to be rather narrow. Hence, choosing a too coarse vertical resolution may result in overestimating collections as the droplets are not supposed to be well-mixed within such deep GBs. In such a case, the ~~AON WM2D variant~~ AON-WM2D version has a conceptional advantage as it does not assume well-mixedness in the vertical direction. The chosen setup specifically aims at demonstrating the possible improvement ~~of~~ by this. Again, the further parameter settings are ~~$nz = 400,\ \Delta z = 10\,\text{m},\ \Delta t = 10\,\text{s},\ nr_{inst} = 20,\ \kappa =$~~

Figure 12 shows vertical profiles at $t = 30$ and 60 minutes for AON-regular, AON-WM2D and BIN. After 30 minutes the cloud roughly covers the top half of the column. Below $z = 2\,\text{km}$, fewer than 0.1 SIPs are present in each GB of LCM1D. This implies that only in 1 or 2 out of the 20 realisations SIPs grow sufficiently large to fall that far. This also explains the jagged λ_2-profiles in the lower part. Below a certain altitude, no SIPs are present at all and hence no mean droplet diameter could be diagnosed. BIN produces non-zero mass and number all the way down to the bottom and allows computing a smooth ~~D_{mean}~~ D_{mean}-profile. As the predicted droplet masses and concentrations become vanishingly small, the derived ~~D_{mean}~~ D_{mean}-values in the lower part are, however, meaningless. Anyhow, this small discrepancy between BIN and LCM1D is a transient phenomenon. Once the cloud is fully developed, the profiles match perfectly (see dotted curve for $t = 60\,\text{min}$). Remarkable is the fact that on average well below 10 SIPs populate GBs in the lower domain half. Nevertheless, the LCM1D results seem to be converged. SIPs at those altitudes are large (~~$D_{mean} > 400\,\mu\text{m}$~~ $D_{\text{mean}} \geq 400\,\mu\text{m}$) and fall fast, which fosters a strong SIP exchange across GBs and is beneficial to convergence (see section 3.1). The AON-LinSamp simulation (not shown) produces

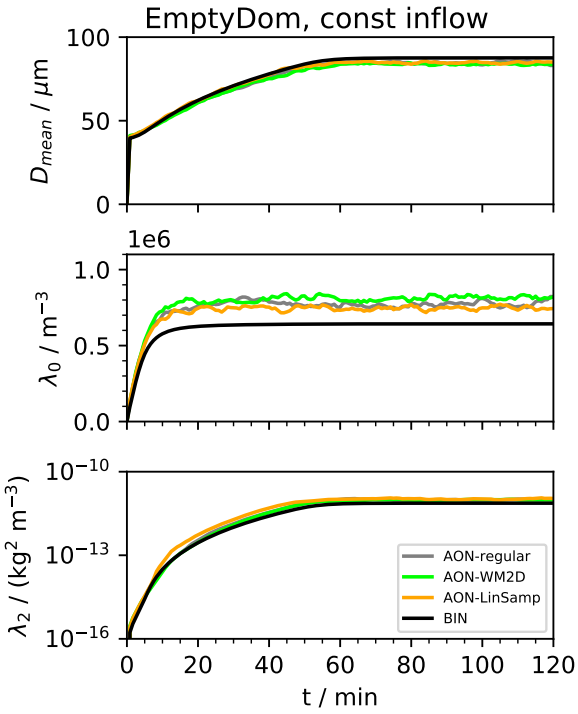

Figure 13. EmptyDom setup: Temporal evolution of ~~D_{mean}~~ D_{mean} and column-averaged moments λ_0 and λ_2 for various model versions (see legend).

again very similar profiles. This is even more remarkable, as on average only 5 SIP pairs are tested for collections per GB in the lower half.

Figure 13 shows the temporal evolution of the mean diameter, column-averaged DNC and Z, here AON-LinSamp curves are added. Within the first 10 minutes, DNC increases quickly. Soon after, collection becomes effective and DNC reaches a quasi steady state. The radar reflectivity increases within the first 60 minutes and then also reaches a quasi steady state. The only discrepancy between the various models are slightly larger ~~DNC-values with LCM1D~~ DNC-values by all AON versions. The reason for this is elucidated next.

Fig. 14 shows the Δz-dependence of the ~~DNC and Z-evolution~~ DNC-evolution in the different models. For $\Delta z = 50$ and $100\,\mathrm{m}$, the SIP numbers in ~~LCM1D~~ AON simulations have been upscaled to maintain ~~$N_{STP,tot}$~~ $N_{\mathrm{SIP,tot}}$-values comparable to the $\Delta z = 10\,\mathrm{m}$-simulation (as already done in the HalfDom-setup). The Z-evolution (~~second row~~see Fig. S19 for a time series) is found to be basically independent of Δz in all three models. For the ~~DNC-evolution~~ DNC-evolution, we find also no Δz-dependence in the WM2D-model as intended. However, in ~~WM3D~~ AON-regular and BIN model, ~~DNC~~ DNC levels off at different values depending on Δz. This ~~latter behavior~~ behaviour is most likely caused by an interaction of the unresolved size sorting and the hence larger range of potential collection partners in ~~AON-WM3D~~ AON-regular and BIN. Apparently, this

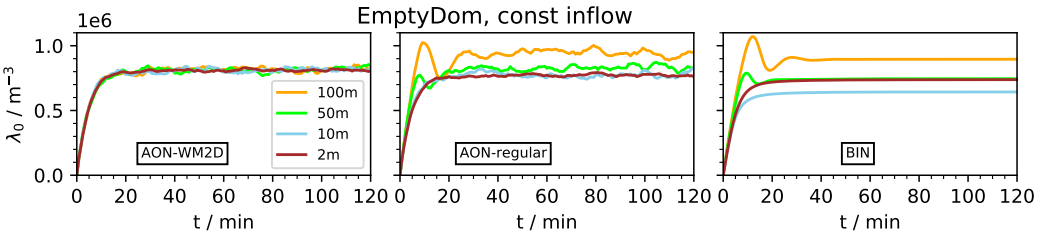

Figure 14. EmptyDom setup: Temporal evolution of column-averaged moments λ_0 and λ_2 for various model versions (AON-WM2D, left; AON-WM3D, middle; Bin, right). Each panel shows a variation of the vertical resolution Δz (see legend). In LCM simulations, SIP numbers for $\Delta z = 100\,\mathrm{m}$ and $50\,\mathrm{m}$-simulations are increased to the level of the $\Delta z = 10\,\mathrm{m}$-simulation.

results in changes in the rate with which the smallest droplets are collected by larger droplets, as indicated by the substantial effect of this process on ~~DNC~~ DNC, but not on ~~Z~~Z.

~~For $\Delta z = 100\,\mathrm{m}$ and $\Delta z = 10\,\mathrm{m}$, Figure ?? shows the DNC-evolution of the WM3D-model with different parameter settings. The green curves shows the default case from before, where the $\Delta z = 100\,\mathrm{m}$-simulation uses a "10x" higher $N_{SIP,GB}$-value. We used LinSamp instead of QuadSamp (red), further decreased the time step from $\Delta = 10\,\mathrm{s}$ to $1\,\mathrm{s}$ or used for both resolutions the same $N_{SIP,GB}$-value (which reduces $N_{SIP,tot}$ of the $\Delta z = 100\,\mathrm{m}$-simulation by a factor of ten). In all cases, the~~ The Δz-dependence ~~appears consistently in all parameter settings.~~ persists in AON-LinSamp simulations and in further AON-regular simulations, where we reduced the time step to $\Delta t = 1\,\mathrm{s}$ or decreased $N_{\mathrm{SIP,tot}}$ (see Fig. S20).

This undesired Δz-dependence in BIN and ~~WM3D~~ AON-regular seems to showcase the superiority of the AON-WM2D ~~implementation~~version. However, the Δz-dependence does not affect higher moments of the DSD, e.g., Z (~~Figs.13 and 14~~as shown in SUPP) or the accumulated size distribution of all droplets that crossed the lower boundary (Fig.~~??~~ S21). Accordingly, precipitation-related quantities seem to be unaffected by changes in the vertical grid spacing. On the other hand, most of the Δz-effect can be attributed to changes in the DNC within the top most $100 - 200\,\mathrm{m}$ of the column (Fig. 12)~~, which might affect the radiative properties of the considered cloud~~. Anyhow, based on the presented results, we cannot definitely answer the question, whether using the AON-WM2D approach has in general any practical benefits over the classical 3D well-mixed approaches~~based on the presented results~~. Further research in this direction is required.

4 Summary and conclusions

Collection, i.e., the coalescence, accretion, and aggregation of hydrometeors, is an important process for the development of precipitation in liquid-, mixed-, and ice-phase clouds, respectively. ~~Moreover, aggregation leads to irregular ice crystal shapes affecting the cloud radiative properties.~~ The correct representation of these processes in cloud microphysical models is, therefore, of utmost importance. In this study, we investigated and validated the representation of collection in LCMs, a relatively new approach that uses simulation particles, so-called SIPs or superdroplets, to represent cloud microphysics.

This study is a continuation of U2017, in which we ~~analyzed~~ analysed various representations of ~~collection~~ collisional growth algorithms in LCMs using zero-dimensional box model simulations. Here, this analysis is extended to one-dimensional column simulations that allow considering the effects of sedimentation explicitly. This study focuses on the AON ~~collection~~ algorithm (Shima et al., 2009; Sölch and Kärcher, 2010) that outperformed other collection ~~approaches~~algorithms, as assessed in our previous study (U2017). Two ~~variants~~ versions of AON are applied that differ in the assumed distribution of droplets represented by a SIP: In ~~WM3D~~the regular AON version, the droplets are assumed to be well-mixed within a three-dimensional volume (which is typically identical to the GB of the dynamical model coupled to the LCM). In WM2D, the height coordinate of each SIP is used explicitly, and the droplets represented by a SIP are assumed to be well-mixed only within a two-dimensional, horizontal plane. Accordingly, collections are only considered if a SIP overtakes another one during a ~~timestep.~~ time step.

Furthermore, two variants of AON-WM3D are tested that differ in the number of SIP combinations that need to be tested during collection. In its simplest form, AON-WM3D depends quadratically on the number of SIPs since every SIP may interact with any other SIP inside a GB (QuadSamp). Additionally, Shima et al. (2009) introduced an approach that depends only linearly on the number of SIPs by appropriately scaling collection probabilities (LinSamp). What we call here AON-LinSamp is also referred to as SDM (SuperDroplet Method) algorithm in the literature.

All results are compared to established Eulerian bin model results (Bott, 1998; Wang et al., 2007). Accordingly, the capability of Lagrangian and Eulerian approaches to advect a droplet ensemble due to sedimentation is tested first — neglecting the influence of collection. Since numerical diffusion is inherent to any Eulerian advection problem, i.e., also sedimentation, its impact might impede any conclusions drawn from the collection simulations. However, by using an appropriate advection scheme (MPDATA, Smolarkiewicz, 1984), numerical diffusion can be reduced to an acceptable degree in the sense that the present simulations focus on the differences driven by collection numerics.

~~To bridge the gap to U2017, the behavior of~~ As a first step and link to U2017-simulations, box model simulations ~~is~~ are emulated in the column model. This is done by initialising each GB of the column with the same droplet size distribution and applying cyclic boundary conditions at the surface and the top. By using this framework, we were able to show that sedimentation increases the model convergence rate significantly compared to box model simulations without sedimentation, i.e., ~~significantly~~ fewer SIPs are required in the column model. The reason for this ~~behavior~~ behaviour is that the largest and hence fastest falling droplets are no longer confined to the same GB and to the same potential collection partners, ~~hence increasing~~ which increases the ensemble of potential collection partners. A similar observation has been made by Schwenkel et al. (2018), who used ~~randomized~~ randomised motions between individual GBs. Overall, these results indicate that a simulation with only 24 SIPs per GB can yield reasonable results if (i) these SIPs are able to move between GBs and (ii) the SIP weighting factors are ideally chosen in the beginning by using an ~~approriate~~ appropriate SIP initialisation technique.

~~A generally~~ In general, a remarkably good agreement of the LCM results with the bin reference has been found for all AON ~~variants. However, they reveal distinct differences in their numerical and computational requirements. LinSamp demands a shorter timestep than QuadSamp as a result of the upscaled collection probabilities to avoid SIPs with a zero (or even negative)weighting factor. And indeed, fully coupled LCM applications with AON and LinSamp are reported to require a relatively short timestep to reach convergence (e.g., Dziekan et al., 2019) . Accordingly, these strong~~ versions (regular AON,

AON-WM2D and AON-LinSamp). AON-LinSamp results are only slightly worse compared to regular AON simulation of the same time step and SIP number. However, these stronger restrictions on the ~~timestep might cancel out~~ time step do by far not outweigh the computational benefit gained by the ~~reduced number of SIP combinations that need to be tested in LinSamp . This indicates that the simpler QuadSamp might be~~ favourable linear computational complexity making the LinSamp version the preferred choice if computation time is a critical factor. In an operational setting, the QuadSamp approach is a valuable alternative to LinSamp as long as the number of SIPs is not prohibitively high.

We further compared the computational requirements for the WM2D and WM3D implementations of AON. We found that WM2D requires ~~to check~~ checking for overtakes in the entire column, not only in the GB in which the SIP is located, as is the case for WM3D. However, this seeming disadvantage is turned into an advantage, since only a minority of SIPs overtakes other SIPs. Accordingly, the overall number of calculations necessary for the application of WM2D is reduced compared to WM3D. The physical reason for this effect is the typical bimodal structure of droplet spectra, which consist of only a few large droplets that sediment and collect other droplets efficiently, while the remaining droplets are usually too small to sediment and collect other droplets.

Finally, we applied ~~these approaches~~ the various AON versions to two more realistic column cases. While both cases use a prescribed inflow of droplets from the top, the first case is initialised with a linearly increasing liquid water content, and the second case is completely devoid of any initial droplets. Overall, the agreement of ~~AON-WM3D~~AON-regular, AON-WM2D, AON-LinSamp and the bin references is remarkable. Only in the second case, which is designed to be heavily prone to size-sorting, a dependence on the vertical grid spacing is detectable for WM3D and the bin reference, which both assume ~~the~~ droplets to be well-mixed within a GB, while the WM2D results are found to be completely independent of the vertical grid spacing.

In all AON variants, simulation results converge for fairly large time steps $\Delta t > 10\,\mathrm{s}$. For such high Δt-values, the largest droplets routinely travel distances larger than the vertical resolution Δz during one time step (as noted above). Whereas in Eulerian advection this would violate the CFL criterion and cause a numerical break-down, Lagrangian numerics do not fail. In higher-dimensional full microphysical models with diffusional growth included and gradients in moist thermodynamic fields physical reasons render it appropriate to apply a time step criterion in the spirit of the CFL condition also in Lagrangian approaches. Solving diffusional growth usually sets stricter bounds on Δt (Arnason and Brown, 1971) . Moreover, the interplay of diffusional and collisional growth, which was not studied here, may raise the time step requirements of AON for physical reasons, e.g. Dziekan et al. (2019) , using AON with linear sampling in 2D and 3D LCM simulations, found convergence only for a rather small time step of $\Delta t = 0.1\,\mathrm{s}$.

All in all, this study has shown that the representation of ~~collection~~ collisional growth in LCMs using AON ~~with WM3D and WM2D~~ successfully reproduces established Eulerian bin results~~successfully~~. This ability, of course, depends foremost on the number of SIPs and the applied ~~timestep~~ time step as already indicated in previous zero-dimensional box model studies. Compared to these zero-dimensional studies, the application of an LCM in a column decreases the required number of SIPs significantly. The consequently lower computational costs raise hopes to use LCMs more frequently in large-scale, multidimensional models in the future.

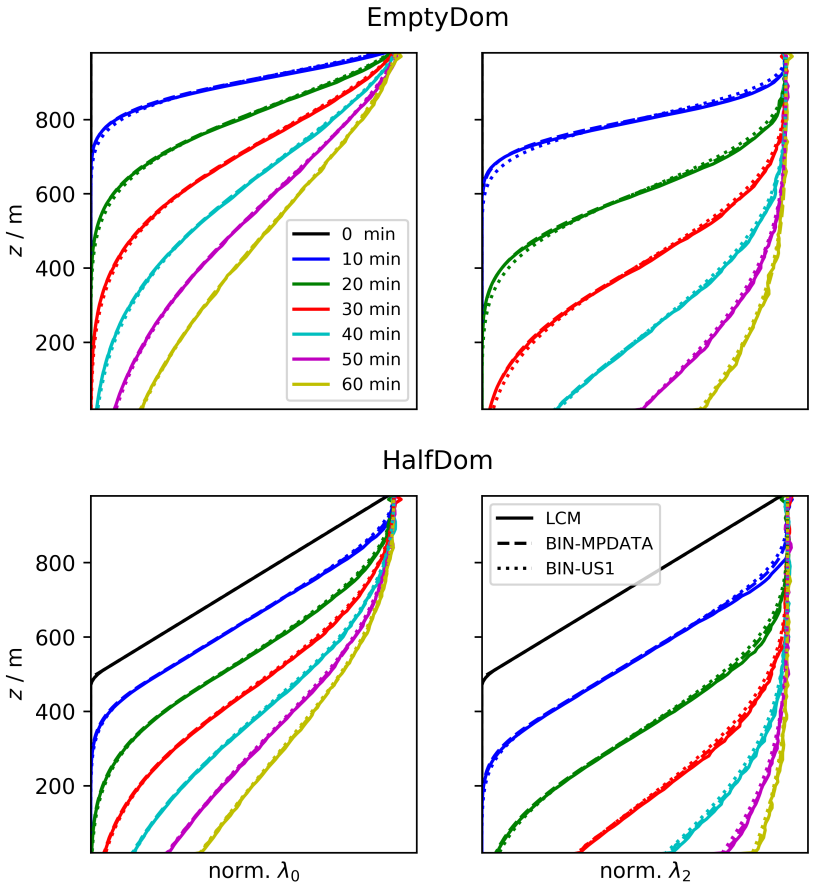

Figure A1. Pure Sedimentation test case: Comparison of BIN and LCM (solid) advection. BIN uses either MPDATA (dashed) or 1st order Upstream scheme (dotted). EmptyDom (upper row) and HalfDom (lower row) setup are used with an exponential distribution with $r_{\text{init}} = 50\,\mu\text{m}$ as influx condition. Displayed are vertical profiles of normalised zeroth and second moment at the indicated points in time.

Code and data availability. The source code of the Lagrangian column model is hosted on GitHub (https://github.com/SimonUnterstrasser/ColumnModel) and released under Apache License 2.0. The (frozen) code version used to produce the simulation data of this study can be obtained from Zenodo (DOI: 10.5281/zenodo.3547539). The data of the BIN and AON simulations together with all plot scripts that are necessary to reproduce the figures of this study, are released in a second Zenodo data set (DOI: 10.5281/zenodo.3547341). **After the review process has been completed, the data sets will be updated and new DOIs will be provided.** The source code of the bin collection algorithms by Bott (1998) and Wang et al. (2007) have been obtained from A. Bott and L. P. Wang, respectively. We are not in the position to make the codes publicly available.

Appendix A: Pure sedimentation test cases

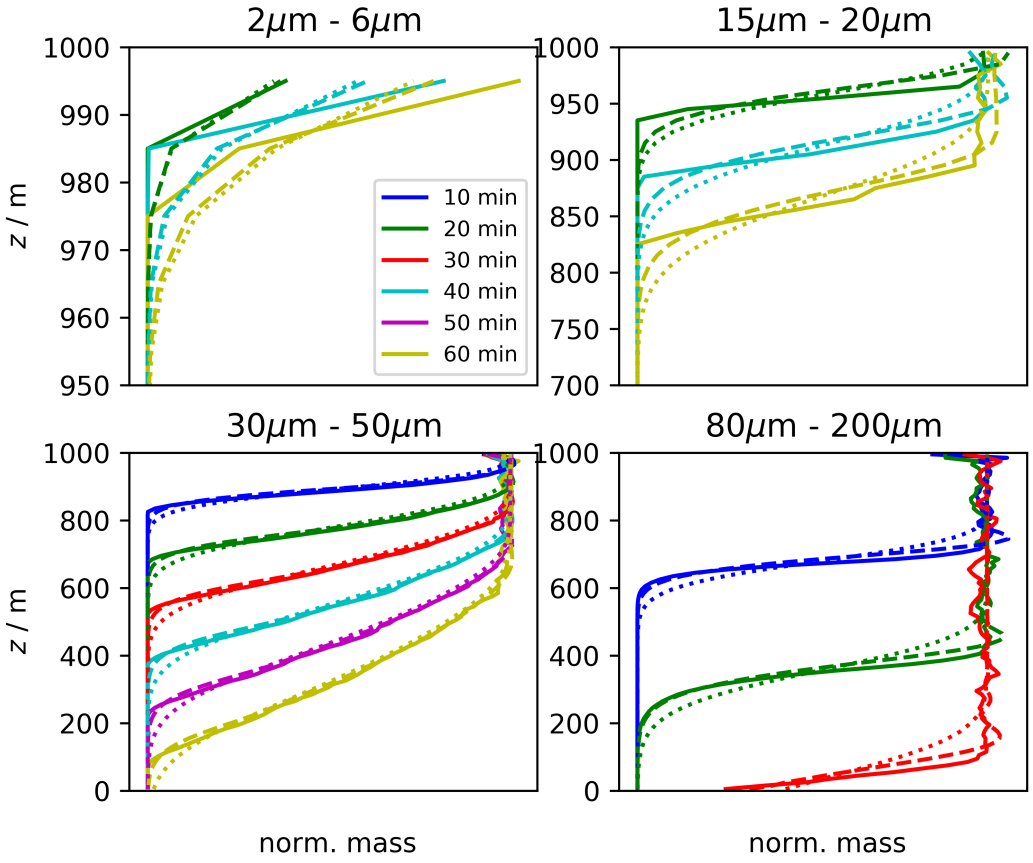

Figure A2. Pure Sedimentation test case: Comparison of BIN and LCM advection. EmptyDom setup with an exponential distribution with $r_{\text{init}} = 50\,\mu\text{m}$ as influx condition. Displayed are vertical profiles of normalised mass within specified size ranges (see on top of each panel) at the indicated points in time. Note that most panels use different y-axis ranges and do not show all six points in time.

This Appendix presents pure sedimentation test cases that are suited to demonstrate that minor differences are introduced by the different numerical treatment of the sedimentation process. Two simple setups with an influx of an exponential DSD with $r_{\text{init}} = 50\,\mu\text{m}$ are tested. In the first case, the domain is initially empty and fills over time (EmptyDom) as in section 3.3.2. In the second case, the upper half of the domain is filled, with LWC_{init} and DNC_{init} decreasing linearly to zero from the domain top to the domain middle (HalfDom) like in section 3.3.1. Figure A1 shows the vertical profiles of normalised zeroth (left) and second (right) moments for EmptyDom (top) and HalfDom (bottom). Because of the lack of numerical diffusion, the solid LCM curves show the exact results, except for the error introduced by discretising the influx DSD with a probabilistic approach. Each panel showcases a convincing agreement between the Eulerian and Lagrangian approach. Only the BIN-US1 solutions are slightly smeared out. The small wiggles in the LCM curves originate from the probabilistic influx condition. Even though the above agreement is favourable, it might be that the advection errors of differently sized droplets compensate each

other in the Eulerian approaches. Hence, in a second validation step, the computation of mass profiles is confined to certain droplet size ranges. Figure A2 shows such vertical profiles for EmptyDom. We see that for all four size ranges, the BIN results are smeared out relative to LCM. For the smallest size ranges both BIN versions are equally "bad" (top left panel). For the three remaining panels, the MPDATA curves (dashed) are closer to the LCM reference than the US1 curves (dotted). On the other hand, the MPDATA curves in the bottom right panel show some wiggles. Overall, the agreement between LCM and BIN-MPDATA is good. The discrepancies introduced by the different sedimentation treatment appear to be small enough to focus on the collisional growth process and its implementations in the main part of the paper.

Moreover, we tested the sensitivity to r_{CFL} and Δt as both parameters in combination determine the local CFL number of each grid box. BIN simulations were carried out for the HalfDomLinDec-setup and with switched on collisional growth (i.e. the setup of section 3.3.1). Fig. S18 demonstrates that this has no impact on the prediction of the total moments.

Author contributions. S. Unterstrasser designed the study, programmed the Lagrangian column model, carried out the simulations, wrote most parts of the manuscript. F. Hoffmann discussed the results with the first author and wrote the introduction and conclusions. A first code version and preliminary results were obtained during the Master's thesis of M. Lerch.

Competing interests. The authors declare that they have no conflict of interest.

Acknowledgements. We thank L. P. Wang and A. Bott for providing box model versions of their collection algorithms. The first author thanks Jan Bohrer (Tropos Leipzig) for carefully examining the AON code and spotting the bug ~~mentionned~~ mentioned in section 3.1.1. Moreover, we appreciate comments on the manuscript by K. Gierens. This research was performed while Fabian Hoffmann held a Visiting Fellowship of the Cooperative Institute for Research in Environmental Sciences (CIRES) at the University of Colorado Boulder and the NOAA Earth System Research Laboratory.

References

L. Alfonso and G. B. Raga. The impact of fluctuations and correlations in droplet growth by collision–coalescence revisited – Part 1: Numerical calculation of post-gel droplet size distribution. *Atmos. Chem. Phys.*, 17(11):6895–6905, 2017. https://doi.org/10.5194/acp-17-6895-2017.

L. Alfonso, G. B. Raga, and D. Baumgardner. The validity of the kinetic collection equation revisited. *Atmos. Chem. Phys.*, 8(4):969–982, 2008. https://doi.org/10.5194/acp-8-969-2008.

M. Andrejczuk, J. M. Reisner, B. Henson, M. K. Dubey, and C. A. Jeffery. The potential impacts of pollution on a nondrizzling stratus deck: Does aerosol number matter more than type? *J. Geophys. Res.*, 113(D19):D19204, 2008. https://doi.org/0.1029/2007JD009445.

M. Andrejczuk, W. W. Grabowski, J. Reisner, and A. Gadian. Cloud-aerosol interactions for boundary layer stratocumulus in the Lagrangian cloud model. *J. Geophys. Res.*, 115:D22214, 2010. https://doi.org/10.1029/2010JD014248.

S. Arabas, A. Jaruga, H. Pawlowska, and W. W. Grabowski. libcloudph++ 1.0: a single-moment bulk, double-moment bulk, and particle-based warm-rain microphysics library in c++. *Geosci. Model Dev.*, 8(6):1677–1707, 2015. https://doi.org/10.5194/gmd-8-1677-2015.

G. Arnason and J. Brown, Philip S. Growth of Cloud Droplets by Condensation: A Problem in Computational Stability. *J. Atmos. Sci.*, 28 (1):72–77, 1971. https://doi.org/10.1175/1520-0469(1971)028<0072:GOCDBC>2.0.CO;2.

M. H. Bayewitz, J. Yerushalmi, S. Katz, and R. Shinnar. The extent of correlations in a stochastic coalescence process. *J. Atmos. Sci.*, 31(6): 1604–1614, 1974. https://doi.org/10.1175/1520-0469(1974)031<1604:TEOCIA>2.0.CO;2.

K. Beard and H. Ochs III. Collection and coalescence efficiencies for accretion. *J. Geophys. Res.*, 89(D5):7165–7169, 1984. https://doi.org/10.1029/JD089iD05p07165.

K. V. Beard. Terminal velocity and shape of cloud and precipitation drops aloft. *J. Atmos. Sci.*, 33(5):851–864, 1976. https://doi.org/10.1175/1520-0469(1976)033<0851:TVASOC>2.0.CO;2.

E. X. Berry. Cloud Droplet Growth by Collection. *J. Atmos. Sci.*, 24(6):688–701, 1967. https://doi.org/10.1175/1520-0469(1967)024<0688:CDGBC>2.0.CO;2.

E. X. Berry and R. L. Reinhardt. An Analysis of Cloud Drop Growth by Collection: Part I. Double Distributions. *J. Atmos. Sci.*, 31(7): 1814–1824, 1974. https://doi.org/10.1175/1520-0469(1974)031<1814:AAOCDG>2.0.CO;2.

A. Bott. A flux method for the numerical solution of the stochastic collection equation. *J. Atmos. Sci.*, 55(13):2284–2293, 1998. https://doi.org/10.1175/1520-0469(1998)055<2284:AFMFTN>2.0.CO;2.

A. Bott. A flux method for the numerical solution of the stochastic collection equation: Extension to two-dimensional particle distributions. *J. Atmos. Sci.*, 57(2):284–294, 2000. https://doi.org/10.1175/1520-0469(2000)057<0284:AFMFTN>2.0.CO;2.

O. Boucher, D. Randall, P. Artaxo, C. Bretherton, G. Feingold, P. Forster, V.-M. Kerminen, Y. Kondo, H. Liao, U. Lohmann, et al. Clouds and aerosols. In *Climate change 2013: the physical science basis. Contribution of Working Group I to the Fifth Assessment Report of the Intergovernmental Panel on Climate Change*, pages 571–657. Cambridge University Press, 2013.

S. Brdar and A. Seifert. McSnow: A Monte-Carlo Particle Model for Riming and Aggregation of Ice Particles in a Multidimensional Microphysical Phase Space. *J. Adv. Model. Earth Syst.*, 10(1):187–206, 2018. https://doi.org/10.1002/2017MS001167.

P. Dziekan and H. Pawlowska. Stochastic coalescence in lagrangian cloud microphysics. *Atmos. Chem. Phys.*, 17(22):13509–13520, 2017. https://doi.org/10.5194/acp-17-13509-2017.

P. Dziekan, M. Waruszewski, and H. Pawlowska. University of Warsaw Lagrangian Cloud Model (UWLCM) 1.0: a modern large-eddy simulation tool for warm cloud modeling with Lagrangian microphysics. *Geosci. Model Dev.*, 12(6):2587–2606, 2019. https://doi.org/10.5194/gmd-12-2587-2019.

D. T. Gillespie. The stochastic coalescence model for cloud droplet growth. *J. Atmos. Sci.*, 29(8):1496–1510, 1972. https://doi.org/10.1175/1520-0469(1972)029<1496:TSCMFC>2.0.CO;2.

W. W. Grabowski, H. Morrison, S.-i. Shima, G. C. Abade, P. Dziekan, and H. Pawlowska. Modeling of Cloud Microphysics: Can We Do Better? *Bull. Am. Meteorol. Soc.*, 100(4):655–672, 2019. https://doi.org/10.1175/BAMS-D-18-0005.1.

W. D. Hall. A detailed microphysical model within a two-dimensional dynamic framework: Model description and preliminary results. *J. Atmos. Sci.*, 37(11):2486–2507, 1980. https://doi.org/10.1175/1520-0469(1980)037<2486:ADMMWA>2.0.CO;2.

F. Hoffmann and G. Feingold. Entrainment and Mixing in Stratocumulus: Effects of a New Explicit Subgrid-Scale Scheme for Large-Eddy Simulations with Particle-Based Microphysics. *J. Atmos. Sci.*, 76(7):1955–1973, 06 2019. https://doi.org/10.1175/JAS-D-18-0318.1.

F. Hoffmann, T. Yamaguchi, and G. Feingold. Inhomogeneous Mixing in Lagrangian Cloud Models: Effects on the Production of Precipitation Embryos. *J. Atmos. Sci.*, 76(1):113–133, 2019. https://doi.org/10.1175/JAS-D-18-0087.1.

Z. Hu and R. C. Srivastava. Evolution of raindrop size distribution by coalescence, breakup, and evaporation: Theory and observations. *J. Atmos. Sci.*, 52(10):1761–1783, 1995. https://doi.org/10.1175/1520-0469(1995)052<1761:EORSDB>2.0.CO;2.

A. Jaruga and H. Pawlowska. libcloudph++ 2.0: aqueous-phase chemistry extension of the particle-based cloud microphysics scheme. *Geosci. Model Dev.*, 11(9):3623–3645, 2018. https://doi.org/10.5194/gmd-11-3623-2018.

E. Kessler. On distribution and continuity of water substance in atmospheric circulations. *Mon. Americal Met. Soc., Boston*, 10:1–84, 1969. https://doi.org/10.1007/978-1-935704-36-2_1.

M. Khairoutdinov and Y. Kogan. A new cloud physics parameterization in a large-eddy simulation model of marine stratocumulus. *Mon. Weather Rev.*, 128(1):229–243, 2000. https://doi.org/10.1175/1520-0493(2000)128<0229:ANCPPI>2.0.CO;2.

A. Kostinski and R. Shaw. Fluctuations and luck in droplet growth by coalescence. *Bull. Am. Meteorol. Soc.*, 86(2):235–244, 2005. https://doi.org/10.1175/BAMS-86-2-235.

S. K. Krueger and A. R. Kerstein. An economical model for simulating turbulence enhancement of droplet collisions and coalescence. *J. Adv. Model. Earth Syst.*, 10(8):1858–1881, 2018. https://doi.org/10.1029/2017MS001240.

P. L'Ecuyer and R. Simard. Testu01: A c library for empirical testing of random number generators. *ACM Trans. Math. Softw.*, 33(4), 2007. https://doi.org/10.1145/1268776.1268777.

R. List, N. R. Donaldson, and R. E. Stewart. Temporal evolution of drop spectra to collisional equilibrium in steady and pulsating rain. *J. Atmos. Sci.*, 44(2):362–372, 1987. https://doi.org/10.1175/1520-0469(1987)044<0362:TEODST>2.0.CO;2.

A. B. Long. Solutions to the droplet collection equation for polynomial kernels. *J. Atmos. Sci.*, 31(4):1040–1052, 1974. https://doi.org/10.1175/1520-0469(1974)031<1040:STTDCE>2.0.CO;2.

M. Matsumoto and T. Nishimura. Mersenne twister: a 623-dimensionally equidistributed uniform pseudo-random number generator. *ACM Transactions on Modeling and Computer Simulation*, 8(1):3–30, 1998. https://doi.org/10.1145/272991.272995.

A. K. Naumann and A. Seifert. A lagrangian drop model to study warm rain microphysical processes in shallow cumulus. *J. Adv. Model. Earth Syst.*, 7(3):1136–1154, 2015. https://doi.org/10.1002/2015MS000456.

H. T. Ochs III and K. Beard. Laboratory measurements of collection efficiencies for accretion. *J. Atmos. Sci.*, 41(5):863–867, 1984. https://doi.org/10.1175/1520-0469(1984)041<0863:LMOCEF>2.0.CO;2.

O. P. Prat and A. P. Barros. Exploring the use of a column model for the characterization of microphysical processes in warm rain: results from a homogeneous rainshaft model. *Advances in Geosciences*, 10:145–152, 2007. https://doi.org/10.5194/adgeo-10-145-2007.

T. Riechelmann, Y. Noh, and S. Raasch. A new method for large-eddy simulations of clouds with Lagrangian droplets including the effects of turbulent collision. *New Journal of Physics*, 14(6):065008, 2012. https://doi.org/10.1088/1367-2630/14/6/065008.

P. G. Saffman and J. S. Turner. On the collision of drops in turbulent clouds. *J. Fluid Mech.*, 1(1):16–30, 1956. https://doi.org/10.1017/S0022112056000020.

J. Schwenkel, F. Hoffmann, and S. Raasch. Improving collisional growth in Lagrangian cloud models: development and verification of a new splitting algorithm. *Geosci. Model Dev.*, 11(9):3929–3944, 2018. https://doi.org/10.5194/gmd-11-3929-2018.

A. Seifert. On the Parameterization of Evaporation of Raindrops as Simulated by a One-Dimensional Rainshaft Model. *J. Atmos. Sci.*, 65 (11):3608–3619, 2008. https://doi.org/10.1175/2008JAS2586.1.

A. Seifert and K. D. Beheng. A double-moment parameterization for simulating autoconversion, accretion and selfcollection. *Atmos. Res.*, 59:265–281, 2001. https://doi.org/10.1016/S0169-8095(01)00126-0.

S. Shima, K. Kusano, A. Kawano, T. Sugiyama, and S. Kawahara. The super-droplet method for the numerical simulation of clouds and precipitation: a particle-based and probabilistic microphysics model coupled with a non-hydrostatic model. *Q. J. R. Meteorol. Soc.*, 135 (642):1307–1320, 2009. https://doi.org/10.1002/qj.441.

S. Shima, Y. Sato, A. Hashimoto, and R. Misumi. Predicting the morphology of ice particles in deep convection using the super-droplet method: development and evaluation of scale-sdm 0.2.5-2.2.0/2.2.1. *Geosci. Model Dev. Discuss.*, pages 1–83, 2019. https://doi.org/10.5194/gmd-2019-294.

M. Simmel, T. Trautmann, and G. Tetzlaff. Numerical solution of the stochastic collection equation - comparison of the linear discrete method with other methods. *Atmos. Res.*, 61(2):135–148, 2002. https://doi.org/10.1016/S0169-8095(01)00131-4.

P. Smolarkiewicz and L. Margolin. MPDATA: A Finite-Difference Solver for Geophysical Flows. *J. Comput. Phys.*, 140(2):459–480, 1998.

P. K. Smolarkiewicz. Multidimensional positive definite advection transport algorithm: an overview. *Int. J. Numer. Methods Fluids*, 50: 1123–1144, 2006. https://doi.org/10.1002/fld.1071.

P. K. Smolarkiewicz. A fully multidimensional positive definite advection transport algorithm with small implicit diffusion. *J. Comput. Phys.*, 54:325–362, 1984. https://doi.org/10.1016/0021-9991(84)90121-9.

M. V. Smoluchowski. Drei Vortrage über Diffusion, Brownsche Bewegung und Koagulation von Kolloidteilchen. *Zeitschrift für Physik*, 17: 557–571, 1916.

I. Sölch and B. Kärcher. A large-eddy model for cirrus clouds with explicit aerosol and ice microphysics and Lagrangian ice particle tracking. *Q. J. R. Meteorol. Soc.*, 136:2074–2093, 2010. https://doi.org/10.1002/qj.689.

B. Stevens and A. Seifert. Understanding macrophysical outcomes of microphysical choices in simulations of shallow cumulus convection. *Journal of the Meteorological Society of Japan. Ser. II*, 86A:143–162, 2008. https://doi.org/10.2151/jmsj.86A.143.

J. W. Telford. A new aspect of coalescence theory. *Journal of Meteorology*, 12(5):436–444, 1955. https://doi.org/10.1175/1520-0469(1955)012<0436:ANAOCT>2.0.CO;2.

S. Tzivion, G. Feingold, and Z. Levin. An efficient numerical solution to the stochastic collection equation. *J. Atmos. Sci.*, 44(21):3139–3149, 1987. https://doi.org/10.1175/1520-0469(1987)044<3139:AENSTT>2.0.CO;2.

S. Tzivion (Tzitzvashvili), G. Feingold, and Z. Levin. The evolution of raindrop spectra. part ii: Collisional collection/breakup and evaporation in a rainshaft. *J. Atmos. Sci.*, 46(21):3312–3328, 1989. https://doi.org/10.1175/1520-0469(1989)046<3312:TEORSP>2.0.CO;2.

S. Unterstrasser, F. Hoffmann, and M. Lerch. Collection/aggregation algorithms in Lagrangian cloud microphysical models: rigorous evaluation in box model simulations. *Geosci. Model Dev.*, 10(4):1521–1548, 2017. https://doi.org/10.5194/gmd-10-1521-2017.

L.-P. Wang, A. S. Wexler, and Y. Zhou. Statistical mechanical descriptions of turbulent coagulation. *Phys. Fluids*, 10(10):2647–2651, 1998. https://doi.org/10.1063/1.869777.

L.-P. Wang, O. Ayala, and Y. Xue. Reconciling the cylindrical formulation with the spherical formulation in the kinematic descriptions of collision kernel. *Phys. Fluids*, 17(6):067103, 2005. https://doi.org/10.1063/1.1928647.

L.-P. Wang, Y. Xue, O. Ayala, and W. W. Grabowski. Effects of stochastic coalescence and air turbulence on the size distribution of cloud droplets. *Atmos. Res.*, 82:416–432, 2006. https://doi.org/10.1063/1.1928647.

L.-P. Wang, Y. Xue, and W. W. Grabowski. A bin integral method for solving the kinetic collection equation. *J. Comput. Phys.*, 226(1): 59–88, 2007. https://doi.org/10.1016/j.jcp.2007.03.029.